Since January 2020 Elsevier has created a COVID-19 resource centre with free information in English and Mandarin on the novel coronavirus COVID-19. The COVID-19 resource centre is hosted on Elsevier Connect, the company's public news and information website.

Elsevier hereby grants permission to make all its COVID-19-related research that is available on the COVID-19 resource centre - including this research content - immediately available in PubMed Central and other publicly funded repositories, such as the WHO COVID database with rights for unrestricted research re-use and analyses in any form or by any means with acknowledgement of the original source. These permissions are granted for free by Elsevier for as long as the COVID-19 resource centre remains active.

Computers in Biology and Medicine 136 (2021) 104609

Contents lists available at ScienceDirect

Computers in Biology and Medicine

journal homepage: www.elsevier.com/locate/compbiomed

Ant colony optimization with Cauchy and greedy Levy mutations for multilevel COVID 19 X-ray image segmentation

Lei Liu [a], Dong Zhao [a,**], Fanhua Yu [a], Ali Asghar Heidari [b,1], Chengye Li [c], Jinsheng Ouyang [c], Huiling Chen [b,*], Majdi Mafarja [d], Hamza Turabieh [e], Jingye Pan [f,g,h,***]

[a] College of Computer Science and Technology, Changchun Normal University, Changchun, Jilin, 130032, China
[b] College of Computer Science and Artificial Intelligence, Wenzhou University, Wenzhou, Zhejiang, 325035, China
[c] Department of Pulmonary and Critical Care Medicine, The First Affiliated Hospital of Wenzhou Medical University, Wenzhou, 325000, China
[d] Department of Computer Science, Birzeit University, POBox 14, West Bank, Palestine
[e] Department of Information Technology, College of Computers and Information Technology, P.O. Box 11099, Taif, 21944, Taif University, Taif, Saudi Arabia
[f] Department of Intensive Care Unit, The First Affiliated Hospital of Wenzhou Medical University, Wenzhou, China
[g] Key Laboratory of IntelligentTreatment and Life Support for Critical Diseases of Zhejiang Provincial, Wenzhou, China
[h] Wenzhou Key Laboratory of Critical Care and Artificial Intelligence, Wenzhou, China

ARTICLE INFO

Keywords:
Ant colony optimization
Diagnosis
Image
Meta-heuristic
COVID-19
Swarm-intelligence

ABSTRACT

This paper focuses on the study of multilevel COVID-19 X-ray image segmentation based on swarm intelligence optimization to improve the diagnostic level of COVID-19. We present a new ant colony optimization with the Cauchy mutation and the greedy Levy mutation, termed CLACO, for continuous domains. Specifically, the Cauchy mutation is applied to the end phase of ant foraging in CLACO to enhance its searchability and to boost its convergence rate. The greedy Levy mutation is applied to the optimal ant individuals to confer an improved ability to jump out of the local optimum. Furthermore, this paper develops a novel CLACO-based multilevel image segmentation method, termed CLACO-MIS. Using 2D Kapur's entropy as the CLACO fitness function based on 2D histograms consisting of non-local mean filtered images and grayscale images, CLACO-MIS was successfully applied to the segmentation of COVID-19 X-ray images. A comparison of CLACO with some relevant variants and other excellent peers on 30 benchmark functions from IEEE CEC2014 demonstrates the superior performance of CLACO in terms of search capability, and convergence speed as well as ability to jump out of the local optimum. Moreover, CLACO-MIS was shown to have a better segmentation effect and a stronger adaptability at different threshold levels than other methods in performing segmentation experiments of COVID-19 X-ray images. Therefore, CLACO-MIS has great potential to be used for improving the diagnostic level of COVID-19. This research will host a webservice for any question at https://aliasgharheidari.com.

1. Introduction

In December 2019, an outbreak of a novel coronavirus, named COVID-19 by the World Health Organization (WHO) [1], occurred in Wuhan, China. In March 2020, the WHO declared COVID-19 a world pandemic. As COVID-19 is spreading around the world, healthcare systems are under tremendous pressure. Although the current diagnostic criteria for COVID-19 are a positive nucleic acid test, the false-negative rate for nucleic acid testing is as high as 17%–25.5%. Therefore, imaging-based diagnostic methods are used to screen for many suspected cases and serve as an effective way to stifle the spread of the disease. Since the outbreak, many researchers have conducted numerous studies using X-ray images of the lungs of infected patients [2–4]. Data science [5] has witnessed significant progress during recent years in dealing with a global epidemic.

* Corresponding author.
** Corresponding author.
*** Corresponding author. Department of Intensive Care Unit, The First Affiliated Hospital of Wenzhou Medical University, Wenzhou, China.
E-mail addresses: leiliu_v@163.com (L. Liu), zd-hy@163.com (D. Zhao), yufanhua@163.com (F. Yu), aliasghar68@gmail.com (A.A. Heidari), ouyangkch@163.com (J. Ouyang), chenhuiling.jlu@gmail.com (H. Chen), mmafarja@birzeit.edu (M. Mafarja), h.turabieh@tu.edu.sa (H. Turabieh), panjingye@wzhospital.cn (J. Pan).
[1] https://aliasgharheidari.com.

https://doi.org/10.1016/j.compbiomed.2021.104609
Received 30 March 2021; Received in revised form 22 June 2021; Accepted 22 June 2021
Available online 3 July 2021
0010-4825/© 2021 Elsevier Ltd. All rights reserved.

Nomenclature

WHO	World Health Organization
COVID-19	An infectious disease of coronavirus infection
MIS	Multilevel threshold image segmentation
WSRT	Wilcoxon signed-rank test
FT	Friedman test
CLACO	A novel variant of ant colony optimization
ACO-MIS	CLACO-based MIS model
PSNR	Peak Signal to Noise Ratio
SSIM	Structural Similarity Index
FSIM	Feature Similarity Index
ξ	The pheromone evaporation rate
k	The archive size
q	The algorithm coefficient
$\theta(j)$	A self-adapting mutation coefficient
$levy$	A Levy distribution random number
y	A number uniformly distributed between $[0,1]$
g	A scaling parameter
$f_{Cauchy(0,g)}$	The Cauchy distribution function
C	A random number
t	The current number of iterations
FEs	The current number of evaluations
$MaxFEs$	The maximum number of evaluations
ε	An algorithm coefficient
$I(p)I(q)$	The gray-scale values of pixels p. and q of image I
m	Population size
$O(p)$	A corresponding filter value
$\omega(p,q)$	The corresponding weight
σ	The corresponding standard deviation
$\mu(p)\mu(q)$	Local area average values
$L(p)$	A $m \times m$ block-oriented at p
$L(q)$	A $m \times m$ block-oriented at q
$I(x,y)$	A gray image
$g(x,y)$	Non-local means image
P_{ij}	The normalized 2D histogram
$\phi(s,t)$	2D Kapur's entropy
L	The gray level
M	The segmentation level
$G^i(x)$	The Gaussian kernel function
$g_l^i(x)$	The Gaussian function
w	The weight vector
μ^i	The mean vecto
p_l	The choosing probability
x_l	The ant individual
dim	Problem dimension
UL	Search space
$bestAnt$	The best ant

These kinds of studies are an essential step in developing effective healthcare or bio-informatic systems [6–8]. It is well known that multilevel threshold image segmentation (MIS) is a simple and efficient image processing method. To further improve the diagnostic level of COVID-19 [9,144,145], this paper focuses on the study of MIS and proposes an MIS method with excellent segmentation results.

In recent years, MIS has gained much attention as an efficient and straightforward image segmentation method. A wide variety of MIS have been proposed and applied to various complex medical image processing. For instance, Zhao et al. [10] proposed a fast 2D Otsu image segmentation algorithm to segment lung tissue images based on enhanced particle swarm optimization (PSO). Rodríguez-Esparza et al. [12] proposed an excellent method for MIS by using the minimum cross-entropy as a fitness function of Harris hawks optimization, which was tested on medical images of digital mammography. Anter et al. [13] developed a robust optimization approach for automatic segmentation of liver and liver lesions based on fast fuzzy c-means, chaos theoretical, and bio-inspired ant-lion optimizer.

Moreover, Abdel-Basset et al. [14] proposed a new hybrid approach by integrating a sticky mode algorithm and whale optimizer according to the threshold segmentation technique of COVID-19 chest X-ray images. Sambandam et al. [15] proposed an adaptive dragonfly optimization approach for performing MIS of medical images. Verma et al. [16] proposed a hybrid MIS method with Fuzzy c-means and the PSO algorithm, which was applied to execute experiments on publicly available real brain datasets. Radha et al. [17] proposed a combination of an intelligent fuzzy level set approach and an improved quantum PSO for magnetic resonance image segmentation. Table 1 compares some related works, which, with relatively weak adaptability, were developed by carrying out a straightforward combination of techniques. Therefore, in the present study, we first propose the CLACO algorithm with excellent performance and then combine it with 2D Kapur's entropy, non-local means, and 2D histogram to achieve a better segmentation effect and a more robust adaptability at different threshold levels.

The MIS method based on the swarm intelligence optimization algorithm is widely adopted. It is also found that the optimum threshold set in the MIS method is highly dependent on the swarm intelligence

Table 1
The comparison between some relevant works.

Study	Method	Image type	The relevant result
Work of this paper	CLACO+ 2D Kapur's entropy + non-local means + 2D histogram	COVID-19 X-ray images	It obtained a better segmentation effect and more robust adaptability at different threshold levels.
Zhao et al. [10]	improved PSO + 2D Otsu	lung tissue images	It not only satisfied the requirement of segmentation precision but also met the requirement of operation speed.
Rodríguez-Esparza et al. [12]	MCET-HHO + Minimum cross entropy	medical images of digital mammography	It produced efficient and reliable results in terms of quality, consistency, and accuracy.
Anter et al. [13]	CAL OF CM + fuzzy c-means	hepatic lesion segmentation from CT scans	It showed good detection and segmentation performance.
Abdel-Basset et al. [14]	HSMA_WOA + Kapur's entropy	COVID-19 chest X-ray images	It outperformed SMA under Kapur's entropy for all the metrics.
Sambandam et al. [15]	SADFO + Kapur's entropy	six medical images of eyes, liver, head and tongue	It effectively optimized the threshold values by exploring the solution space.
Verma et al. [16]	hybrid fuzzy c-means and PSO	real brain datasets	It improved up to 30% for real brain images.
Radha et al. [17]	IQPSO + intelligent fuzzy level set method	magnetic image resonance images	It showed a promising significant improvement in the image segmentation process.

optimization algorithm. In other words, a swarm intelligence optimization algorithm with high performance can greatly improve the results of MIS. Complex feature spaces often are challenging enough to be dealt with [18,19], especially in the medical area [20] and image quality assessment [132]. Hence, more attention should be paid to the accuracy and efficacy of the procedure used to tackle the model [21,22]. The swarm intelligence optimization algorithm has shown great potential in solving a multitude of practical problems, including but not limited to, detection of feature selection cases [23–25], parameter optimization [26–28], imaging array [128], communication systems [129], and engineering problems [29–31]. Also, we can refer to PID optimization control [32–34], prediction problems in educational field [35–37], the hard maximum satisfiability problem [38,39], foreign fiber in cotton [40,41], medical diagnosis [42–44], scheduling problem [45,46], wind speed prediction [47], bankruptcy prediction [48–50], fault diagnosis of rolling bearings [51,52], and gate resource allocation [53,54].

As far as swarm intelligence optimization algorithms are concerned, a number of related algorithms have been proposed, including PSO [57], Harris hawks optimization (HHO)[2] [61], slime mould algorithm (SMA)[3] [62], hunger games search (HGS)[4] [63], Runge Kutta optimizer (RUN)[5] [64], modified SCA (m_SCA) [65], boosted GWO (OBLGWO) [66], opposition-based SCA (OBSCA) [67], A-C parametric WOA (ACWOA) [68], biogeography-based learning PSO (BLPSO) [69], comprehensive learning PSO (CLPSO) [70], moth-flame optimizer with sine cosine mechanisms (SMFO) [71], enhanced comprehensive learning particle swarm optimizer (GCLPSO) [72], enhanced GWO with a new hierarchical structure (IGWO) [73], improved WOA (IWOA) [74], and ant colony optimization (ACO) for continuous domains (ACOR) [75]. Notably, it is well known that ACO [76,77] is an algorithm for solving discrete optimization problems, whereas ACOR can be used to solve optimization problems other than discrete ones.

Accordingly, in recent years, a broad array of related studies have been carried out on original optimizers such as PSO [136–138], and its variants [139–142], and more methods based on well-known swarm--based method continuous ACO algorithms. Zhao et al. [78] proposed a modified continuous ACO algorithm by refining the selection scheme and applying horizontal cross-search and vertical cross-search to ACOR. Chen et al. [79] proposed a new elite hybrid continuous ACO method based on the central initialization of the population. Zhao et al. [80] proposed a novel variant of the continuous ACO by applying a stochastic standby strategy and a chaotic reinforcement strategy based on the original ACO. Wu et al. [81] described a multi-modular and continuous ACO algorithm and devised an efficient method as a local search operation. Kumar et al. [82] proposed a novel continuous ACO algorithm by incorporating an interaction scheme between ants based on the Laplace distribution. Chen et al. [83] developed a modified continuous ACO with crossover operators, where there are three crossover methodologies adopted to yield some new sets of probability density functions. Karakonstantis et al. [84] presented a hybrid variant of ACO for continuous domains, which can handle continuous optimization problems either with or without constraints.

Although these proposed various variants of the continuous ACO algorithm outperform the original ACOR on specific problems, they suffer from some performance problems and thus need improving. It is possible that, they might fail to obtain satisfactory results when applied to different fields due to their poor search capability, slow convergence rate, and tendency to fall into local optimum in the process of solving specific problems. To tackle these problems and obtain a high-quality threshold set in multi-threshold COVID-19 X-ray image segmentation, this paper proposes a novel variant of ACO with the Cauchy mutation and the greedy Levy mutation for continuous domains (CLACO). Specifically, the Cauchy mutation introduced to the end stage of foraging in CLACO effectively enhances the searchability and convergence speed. The greedy Levy variant applied to the optimal ant individuals confers an improved ability to jump out of the local optimum. The optimal individuals have enhanced experiential information and the ability to learn on their own. In this paper, the variant algorithms consisting of the Cauchy mutation and the greedy Levy mutation were compared to demonstrate the superior performance of CLACO, using 30 test functions from IEEE CEC2014. Then, CLACO was also experimentally compared with ten other similar algorithms. Finally, all experimental results obtained were re-analyzed and compared using the Wilcoxon signed-rank test (WSRT) [85] and the Friedman test (FT) [86]. A careful analysis and comparison of experimental results demonstrate that CLACO is superior in searchability, convergence speed and ability to jump out of the local optimum.

Meanwhile, to improve the diagnostic level of COVID-19, a new CLACO-based MIS model (CLACO-MIS), which can obtain high-quality segmentation results, is proposed in this paper and applied to segment X-ray images from patients with COVID-19. In CLACO-MIS, to obtain an optimal threshold set, 2D histograms are adopted composed of non-local mean filtered images and grayscale images and 2D Kapur's entropy is taken as the CLACO fitness function based on the composed 2D histograms. To demonstrate that CLACO-MIS has a superior segmentation effect and stronger adaptability to different threshold levels, based on 9 X-ray images of COVID-19 patients, CLACO-MIS and eight other similar methods were compared in segmentation experiments not only at levels 4, 5, and 6, representing low threshold levels, but also at levels 15, 20, and 25, representing high threshold levels, Finally, we evaluated the COVID-19 X-ray image segmentation results using Peak Signal to Noise Ratio (PSNR) [87], Structural Similarity Index (SSIM) [88], Feature Similarity Index (FSIM) [89] to effectively account for the segmentation results. In addition, we compared the evaluation results using mean and variance together with the WSRT [85] and FT [86]. The comparative results show that, compared with other similar methods, CLACO-MIS has a better segmentation effect and a stronger adaptability to different threshold levels in performing multi-threshold COVID-19 X-ray image segmentation.

The other sections of this paper are organized as follows. Section 2 describes the Cauchy mutation and the greedy Levy mutation and proposes a new ACOR (CLACO) version. Section 3 describes non-local means for the 2D histogram, 2D Kapur's entropy, and presents a novel multilevel COVID-19 X-ray image segmentation method based on CLACO. In section 4, some comparative experiments are carried out to demonstrate the performance of CLACO and CLACO-MIS. The conclusions of the whole paper and some future works are presented in section 5.

In conclusion, this paper's main innovations and contributions lie in the following aspects.

- A new enhanced ACOR version combining the Cauchy mutation and the greedy Levy mutation, called CLACO, is first proposed based on the original ACOR.
- CLACO is compared with many similar methods using IEEE CEC2014, and the core advantages of CLACO are fully demonstrated.
- Using non-local means, 2D histogram and 2D Kapur's entropy, a CLACO-based MIS method, called CLACO-MIS, is first developed.
- In a comparative experiment between CLACO-MIS and its peers at several threshold levels, its segmentation effect is well demonstrated using COVID-19 real pathology images.
- Compared with other peers, CLACO obtains a more significant improvement in benchmark function problems and image segmentation quality.

[2] https://aliasgharheidari.com/HHO.html.
[3] https://aliasgharheidari.com/SMA.html.
[4] https://aliasgharheidari.com/HGS.html.
[5] https://aliasgharheidari.com/RUN.html.

2. Proposed CLACO

2.1. Cauchy mutation

Based on the description of ACOR in Appendix C, in this subsection, the Cauchy mutation strategy is briefly illustrated to enhance the search capability of CLACO. It is also found that some relevant experimental results proved that the Cauchy mutation strategy has a powerful search ability in literature [90]. Therefore, based on the above inspiration, the Cauchy mutation is introduced into CLACO to improve the search power of CLACO, which also further enhances the convergence rate. The Cauchy distribution function, in this case, can be represented as Eqs. (1) and (2) [91].

$$y=\frac{1}{2}+\frac{1}{\pi}arctan\left(\frac{\gamma}{g}\right) \tag{1}$$

The corresponding density function is defined as follows,

$$f_{Cauchy(0,g)}(\gamma)=\frac{1}{\pi}\frac{g}{g^2+\gamma^2} \tag{2}$$

where $g=1$ is the scaling parameter [92], y is a number uniformly distributed between $[0,1]$, and $\gamma=\tan(\pi(y-1/2))$. Although the corresponding density function is similar between Gaussian distribution and Cauchy distribution, differences can be found between them. The main distinguishing feature is that the Cauchy distribution is smaller than the Gaussian distribution in the vertical direction, but it is broader than the Gaussian distribution in the horizontal direction. The search capability of search individuals can be improved by adding some neighbors in every generation because it guarantee that individuals can enhance themselves within the main scope and easily jump out of the local optimum. Therefore, the Cauchy distribution, which can be regarded as an effective mutation operation, is applied to the end of the foraging phase of an ant colony in CLACO while $FEs/MaxFEs>0.5$. This process can be illustrated by Eqs. (1) and (2) [91].

At the end of the foraging phase, the Cauchy mutation is introduced to confer a better ability to utilize the prospective space. Therefore, it is possible to improve solution quality with the Cauchy mutation over the whole simulation process. The generated random number is applied to the end of the foraging phase of an ant colony and is shown as Eq. (3) [91].

$$x_i^{'}=x_i\times(1+C(\gamma)) \tag{3}$$

where C is a random number sampled from the Cauchy distribution.

2.2. Greedy Levy mutation

In the basic ACOR, some optimal individuals guide the entire group in the search direction. However, the best individuals face a lack of experiential information and thus the ability to learn independently. Therefore, it may be difficult for them to be improved and thus they tend to fall into the local optimum. A greedy Levy mutation-based optimal individual strategy is proposed in order to avoid falling into the local optimum and to overcome inefficiency in the later period. As a result, the individuals can jump out of the original optimal position previously searched by the mutation operation, thus preserving the population diversity. The Greedy Levy mutation-based optimal individual methodology is represented as Eq. (4) [93].

$$x_{best,j}^{t+1}=x_{best,j}^{t}+\theta(j)\times levy\times x_{best,j}^{t} \tag{4}$$

where $levy$ is the random number obtained by the Levy distribution, $\theta(j)$ is a self-adapting mutation coefficient, and $x_{best,j}^{t}$ is the jth dimension value of the optimal individual position at iteration t.

Due to the difficulty of integrating the probability density function of the Levy distribution, in the greedy Levy mutation, it has been shown that the Mantegna algorithm can be implemented as an equivalent calculation [94]. It can be calculated by Eq. (5) [93].

$$levy\approx\frac{u}{|v|^{1/\beta}} \tag{5}$$

where $u\sim N(0,\sigma_u^2)$, $v\sim N(0,\sigma_v^2)$, $\sigma_v=1$, $\beta=3/2$, and σ_u can be calculated by Eq. (6) [93].

$$\sigma_u=\left\{\frac{\Gamma(1+\beta)\times\sin(\pi\times\beta/2)}{\Gamma[(1+\beta)/2]\times\beta\times2^{(\beta-1)/2}}\right\}^{1/\beta} \tag{6}$$

where Γ indicates the standard Gamma function.

Besides, aiming to obtain a large mutation in the initial stage of ant foraging to perform global interference, and to diminish the mutation in the late-foraging stage to accelerate the local search, the self-adaptive mutation control coefficient $\theta(j)$ can be expressed as given in Eqs. (7)–(9) [93].

$$\theta(j)=e^{(-\varepsilon\times FEs/MaxFEs)(1-r(j)/r_{max}(j))} \tag{7}$$

$$r(j)=\left|x_{best,j}^{t}-\frac{1}{n}\sum_{i=1}^{k}x_{i,j}^{t}\right| \tag{8}$$

$$r_{max}(j)=max\left(x_{:,j}^{t}\right)-min\left(x_{:,j}^{t}\right) \tag{9}$$

where t is the current number of iterations, FEs is the current number of evaluations, $MaxFEs$ is the maximum number of evaluations, ε is an algorithm coefficient, $r(j)$ is the difference between the value of the jth position vector of the current optimal individual and the average of the values of the jth position vector of each individual in the archive, and $r_{max}(j)$ is the difference between the maximum and minimum values among the jth position vector values in the archive.

2.3. The proposed CLACO

Given that satisfactory results are often not obtained when ACOR was applied to different domains for its poor search capability, slow convergence speed and tendency to fall into local optima in solving specific problems, we propose a new version of ACOR, called CLACO. The introduction of the Cauchy mutation to the end stage of ant foraging in CLACO effectively enhances not only the search capability but also the convergence speed of foraging ants. Aiming to confer an improved ability to jump out of local optima, the greedy Levy mutation is applied to optimal ant individuals, conferring enhanced experiential information and an ability to learn independently. By analyzing the effects of the Cauchy mutation and the greedy Levy mutation on the process of ant foraging, a flowchart of CLACO is presented in Fig. 1.

3. Proposed MIS method

3.1. Non-local means for 2D histogram

Non-local means, a novel denoising technique, was developed by Buades et al. [95]. Taking full advantage of the redundant information in the image, this method can preserve the image's detailed features as much as possible while de-noising. Assuming that $I(p)$ and $I(q)$ are the corresponding gray-scale values of pixels p and q of image I, it is possible to calculate the non-local mean values from Eqs. 10–13 [95] for image I.

$$O(p)=\frac{\sum_{q\in I}I(q)\omega(p,q)}{\sum_{q\in I}\omega(p,q)} \tag{10}$$

$$\omega(p,q)=exp^{-\frac{|\mu(p)-\mu(q)|^2}{\sigma^2}} \tag{11}$$

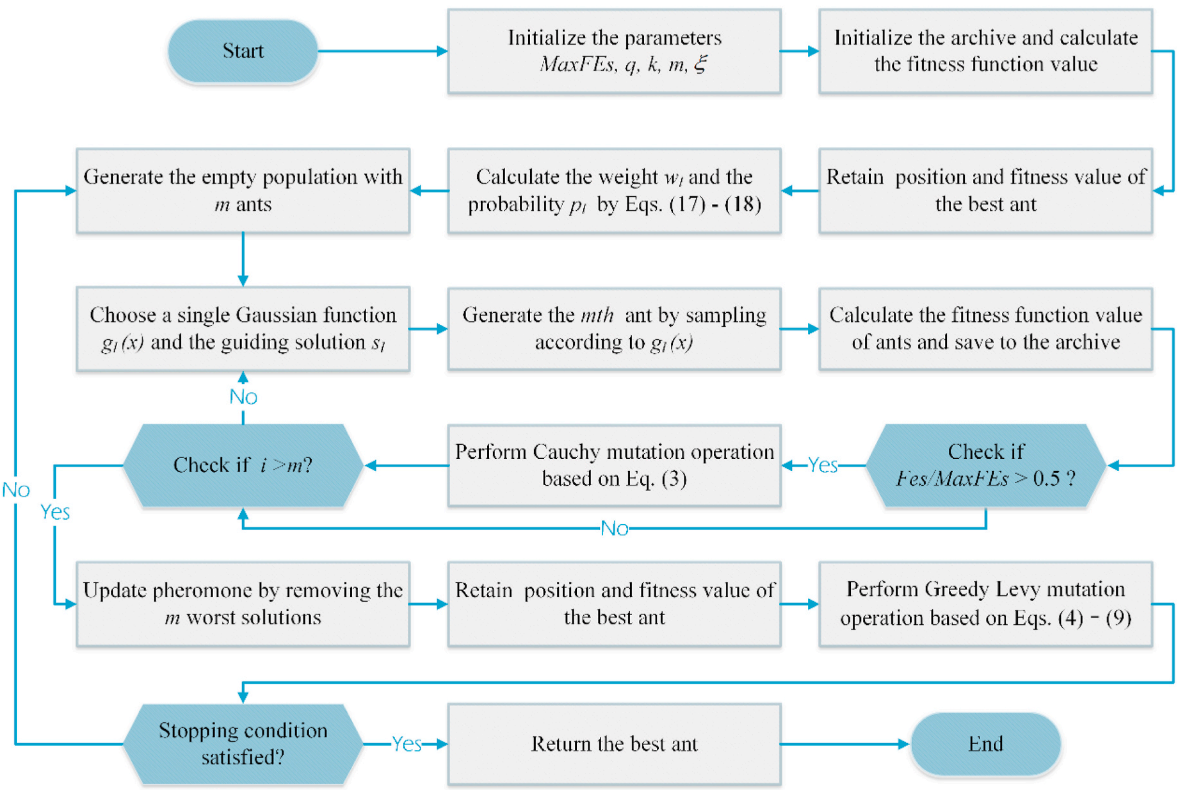

Fig. 1. The flowchart of CLACO.

$$\mu(p) = \frac{1}{m \times m} \sum_{i \in L(p)} I(i) \tag{12}$$

$$\mu(q) = \frac{1}{m \times m} \sum_{i \in L(q)} I(i) \tag{13}$$

where $O(p)$ is a corresponding filter value, $\omega(p,q)$ is the corresponding weight, σ is the corresponding standard deviation, $\mu(p)$ and $\mu(q)$ are local area average values, $L(p)$ is a $m \times m$ block-oriented at p, and L(q) is an m × m block-oriented at q.

An image's 2D histogram can be constructed using a non-local mean image and grayscale image. If we suppose that a gray image $I(x,y)$ has levels $[0, L-1]$ and the image size is $M \times N$, the image $g(x,y)$ obtained by non-local means filtering also has levels $[0, L-1]$ and the image size is also $M \times N$. As a result, the point (i,j) can be constructed using the levels and gray values of $I(x,y)$ and $g(x,y)$. i denotes the gray value of the pixel in $I(x,y)$ and j denotes the gray value of the corresponding pixel in $g(x, y)$. Consequently, it is possible to have the number of pixels $h(i,j)$ that appear at this point (s,t), as well. The 2D histogram developed above in this way is normalized by Eq. (14) [96]. We can produce a final 2D histogram shown in Fig. 2 and the corresponding plane view.

$$P_{ij} = \frac{h(i,j)}{M \times N} \tag{14}$$

3.2. 2D Kapur's entropy

As we have the definition of non-local mean 2D histogram above, it is possible to construct correspondingly the 2D histogram and 2D plane view in Fig. 2, where $\{t_1, t_2 \ldots, L-1\}$ represents the greyscale image levels, and $\{s_1, s_2 \ldots, L-1\}$ characterizes levels in the non-local mean image.

Based on the 2D histogram presented above, we can construct the corresponding 2D Kapur's entropy. Since the primary alignment of the 2D histogram contains the most image information, the 2D Kapur's entropy is calculated only for the n subregions on the central diagonal to make the calculation correct and straightforward. Consequently,

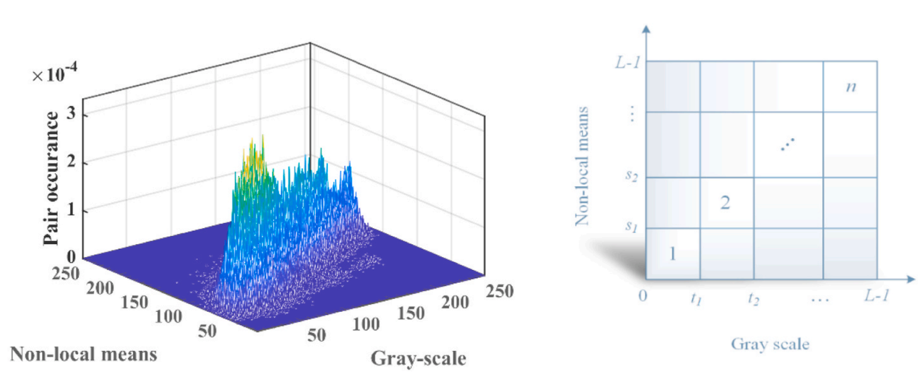

Fig. 2. The 2D histogram and the 2D plan view.

through the description above, the 2D Kapur's entropy is expressed as Eq. (15) [80] in the image. Therefore, the threshold set $\{t_1, t_2, \ldots, t_{n-1}\}$ that maximizes $\phi(s,t)$ is the optimal threshold set, when the 2D Karpur's entropy is considered as the objective function of CLACO.

$$\phi(s,t) = -\sum_{i=0}^{s_1}\sum_{j=0}^{t_1}\frac{P_{ij}}{P_1}\ln\frac{P_{ij}}{P_1} - \sum_{i=t_1+1}^{s_2}\sum_{j=t_1+1}^{t_2}\frac{P_{ij}}{P_2}\ln\frac{P_{ij}}{P_2} - \ldots - \sum_{i=s_{L-2}+1}^{s_{L-1}} \times \sum_{j=t_{L-2}+1}^{t_{L-1}}\frac{P_{ij}}{P_{L-1}}\ln\frac{P_{ij}}{P_{L-1}}. \tag{15}$$

where

$$P_1 = \sum_{i=0}^{s_1}\sum_{j=0}^{t_1}P_{ij}\ P_2 = \sum_{i=t_1+1}^{s_2}\sum_{j=t_1+1}^{t_2}P_{ij}\ P_{L-1} = \sum_{i=s_{L-2}+1}^{s_{L-1}}\sum_{j=t_{L-2}+1}^{t_{L-1}}P_{ij}$$

3.3. The proposed MIS method

The main purpose of threshold-based segmentation is to find a reasonable threshold set to distinguish the target from the background in an image, a compelling image segmentation method. Furthermore, MIS is defined as the process of finding a threshold set in an image, segmenting the image into multiple parts using a threshold set. To achieve better one-threshold image segmentation, Pun [97] presented a maximum entropy-based thresholding algorithm, which regards the histogram of an image as a probability distribution and calculates the maximum entropy to identify an optimal threshold value. Ler, Kapur et al. [98] introduced a modified maximum entropy-based threshold segmentation algorithm, which is simple to compute and yields better segmentation results called Kapur's entropy. It is theoretically easy to extend the maximum entropy-based one-threshold image segmentation algorithm to MIS. Nevertheless, Given repeated calculations that are involved in MIS, its computational efficiency is relatively low. For instance, by applying the exhaustive method to multilevel maximum entropy threshold segmentation, the time complexity is $O((L-M+1)^{M-1})$, and it is increasing exponentially, in which L denotes the grayscale range of the image and M is the number of levels in the segmentation. Moreover, for the 1D histogram-based segmentation method, a serious misclassification phenomenon occurs when the target occupies a relatively small area in an image, rendering the segmentation results vulnerable to noise interference. By contrast, the conventional 2D histogram segmentation method based on the local mean does not consider some detailed information in an image, such as some points, lines, and planes [95].

As a result, the proposed MIS method is based on 2D histograms with non-local means to minimize the above drawbacks, and it employs 2D Kapur's entropy as the fitness function of CLACO. In addition, it is applied to multilevel COVID-19 X-ray image segmentation, and is described in detail in Fig. 3.

4. Experiments and results

In this section, it is mainly to verify the performance of CLACO experimentally and to evaluate the segmentation effect of CLACO-MIS. First, ACOR variants consisting of the Cauchy mutation and the greedy Levy mutation were compared, and then CLACO was compared with ten other similar algorithms on the 30 test functions from IEEE CEC2014. Subsequently, based on 9 COVID-19 X-ray images, a segmentation experiment using CLACO and eight other similar methods was performed not only at levels 4, 5, and 6, representing low threshold levels, but also at levels 15, 20, and 25, representing high threshold levels.

4.1. Experiment setup

In the experiments on the IEEE CEC2014 benchmark functions shown in Table 2, which contains a convincing test suite of unimodal functions, simple multimodal functions, hybrid functions, and composition functions. Its main purpose is to demonstrate that CLACO has a high performance. At first, different ACOR variants, namely, LACO, CACO, and CLACO, are constructed using the Cauchy mutation and the greedy Levy mutation, and the constructed variant algorithms are employed for strategy comparison experiments. Subsequently, the comparison experiments with similar algorithms were mainly carried out by comparing CLACO with GWO [134], MFO [135], PSO, ACOR, SCA [135], WOA [135], OBLGWO, m_SCA, OBSCA, and ACWOA. In the process of conducting the relevant experiments, all the algorithms involved in the comparison were carried out under the same conditions to guarantee the fairness and reliability of the experimental results [133], where the population size was set to 30, and the maximum number of evaluations was uniformly set to 300,000. Furthermore, all algorithms were independently trained 30 times to minimize the influence of random conditions. Notably, both the WSRT and FT were utilized to analyze and compare the obtained experimental results once again. After careful analysis and comparison on a series of experimental results, CLACO was shown to have an enhanced search capability, a faster convergence speed, and a higher convergence accuracy as well as an improved ability to step out of the local optimum.

Experiments were conducted for segmentation using 9 COVID-19 X-ray images shown in Fig. 4 from a public database collected by Cohen et al. [99]. Their corresponding 2D histograms are represented by A, B, C, D, E, F, G, H, and I, respectively. It is mainly to demonstrate that the proposed CLACO-MIS method can obtain relatively good segmentation results and has a strong adaptability to different threshold levels. Firstly, CLACO and eight other similar methods were used to perform segmentation experiments at levels 4, 5, and 6, representing low threshold levels, and secondly, we also performed segmentation experiments at levels 15, 20, and 25, representing high threshold levels. In the segmentation experiments, the 8 similar comparison methods involved were ACOR-MIS, MVO-MIS, HHO-MIS, SCA-MIS, BLPSO-MIS, IGWO--MIS, IWOA-MIS, and CLPSO-MIS. During the process of performing the experiments, all segmentation experiments were performed in 100 times iterations to assure the fairness as well as the reliability of the experimental results, where the chosen segmentation image size was defined as 512 × 400, and the population size was set to 20 for all the segmentation methods involved in the comparison. To eliminate the

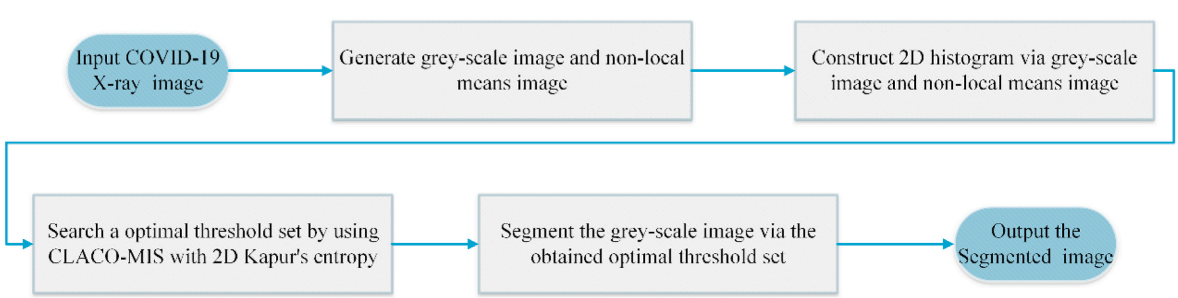

Fig. 3. The flowchart of the CLACO-MIS method.

Table 2
Descriptions of the CEC2014 functions.

Class	ID	Description	Range	$F_i^* = F_i(x^*)$
Unimodal Functions	1	Rotated High Conditioned Elliptic Function	$[-100, 100]$	100
	2	Rotated Bent Cigar Function	$[-100, 100]$	200
	3	Rotated Discus Function	$[-100, 100]$	300
Simple Multimodal Functions	4	Shifted and Rotated Rosenbrock's Function	$[-100, 100]$	400
	5	Shifted and Rotated Ackley's Function	$[-100, 100]$	500
	6	Shifted and Rotated Weierstrass Function	$[-100, 100]$	600
	7	Shifted and Rotated Griewank's Function	$[-100, 100]$	700
	8	Shifted Rastrigin's Function	$[-100, 100]$	800
	9	Shifted and Rotated Rastrigin's Function	$[-100, 100]$	900
	10	Shifted Schwefel's Function	$[-100, 100]$	1000
	11	Shifted and Rotated Schwefel's Function	$[-100, 100]$	1100
	12	Shifted and Rotated Katsuura Function	$[-100, 100]$	1200
	13	Shifted and Rotated HappyCat Function	$[-100, 100]$	1300
	14	Shifted and Rotated HGBat Function	$[-100, 100]$	1400
	15	Shifted and Rotated Expanded Griewank's plus Rosenbrock's Function	$[-100, 100]$	1500
	16	Shifted and Rotated Expanded Schaffer's F6 Function	$[-100, 100]$	1600
Hybrid Functions	17	Hybrid Function 1 ($N = 3$)	$[-100, 100]$	1700
	18	Hybrid Function 2 ($N = 3$)	$[-100, 100]$	1800
	19	Hybrid Function 3 ($N = 4$)	$[-100, 100]$	1900
	20	Hybrid Function 4 ($N = 4$)	$[-100, 100]$	2000
	21	Hybrid Function 5 ($N = 5$)	$[-100, 100]$	2100
	22	Hybrid Function 6 ($N = 5$)	$[-100, 100]$	2200
Composition Functions	23	Composition Function 1 ($N = 5$)	$[-100, 100]$	2300
	24	Composition Function 2 ($N = 3$)	$[-100, 100]$	2400
	25	Composition Function 3 ($N = 3$)	$[-100, 100]$	2500
	26	Composition Function 4 ($N = 5$)	$[-100, 100]$	2600
	27	Composition Function 5 ($N = 5$)	$[-100, 100]$	2700
	28	Composition Function 6 ($N = 5$)	$[-100, 100]$	2800
	29	Composition Function 7 ($N = 3$)	$[-100, 100]$	2900
	30	Composition Function 8 ($N = 3$)	$[-100, 100]$	3000

experimental randomness, all experiments were run 30 times independently. The experimental results obtained were evaluated using PSNR, SSIM, and FSIM, and a comparative analysis was performed using the mean and variance as well as WSRT and FT. By analyzing and comparing a series of experimental results, the superior segmentation effect of CLACO-MIS and its stronger adaptability to different threshold levels were well demonstrated when CLACO-MIS was compared with other similar methods to segment COVID-19 X-ray images with multi-threshold levels.

In addition, considering that the parameters of CLACO are crucial, we applied a trial-and-error approach to obtain values of the relevant parameters shown in Table 3. The corresponding parameters of CLACO-MIS also adopted the same values as CLACO. Furthermore, all experiments were performed on a desktop computer with an Intel(R) Core(TM) i7-10750H CPU @2.60 GHz, and all programs were coded on MATLAB 2018B.

4.2. Benchmark function validation

In this subsection, the performance of CLACO is demonstrated mainly from two aspects. The first is the experiment comparing CLACO with other variants on 30 benchmark functions; and the second is the experiment comparing CLACO with 10 other similar methods on 30 benchmark functions. Through the variance, mean, and WSRT and FT analysis, the obtained experimental results demonstrate that CLACO is superior in search capability, convergence speed, and convergence accuracy as well as inability to avoid local optimum.

4.2.1. The impact of Cauchy and greedy Levy mutations

Table 4 presents the composition of the various versions of ACOR, where CM denotes Cauchy mutation, GLM denotes greedy Levy mutation, '1′ means that the corresponding ACOR version has this mutation operation, and '0′ means that the corresponding ACOR version does not have this mutation operation. As shown in Table 4, ACOR is the original version, LACO is the version with the greedy Levy mutation, CACO is the version with the Cauchy mutation, and CLACO is the version with both.

Table A1 lists the means and variances obtained by four different versions of ACOR after 30 randomized experiments on 30 test functions, where 'AVG' indicates the mean value obtained by the algorithm on the benchmark function and 'STD' indicates the algorithm variance obtained. As can be seen from Table A1, the original algorithm ACOR obtained optimal results on only 1 benchmark function, CACO on nine functions, LACO on five functions, and CLACO on 15 functions. Therefore, CACO, LACO, and CLACO all have a certain degree of improvement on ACOR performance, with CLACO being a variant of ACOR with the best performance.

In Table 5, the analysis results of the WSRT are presented, where '+' indicates the number of functions in which CLACO's overall performance is better than that of the other methods among the 30 tested functions, '-' indicates the number of functions in which CLACO's overall performance is worse than that of the other methods, ' = ' indicates that CLACO and the other methods perform equally, 'Mean' indicates the overall ranking means obtained by each method, and 'Rank' indicates the final ranking result based on the performance of each algorithm. As can be seen from Table 5, CLACO is superior in overall performance to CACO, LACO, and ACOR. Specifically, CLACO performed worse than CACO in only 3 functions, and CLACO was not worse than LACO and ACOR in all functions. On the overall ranking mean, CLACO also obtained the No. 1 result with 1.677, indicating that CLACO is a high-performance variant of ACOR. Besides, the results of the FT analysis given in Fig. 5 also show that CLACO outperforms CACO, LACO, and ACOR. The convergence curves of different variants of ACOR shown in Fig. B1 further demonstrate that, compared with CACO, LACO, and ACOR, CLACO has not only an improved ability to obtain the optimal solution quality and to jump out of the local optimum but also an elevated convergence rate.

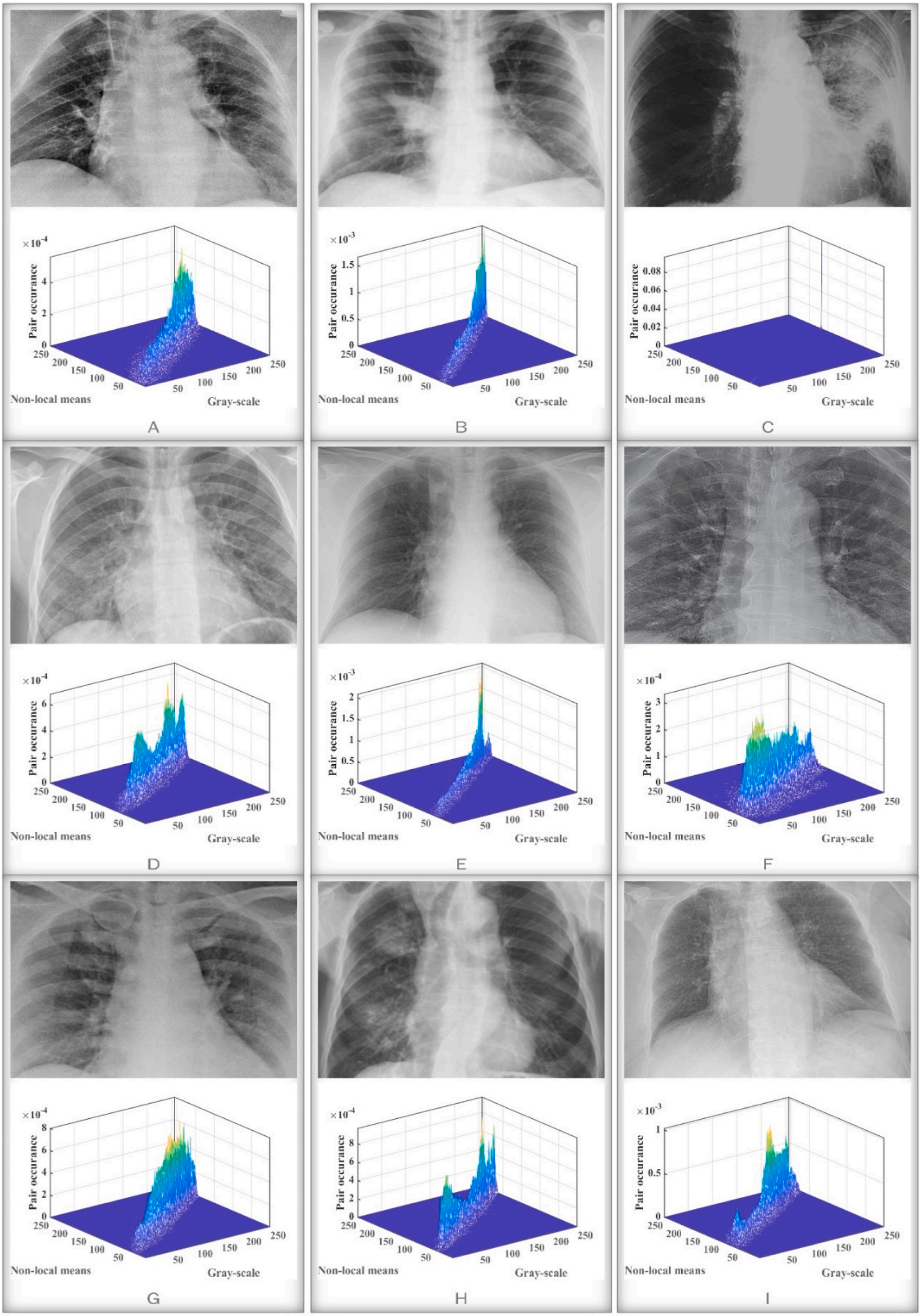

Fig. 4. The original COVID-19 X-ray images and the corresponding 2D histograms.

Table 3
Some parameter descriptions of CLACO.

Variable name	Variable description	Variable value
ξ	The pheromone evaporation rate	1
k	The archive size	10
q	The coefficient	0.5

Table 4
Various variants with different mutation strategies.

	CM	GLM
ACOR	0	0
LACO	0	1
CACO	1	0
CLACO	1	1

Table 5
Comparison results of four variants based on WSRT.

Item	CLACO	ACOR	CACO	LACO
+/−/ =	~	21/0/9	15/3/12	2/0/28
Mean	1.667	3.533	2.467	2.333
Rank	1	4	3	2

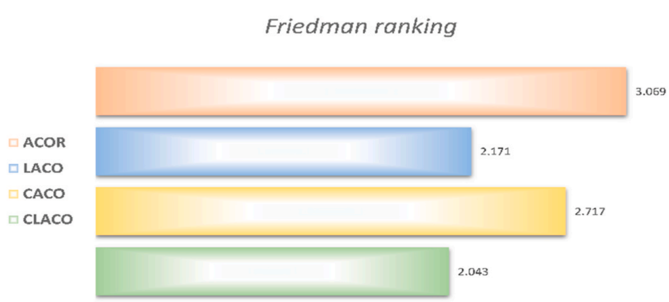

Fig. 5. The Friedman ranking of different versions of ACOR.

4.2.2. Comparison with some peers

In this section, the core advantages of CLACO are verified by comparing CLACO with ten other similar high-performance algorithms including GWO, MFO, PSO, ACOR, SCA, WOA, OBLGWO, m_SCA, OBSCA, and ACWOA. To make the experimental results more convincing, not only some traditional basic algorithms but also some variant algorithms were included. Moreover, we followed fair evaluation instructions [100–102]. Table A2 gives the means and variances obtained by CLACO and ten peers for different test functions, where CLACO obtained the smallest mean on 20 functions and obtained the minor variance on 14 functions, demonstrating the strong ability of CLACO to obtain high-quality solutions. Table A3 gives the results of further analysis of the obtained experimental results using the WSRT, where CLACO obtained the No. 1 result with a total ranked mean value of 1.800 and performed better than OBLGWO (ranked No. 2) on 25 functions. The p-values obtained by the WSRT are given in Table A4, where only a small number of values are more significant than 0.05, indicating that the results obtained for the experimental analysis are credible. The results of the analysis of the experimental results using Friedman are presented in Fig. 6, and they further illustrate that CLACO has a more robust performance than the original ACOR and the ten other similar methods. Fig. B2 gives the convergence curves of CLACO and its similar methods, where F2, F8, F12, F28, F29, F30 demonstrated the faster convergence speed and higher convergence accuracy of CLACO, and F1, F17, F21 demonstrated a better ability of CLACO to jump out of the local optimum.

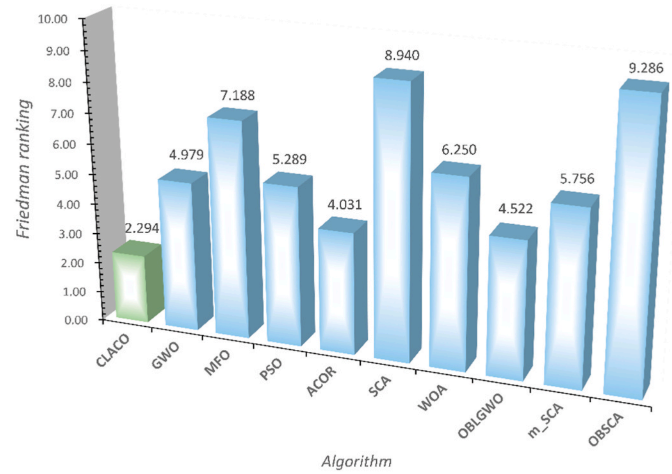

Fig. 6. The Friedman ranking of CLACO and its peers.

Therefore, the experiments comparing CLACO with other ACOR variants on 30 benchmark functions and ten other similar methods fully demonstrate that CLACO has a significantly enhanced search capability over ACOR, a faster convergence speed, a higher convergence accuracy, and a better ability to escape from the local optimum.

4.3. Experiment on multilevel COVID-19 X-ray image segmentation

In this subsection, the segmentation effect of CLACO-MIS on the COVID-19 X-ray image is demonstrated not only at the low threshold levels (4, 5, and 6) but also at the high threshold levels (15, 20, and 25). The segmentation methods used for comparison were CLACO-MIS, ACOR-MIS, MVO-MIS, HHO-MIS, SCA-MIS, BLPSO-MIS, IGWO-MIS, IWOA-MIS, and CLPSO-MIS.

4.3.1. Performance evaluation indicators

In order to comprehensively analyze the obtained experimental results, three commonly adopted evaluation methods were applied in this paper, namely Peak Signal to Noise Ratio (PSNR) [87], Structural Similarity Index (SSIM) [88], Feature Similarity Index (FSIM) [89]. Table 6 presents the relevant descriptions, where the larger values of the evaluation results of PSNR, SSIM, and FSIM indicate a better segmentation effect obtained by each method. In addition, we conducted a comparative analysis of the evaluation results obtained using PSNR, FSIM, and SSIM using mean and variance and WSRT [85] and FT [86].

4.3.2. Experimental result analyses

In the area of image and video processing [103], it is critical to apply efficient methods for quality assessment [104–106]. Tables A5 - A7 present the mean and variance results obtained by all segmentation methods under the three performance evaluation metrics, where

Table 6
The definitions and descriptions of the three evaluation indicators.

Indicators	Formulation	Remark
Peak Signal to Noise Ratio (PSNR)	$PSNR = 20 \times \log_{10}\left(\frac{255}{RMSE}\right)$	Assess the difference between the split image and the original image
Structural Similarity Index (SSIM)	$SSIM = \frac{(2\mu_I\mu_{Seg}+c_1)(2\sigma_{I,Seg}+c_2)}{(\mu_I^2+\mu_{Seg}^2+c_1)(\sigma_I^2+\sigma_{Seg}^2+c_2)}$	Finds the similarity between segmented image and uncompressed or distortion-free image.
Feature Similarity Index (FSIM)	$FSIM = \frac{\sum_{I\in\Omega} S_L(X)PC_m(X)}{\sum_{I\in\Omega} PC_m(X)}$	Defines the quality score, which reflects the significance of a local structure.

CLACO-MIS obtained the highest number of both maximum mean and minimum variance at different threshold levels, which is also a very strong indication that it can obtain better segmentation results in most cases. Tables A8 – A10 give the results of WSRT for further analysis of PSNR, FSIM, and SSIM, and it can be seen that CLACO-MIS is second to none in PSNR, FSIM, and SSIM at all threshold levels for its ranking, and in most cases, the segmentation results of other segmentation methods are not better than CLACO-MIS. Additionally, Table A11 gives the maximum 2D Kapur's entropy obtained by each segmentation model during the segmentation process. CLACO-MIS obtained 44 times the maximum 2D Kapur's entropy in all segmentation cases, ACOR-MIS obtained only seven times the maximum 2D Kapur's entropy, and MVO-MIS obtained only three times the maximum 2D Kapur's entropy. Therefore, the ability of CLACO-MIS to obtain the optimal solution during the segmentation process is unquestionable, and it obtains the maximum 2D Kapur's entropy in most cases, which also indicates that the optimal segmentation threshold set found using CLACO-MIS is also reliable. In addition, Figs. B3 - B5 give the results of further analysis of PSNR, FSIM, and SSIM using FT, where CLACO-MIS also obtained optimal values in all evaluated cases, which further illustrates that CLACO-MIS has better segmentation performance for COVID-19 X-ray images and can obtain high-quality segmentation results.

Based on the evaluation results of PSNR, FSIM, and SSIM, Figs. B6–B8 give the mean performance of the segmentation results of each segmentation method at each threshold level. By observing the mean performance under each threshold level, we can find that CLACO-MIS can obtain the maximum value in all cases. Moreover, Figs. 7–9 give the mean values obtained by each segmentation method concerning all the threshold levels, where CLACO-MIS can obtain the maximum value under each evaluation metric. Therefore, CLACO-MIS obtains excellent results for COVID-19 X-ray image segmentation. Furthermore, the convergence curves of each segmentation method on the 2D Kapur's entropy are given in Figs. B9 – B10 in the process of searching for the optimal threshold set. From the given convergence curves, it can be seen that the convergence speed of CLACO-MIS is the fastest, and it is not easy to fall into local optimum in the process of convergence, and thus can obtain the maximum 2D Kapur's entropy. In addition, the ability of CLACO-MIS to obtain the optimal threshold set is significantly enhanced at the threshold level 25. Therefore, in addition to obtaining better segmentation effects, CLACO-MIS also has better adaptability to different threshold levels. In other words, as the threshold level increases, the advantages of CLACO-MIS become more apparent.

Furthermore, when the threshold level is 6, Figs. B11 - B19 give the specific optimal segmentation thresholds obtained by all segmentation methods, and Fig. B29 gives the specific segmentation results of all images obtained by all methods. Also, the specific optimal segmentation thresholds obtained by all methods at the threshold level 25 are given in

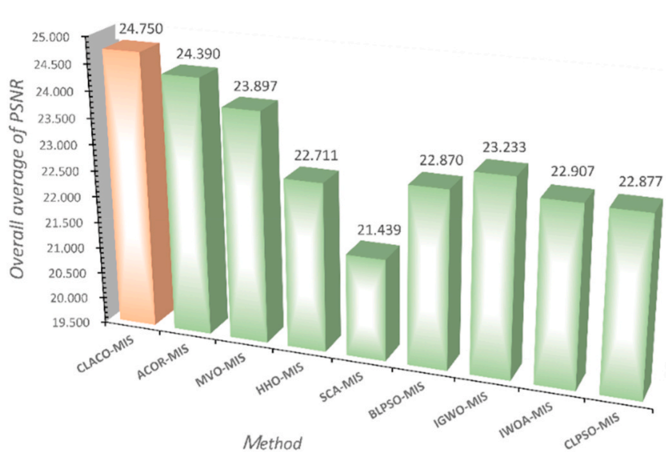

Fig. 7. Overall average results of PSNR evaluation of all threshold levels.

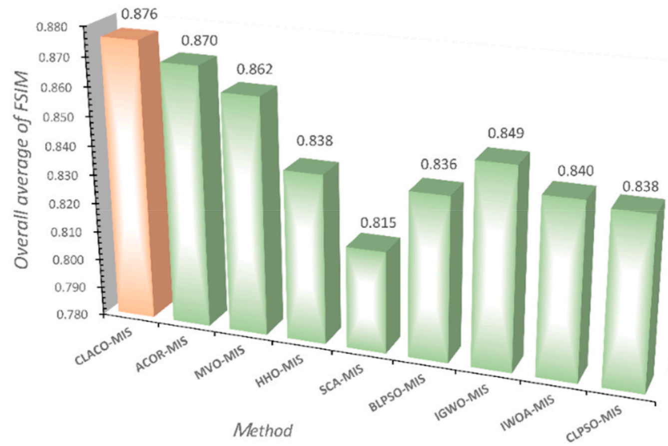

Fig. 8. Overall average results of FSIM evaluation of all threshold levels.

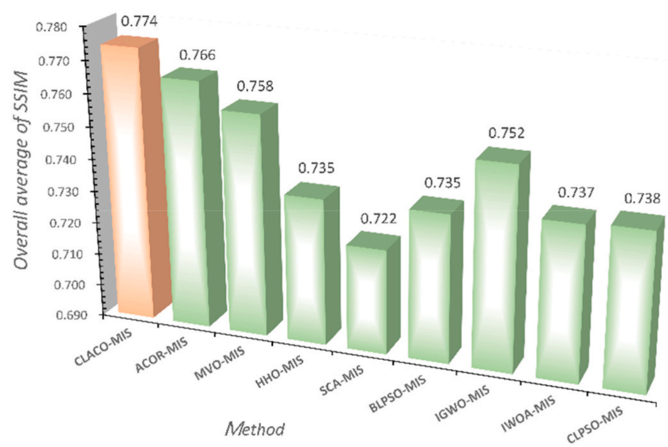

Fig. 9. Overall average results of SSIM evaluation of all threshold levels.

Figs. B20 - B28, and the specific segmentation results obtained by all methods at the threshold level 25 are given in Fig. B30. Based on the observation and analysis of the optimal segmentation thresholds and the segmentation results, it is further demonstrated that CLACO-MIS can obtain better segmentation results and verified that CLACO-MIS has good adaptability to different threshold levels. As exploration and exploration of the method exposes, the experts can also utilize the proposed ACO-based optimizer to tackle multi-faced feature spaces in other families of problems such as works in Refs. [107–109]. For future work, since CLACO is a superior swarm intelligence optimization algorithm, we will consider applying it to more fields, such as face recognition and micro-expression recognition [110,111], 3D deformable shape analysis [112,113], micro-expression spotting [111,114], and service ecosystem [115,116]. Also, we can suggest areas such as Lunar impact crater identification and age estimation [117], large scale network analysis [118], energy storage planning and scheduling [119], medical diagnosis [120–122], structure designs [130], power generation [131], and prediction of brain-behavior [123,124].

5. Conclusions and future works

This paper presents the first ACO with the Cauchy mutation and the greedy Levy mutation, namely CLACO, for continuous domains. Besides, to improve the diagnostic level of COVID-19, this paper proposes a novel CLACO-based MIS model, namely CLACO-MIS, and applies it to the segmentation of COVID-19 X-ray images and obtains segmentation results with high quality. The Cauchy mutation has been effectively applied to the end phase of ant foraging in CLACO, which has achieved an effective enhancement of the searchability of ants; in other words, the lack of searchability of ACOR has been successfully enhanced as well as the convergence speed has been dramatically boosted. To make CLACO have a solid ability to step out of the local optimum, the greedy Levy mutation is applied to optimal individuals to make the optimal individuals enhance the experiential knowledge and learn by themselves. To provide a robust demonstration of CLACO's performance based on the 30 test functions from IEEE CEC2014, the variant algorithms, which are made up of the Cauchy mutation and the greedy Levy mutation, were first compared experimentally with each other. CLACO was then compared experimentally with ten other peer algorithms.

At last, we analyzed and compared all the experimental results obtained again using WSRT and FT, which powerfully illustrate that CLACO has an enhanced search capability, a further improvement in convergence speed, and an improved ability to jump out of the local optimum. In CLACO-MIS, it mainly adopts 2D histograms made up of non-local mean filtered images and grayscale images and takes 2D Kapur's entropy as the CLACO fitness function based on 2D histograms to obtain an optimal threshold set. Based on 9 COVID-19 X-ray images, CLACO-MIS and eight other similar methods at levels 4, 5, and 6, representing low threshold levels, and at levels 15, 20, and 25, representing high threshold levels, have been applied to perform COVID-19 X-ray image segmentation experiments. Then, we evaluated the image segmentation results using PSNR, FSIM, and SSIM to illustrate the effectiveness of the segmentation results effectively, and the comparative analysis results were also obtained by using the mean, variance, and WSRT and FT. Therefore, CLACO-MIS has a better segmentation effect and a stronger adaptability to different threshold levels, compared with other similar methods. However, due to the introduction of the Cauchy mutation and the greedy Levy mutation, the time complexity of CLACO-MIS inevitably increases, and the CPU computation time required for its segmentation has a corresponding extension. Thus, parallel computation is used in the experimental process to improve CPU utilization and reduce CPU computation time.

In future, as the CLACO-MIS model is also a segmentation method that can obtain high-quality segmentation results, we will consider using it to segment more pathological images to realize greater value and make our due contribution to the advancement of medical diagnosis technology.

Declaration of competing interest

The authors declare that there is no conflict of interests regarding the publication of article.

Acknowledgments

This research was supported by the National Natural Science Foundation of China (62076185, U1809209), Guangxi Key Laboratory of Trusted Software (KX202049), Guangxi science and technology base and talent project (20325004 CE), "Thirteenth Five-Year" Science and Technology Project of Jilin Provincial Department of Education (JJKH20200829KJ), Changchun Normal University Ph.D. Research Startup Funding Project(BS [2020]). Taif University Researchers Supporting Project Number (TURSP-2020/125), Taif University, Taif, Saudi Arabia, Wenzhou Key Technology Breakthrough Program on Prevention and Treatment for COVID-19 Epidemic, No. ZG2020012, Wenzhou University Application Technology Collaborative Innovation Center, Smart Medical Education Collaborative Innovation Center.

Appendix A

Table A1
The mean and variance values gained by relevant variants on IEEE CEC2014

Fun	Item	CLACO	CACO	LACO	ACOR
F1	AVG	3.2250 E+06	**1.6559E + 06**	2.8502 E+06	6.4907 E+06
	STD	3.1387 E+06	**7.9411E + 05**	2.0672 E+06	1.0097 E+07
F2	AVG	1.3543 E+04	**1.1570E + 04**	1.2641 E+08	3.1627 E+08
	STD	1.2715 E+04	**1.2552E + 04**	6.9232 E+08	1.3099 E+09
F3	AVG	8.7428 E+02	**5.9578E + 02**	2.8025 E+03	1.2320 E+04
	STD	7.3854 E+02	**4.4795E + 02**	3.3751 E+03	1.5983 E+04
F4	AVG	**4.4999E + 02**	4.6261 E+02	4.6011 E+02	4.7870 E+02
	STD	**3.0968E + 01**	4.6270 E+01	3.5970 E+01	4.5320 E+01
F5	AVG	**5.2000E + 02**	5.2091E+02	5.2000E+02	5.2092E+02
	STD	**1.4892E-03**	5.8613E-02	6.7377E-03	5.2908E-02
F6	AVG	6.1335 E+02	6.1307 E+02	6.1592 E+02	**6.1264E + 02**
	STD	5.7492 E+00	**2.9805E + 00**	5.9321 E+00	3.4019 E+00
F7	AVG	**7.0001E + 02**	7.0001 E+02	7.0001 E+02	7.0312 E+02
	STD	**1.1587E-02**	1.7870E-02	1.5846E-02	1.2478 E+01
F8	AVG	**8.0673E + 02**	8.3748 E+02	8.0879 E+02	8.5970 E+02
	STD	**4.8721E + 00**	7.0867 E+00	5.0469 E+00	2.0022 E+01
F9	AVG	1.0068 E+03	**9.7383E + 02**	1.0526 E+03	1.0311 E+03
	STD	3.3213 E+01	**1.8224E + 01**	3.3067 E+01	5.9325 E+01
F10	AVG	1.2353 E+03	2.1862E+03	**1.1939E + 03**	3.0943 E+03
	STD	1.9363 E+02	4.2033E+02	**1.6338E + 02**	5.2288 E+02
F11	AVG	4.1261 E+03	**3.8004E + 03**	4.2291 E+03	4.2145 E+03
	STD	7.1379 E+02	6.9068 E+02	**4.5399E + 02**	1.8687 E+03
F12	AVG	**1.2002E + 03**	1.2013E+03	1.2002E+03	1.2024E+03
	STD	5.9746E-02	2.6751E-01	**4.9470E-02**	2.7249E-01
F13	AVG	**1.3003E + 03**	1.3005 E+03	1.3004 E+03	1.3005 E+03
	STD	8.2923E-02	1.2138E-01	**8.0065E-02**	1.5488E-01
F14	AVG	**1.4004E + 03**	1.4007 E+03	1.4004 E+03	1.4012 E+03
	STD	2.2038E-01	3.0139E-01	**1.8310E-01**	3.2256 E+00
F15	AVG	**1.5103E + 03**	1.5159 E+03	1.5103 E+03	1.6409 E+03
	STD	4.0081 E+00	**2.1711E + 00**	3.9374 E+00	3.4416 E+02
F16	AVG	1.6113 E+03	**1.6112E + 03**	1.6114 E+03	1.6117 E+03
	STD	4.6112E-01	4.4951E-01	7.6039E-01	**3.6573E-01**
F17	AVG	1.8523 E+05	**1.1702E + 05**	3.3839 E+05	2.3134 E+05

(*continued on next page*)

Table A1 (*continued*)

Fun	Item	CLACO	CACO	LACO	ACOR
	STD	1.5170 E+05	**7.9534E + 04**	6.3085 E+05	7.4030 E+05
F18	AVG	9.8507 E+03	1.1328 E+04	**7.9694E + 03**	1.0173 E+04
	STD	1.0449 E+04	8.9895 E+03	8.9481 E+03	**8.2862E + 03**
F19	AVG	1.9137 E+03	1.9098 E+03	**1.9086E + 03**	1.9256 E+03
	STD	1.8959 E+01	2.6922 E+00	**2.6371E + 00**	3.2742 E+01
F20	AVG	2.9337 E+03	**2.5918E + 03**	5.5125 E+03	8.7828 E+03
	STD	9.1804E+02	**5.9689E + 02**	4.8704 E+03	1.7187 E+04
F21	AVG	1.0968 E+05	**7.3751E + 04**	1.0965 E+05	8.3913 E+04
	STD	8.8399 E+04	**6.2751E + 04**	1.2531 E+05	9.5793 E+04
F22	AVG	**2.4826E + 03**	2.6282 E+03	2.5470 E+03	2.5969 E+03
	STD	**1.7921E + 02**	2.5538 E+02	1.9402 E+02	2.3312 E+02
F23	AVG	**2.6143E + 03**	2.6152 E+03	2.6144 E+03	2.6175 E+03
	STD	1.9431E-01	**1.9659E-12**	4.7907E-01	3.1485 E+00
F24	AVG	**2.6221E + 03**	2.6389 E+03	2.6238 E+03	2.6404 E+03
	STD	1.0423 E+01	**6.8135E + 00**	8.9071 E+00	8.4687 E+00
F25	AVG	**2.7008E + 03**	2.7067 E+03	2.7008 E+03	2.7066 E+03
	STD	3.9740E-01	3.2956 E+00	**3.4021E-01**	2.4838 E+00
F26	AVG	**2.7003E + 03**	2.7285 E+03	2.7004 E+03	2.7241 E+03
	STD	1.0667E-01	7.6358 E+01	**1.0244E-01**	7.2059E+01
F27	AVG	**3.3992E + 03**	3.4280 E+03	3.4262 E+03	3.4093 E+03
	STD	1.5674 E+02	**8.6849E + 01**	1.7446 E+02	9.1329 E+01
F28	AVG	3.2587 E+03	3.8482 E+03	**3.2540E + 03**	3.8560 E+03
	STD	6.7389 E+01	1.7913 E+02	**5.9706E + 01**	1.9388 E+02
F29	AVG	3.1183 E+03	1.4150 E+06	**3.1169E + 03**	3.6582 E+06
	STD	2.5634 E+01	3.2038E+06	**2.1513E + 01**	5.0062 E+06
F30	AVG	**3.8475E + 03**	6.4474 E+03	3.8544 E+03	1.0754 E+04
	STD	**2.6490E + 02**	1.0036 E+03	2.7471 E+02	6.2312 E+03

Table A2
Comparison results of CLACO and some excellent peers

Fun	Item	CLACO	GWO	MFO	PSO	ACOR	SCA	WOA	OBLGWO	m_SCA	OBSCA	ACWOA
F1	AVG	**3.036E + 06**	5.808 E+07	1.159 E+08	8.536 E+06	5.158 E+06	2.321 E+08	2.742 E+07	1.849 E+07	4.770 E+07	4.252 E+08	1.277 E+08
	STD	**2.456E + 06**	3.796 E+07	1.161 E+08	2.925 E+06	5.713 E+06	5.580 E+07	1.059 E+07	7.737 E+06	2.759 E+07	1.064 E+08	5.309 E+07
F2	AVG	**1.119E + 04**	2.284 E+09	1.284 E+10	1.440 E+08	1.878 E+08	1.717 E+10	7.023 E+06	1.480 E+07	6.955 E+09	2.418 E+10	6.188 E+09
	STD	**1.214E + 04**	2.295 E+09	8.474 E+09	1.796 E+07	5.495 E+08	3.336 E+09	1.151 E+07	8.211 E+06	3.848 E+09	4.000 E+09	2.933 E+09
F3	AVG	**8.839E + 02**	3.111 E+04	1.051 E+05	9.154 E+02	9.564 E+03	3.554 E+04	3.692 E+04	9.242 E+03	2.481 E+04	5.106 E+04	5.069 E+04
	STD	6.470 E+02	8.956 E+03	5.982 E+04	**1.175E + 02**	1.216 E+04	6.026 E+03	2.677 E+04	3.333 E+03	7.957 E+03	8.727 E+03	7.977 E+03
F4	AVG	**4.552E + 02**	6.555 E+02	1.433 E+03	4.573 E+02	4.945 E+02	1.400 E+03	5.731 E+02	5.565 E+02	7.609 E+02	2.333 E+03	1.281 E+03
	STD	3.970 E+01	9.229 E+01	8.496 E+02	**3.468E + 01**	6.674 E+01	2.373 E+02	4.363 E+01	4.842 E+01	1.031 E+02	5.944 E+02	3.929 E+02
F5	AVG	**5.200E + 02**	5.209 E+02	5.203 E+02	5.209 E+02	5.209 E+02	5.209 E+02	5.203 E+02	5.210 E+02	5.206 E+02	5.210 E+02	5.207 E+02
	STD	**9.800E-04**	4.807E-02	1.674E-01	4.711E-02	4.875E-02	5.833E-02	1.732E-01	5.601E-02	1.558E-01	5.622E-02	2.045E-01
F6	AVG	6.142 E+02	6.138 E+02	6.228 E+02	6.218 E+02	**6.132E + 02**	6.337 E+02	6.352 E+02	6.192 E+02	6.215 E+02	6.324 E+02	6.346 E+02
	STD	5.902 E+00	2.705 E+00	3.139 E+00	3.302 E+00	2.881 E+00	2.455 E+00	3.386 E+00	4.169 E+00	2.603 E+00	**1.388E + 00**	2.575 E+00
F7	AVG	**7.000E + 02**	7.214 E+02	7.990 E+02	7.023 E+02	7.078 E+02	8.281 E+02	7.010 E+02	7.012 E+02	7.579 E+02	9.105 E+02	7.455 E+02
	STD	**1.043E-02**	1.958 E+01	6.811 E+01	1.361E-01	1.693 E+01	2.301 E+01	6.914E-02	9.422E-02	3.753 E+01	4.347 E+01	2.581 E+01
F8	AVG	**8.073E + 02**	8.771 E+02	9.436 E+02	9.736 E+02	8.624 E+02	1.038 E+03	9.771 E+02	9.245 E+02	9.379 E+02	1.064 E+03	9.911 E+02
	STD	**4.780E + 00**	2.162 E+01	3.559 E+01	1.792 E+01	2.201 E+01	1.836 E+01	3.629 E+01	2.478 E+01	2.217 E+01	1.598 E+01	2.392 E+01
F9	AVG	1.018 E+03	**9.965E + 02**	1.119 E+03	1.113 E+03	1.016 E+03	1.170 E+03	1.113 E+03	1.072 E+03	1.052 E+03	1.198 E+03	1.126 E+03
	STD								3.315 E+01			

(*continued on next page*)

Table A2 (*continued*)

Fun	Item	CLACO	GWO	MFO	PSO	ACOR	SCA	WOA	OBLGWO	m_SCA	OBSCA	ACWOA
		3.264 E+01	1.927 E+01	5.523 E+01	2.971 E+01	6.235 E+01	1.976 E+01	5.208 E+01		2.689 E+01	**1.715E + 01**	2.134 E+01
F10	AVG	**1.196E + 03**	3.021 E+03	4.389 E+03	5.095 E+03	3.173 E+03	6.678 E+03	4.928 E+03	3.952 E+03	4.161 E+03	6.274 E+03	4.885 E+03
	STD	**1.482E + 02**	4.575 E+02	1.022 E+03	6.714 E+02	4.620 E+02	6.080 E+02	9.012 E+02	7.783 E+02	6.723 E+02	3.362 E+02	1.047 E+03
F11	AVG	4.256 E+03	**3.824E + 03**	5.136 E+03	5.933 E+03	4.851 E+03	8.018 E+03	6.243 E+03	5.085 E+03	4.713 E+03	7.336 E+03	6.138 E+03
	STD	3.747 E+02	4.865 E+02	7.883 E+02	5.176 E+02	2.137 E+03	**3.082E + 02**	8.276 E+02	7.697 E+02	7.867 E+02	4.433 E+02	6.486 E+02
F12	AVG	**1.200E + 03**	1.202 E+03	1.201 E+03	1.202 E+03	1.202 E+03	1.202 E+03	1.202 E+03	1.202 E+03	1.201 E+03	1.202 E+03	1.202 E+03
	STD	**4.637E-02**	1.140 E+00	2.669E-01	3.026E-01	4.616E-01	3.024E-01	5.497E-01	5.424E-01	3.630E-01	3.556E-01	4.680E-01
F13	AVG	**1.300E + 03**	1.300 E+03	1.302 E+03	1.300 E+03	1.300 E+03	1.303 E+03	1.300 E+03	1.301 E+03	1.301 E+03	1.304 E+03	1.302 E+03
	STD	1.066E-01	3.810E-01	1.242 E+00	**6.654E-02**	1.231E-01	3.738E-01	1.189E-01	1.092E-01	5.461E-01	4.043E-01	1.067 E+00
F14	AVG	1.400 E+03	1.403 E+03	1.426 E+03	1.400 E+03	1.401 E+03	1.445 E+03	**1.400E + 03**	1.400 E+03	1.416 E+03	1.470 E+03	1.419 E+03
	STD	1.895E-01	4.911 E+00	2.055 E+01	**1.196E-01**	3.133E-01	1.091 E+01	1.385E-01	1.889E-01	1.041 E+01	1.092 E+01	1.508 E+01
F15	AVG	**1.510E + 03**	1.648 E+03	1.306 E+05	1.517 E+03	1.663 E+03	3.334 E+03	1.577 E+03	1.517 E+03	2.294 E+03	1.584 E+04	1.858 E+03
	STD	3.108 E+00	3.117 E+02	2.563 E+05	**1.079E + 00**	4.544 E+02	1.720 E+03	3.135 E+01	5.842 E+00	1.242 E+03	8.689 E+03	4.358 E+02
F16	AVG	1.611 E+03	**1.611E + 03**	1.613 E+03	1.612 E+03	1.612 E+03	1.613 E+03	1.612 E+03	1.612 E+03	1.612 E+03	1.613 E+03	1.612 E+03
	STD	4.184E-01	7.339E-01	6.048E-01	3.471E-01	5.269E-01	2.519E-01	4.408E-01	6.478E-01	5.979E-01	**1.996E-01**	5.898E-01
F17	AVG	**1.554E + 05**	1.779 E+06	2.691 E+06	2.963 E+05	2.879 E+05	5.590 E+06	3.519 E+06	1.656 E+06	1.514 E+06	1.258 E+07	1.221 E+07
	STD	**9.896E + 04**	1.835 E+06	4.838 E+06	1.302 E+05	5.370 E+05	2.623 E+06	2.440 E+06	1.158 E+06	9.395 E+05	6.114 E+06	8.528 E+06
F18	AVG	**1.002E + 04**	1.027 E+07	4.257 E+07	2.100 E+06	1.013 E+04	1.610 E+08	1.484 E+04	3.356 E+04	2.122 E+07	1.747 E+08	5.337 E+07
	STD	8.524 E+03	2.107 E+07	1.900 E+08	6.321 E+05	**7.519E + 03**	9.837 E+07	3.941 E+04	2.065 E+04	4.410 E+07	9.461 E+07	4.848 E+07
F19	AVG	**1.911E + 03**	1.938 E+03	1.969 E+03	1.917 E+03	1.913 E+03	1.999 E+03	1.947 E+03	1.916 E+03	1.945 E+03	2.011 E+03	2.007 E+03
	STD	1.343 E+01	2.832 E+01	5.062 E+01	**2.171E + 00**	1.107 E+01	2.330 E+01	4.620 E+01	2.175 E+01	2.056 E+01	2.409 E+01	2.777 E+01
F20	AVG	2.761 E+03	1.466 E+04	5.651 E+04	**2.326E + 03**	6.893 E+03	1.615 E+04	2.988 E+04	6.319 E+03	1.176 E+04	2.998 E+04	4.063 E+04
	STD	6.735 E+02	5.761 E+03	2.948 E+04	**6.807E + 01**	7.837 E+03	5.458 E+03	1.631 E+04	2.967 E+03	2.858 E+03	9.515 E+03	1.660 E+04
F21	AVG	**6.879E + 04**	1.437 E+06	6.577 E+05	1.156 E+05	7.994 E+04	1.322 E+06	9.813 E+05	5.627 E+05	5.401 E+05	2.367 E+06	5.185 E+06
	STD	**4.844E + 04**	2.788 E+06	1.379 E+06	6.616 E+04	8.029 E+04	6.478 E+05	8.023 E+05	3.860 E+05	9.181 E+05	1.530 E+06	4.285 E+06
F22	AVG	**2.466E + 03**	2.549 E+03	2.995 E+03	2.871 E+03	2.585 E+03	2.990 E+03	2.957 E+03	2.670 E+03	2.585 E+03	3.161 E+03	3.080 E+03
	STD	1.509 E+02	1.934 E+02	2.577 E+02	1.843 E+02	2.658 E+02	**1.103E + 02**	1.982 E+02	1.849 E+02	1.706 E+02	1.650 E+02	2.669 E+02
F23	AVG	2.614 E+03	2.633 E+03	2.662 E+03	2.616 E+03	2.620 E+03	2.665 E+03	2.633 E+03	2.614 E+03	2.640 E+03	2.688 E+03	**2.533E + 03**
	STD	**1.920E-01**	7.936 E+00	2.917 E+01	8.120E-01	7.911 E+00	1.252 E+01	1.068 E+01	2.168 E+01	8.011 E+00	2.114 E+01	7.451 E+01
F24	AVG	2.625 E+03	2.600 E+03	2.678 E+03	2.628 E+03	2.646 E+03	2.600 E+03	2.606 E+03	**2.600E + 03**	2.600 E+03	2.600 E+03	2.600 E+03
	STD	1.347 E+01	6.699E-04	2.975 E+01	5.123 E+00	1.360 E+01	5.016E-02	4.542 E+00	**0.000E + 00**	7.328E-04	3.720E-04	4.522E-06
F25	AVG	2.701 E+03	2.710 E+03	2.716 E+03	2.712 E+03	2.708 E+03	2.725 E+03	2.718 E+03	**2.700E + 03**	2.713 E+03	2.700 E+03	2.700 E+03
	STD	2.067E-01	5.112 E+00	9.123 E+00	6.679 E+00	3.560 E+00	1.059 E+01	1.720 E+01	**0.000E + 00**	2.277 E+00	3.047E-05	0.000 E+00
F26	AVG	**2.700E + 03**	2.750 E+03	2.702 E+03	2.774 E+03	2.732 E+03	2.702 E+03	2.704 E+03	2.701 E+03	2.701 E+03	2.704 E+03	2.744 E+03
	STD	**9.519E-02**					6.001E-01		1.662E-01	4.006E-01	4.246E-01	

(*continued on next page*)

Table A2 (*continued*)

Fun	Item	CLACO	GWO	MFO	PSO	ACOR	SCA	WOA	OBLGWO	m_SCA	OBSCA	ACWOA
			5.066 E+01	1.195 E+00	4.504 E+01	6.513 E+01		1.818 E+01				5.000 E+01
F27	AVG	3.356 E+03	3.365 E+03	3.612 E+03	3.449 E+03	3.388 E+03	3.499 E+03	3.842 E+03	**3.118E + 03**	3.173 E+03	3.235 E+03	3.700 E+03
	STD	1.740 E+02	1.247 E+02	1.931 E+02	2.817 E+02	1.004 E+02	3.312 E+02	3.207 E+02	3.277 E+02	1.247 E+02	**3.522E + 01**	3.246 E+02
F28	AVG	**3.228E + 03**	3.912 E+03	3.938 E+03	6.858 E+03	3.839 E+03	4.868 E+03	5.065 E+03	3.588 E+03	3.995 E+03	5.509 E+03	3.947 E+03
	STD	**3.766E + 01**	2.974 E+02	1.846 E+02	1.304 E+03	1.691 E+02	3.190 E+02	6.872 E+02	5.042 E+02	2.964 E+02	3.695 E+02	1.194 E+03
F29	AVG	**3.120E + 03**	1.366 E+06	3.827 E+06	4.851 E+04	1.614 E+06	1.298 E+07	6.882 E+06	3.199 E+06	1.953 E+06	1.985 E+07	2.333 E+07
	STD	**2.925E + 01**	3.309 E+06	4.157 E+06	1.052 E+05	3.692 E+06	7.052 E+06	4.256 E+06	4.245 E+06	4.241 E+06	1.089 E+07	1.819 E+07
F30	AVG	**3.820E + 03**	5.026 E+04	5.129 E+04	1.340 E+04	9.502 E+03	2.530 E+05	9.652 E+04	2.062 E+04	4.338 E+04	3.971 E+05	3.810 E+05
	STD	**2.502E + 02**	3.678 E+04	3.743 E+04	5.947 E+03	5.088 E+03	8.221 E+04	5.700 E+04	1.179 E+04	2.399 E+04	1.226 E+05	3.127 E+05

Table A3
The analysis result by using the WSRT

Methods	CLACO	GWO	MFO	PSO	ACOR	SCA	WOA	OBLGWO	m_SCA	OBSCA	ACWOA
+/−/ =	~	23/4/3	29/0/1	23/1/6	20/0/10	28/1/1	27/1/2	25/4/1	28/2/0	27/3/0	26/3/1
Mean	**1.800**	4.933	7.733	5.200	4.067	9.000	6.467	4.067	5.367	9.533	7.800
Rank	**1**	4	8	5	2	10	7	2	6	11	9

Table A4
The p-values obtained by conducting the WSRT

Fun	GWO	MFO	PSO	ACOR	SCA	WOA	OBLGWO	m_SCA	OBSCA	ACWOA
F1	1.734E-06	1.921E-06	8.466E-06	**9.368E-02**	1.734E-06	1.921E-06	1.921E-06	1.734E-06	1.734E-06	1.734E-06
F2	1.734E-06	1.734E-06	1.734E-06	**8.936E-01**	1.734E-06	1.734E-06	1.734E-06	1.734E-06	1.734E-06	1.734E-06
F3	1.734E-06	1.734E-06	**6.143E-01**	2.879E-06	1.734E-06	1.734E-06	1.734E-06	1.734E-06	1.734E-06	1.734E-06
F4	1.734E-06	1.734E-06	**3.820E-01**	3.162E-03	1.734E-06	1.734E-06	3.182E-06	1.734E-06	1.734E-06	1.734E-06
F5	1.734E-06	1.921E-06	1.734E-06	1.734E-06	1.734E-06	1.734E-06	1.734E-06	1.734E-06	1.734E-06	1.734E-06
F6	**8.130E-01**	3.182E-06	3.724E-05	**4.165E-01**	1.734E-06	1.734E-06	1.114E-03	2.597E-05	1.734E-06	1.734E-06
F7	1.734E-06	1.734E-06	1.734E-06	3.331E-03	1.734E-06	1.734E-06	1.734E-06	1.734E-06	1.734E-06	1.734E-06
F8	1.734E-06	1.734E-06	1.734E-06	1.734E-06	1.734E-06	1.734E-06	1.734E-06	1.734E-06	1.734E-06	1.734E-06
F9	4.114E-03	2.127E-06	1.734E-06	**8.130E-01**	1.734E-06	3.182E-06	1.150E-04	9.627E-04	1.734E-06	1.734E-06
F10	1.734E-06	1.734E-06	1.734E-06	1.734E-06	1.734E-06	1.734E-06	1.734E-06	1.734E-06	1.734E-06	1.734E-06
F11	7.157E-04	1.639E-05	1.921E-06	**3.086E-01**	1.734E-06	2.353E-06	8.188E-05	1.319E-02	1.734E-06	1.734E-06
F12	6.892E-05	1.734E-06	1.734E-06	1.734E-06	1.734E-06	1.734E-06	1.734E-06	1.734E-06	1.734E-06	1.734E-06
F13	3.001E-02	1.734E-06	**8.972E-02**	1.057E-04	1.734E-06	4.449E-05	1.494E-05	1.734E-06	1.734E-06	1.921E-06
F14	2.183E-02	1.734E-06	**1.915E-01**	1.150E-04	1.734E-06	**1.414E-01**	**2.289E-01**	2.603E-06	1.734E-06	2.879E-06
F15	1.025E-05	1.734E-06	3.182E-06	3.112E-05	1.734E-06	1.734E-06	2.225E-04	1.734E-06	1.734E-06	1.734E-06
F16	2.765E-03	2.879E-06	2.603E-06	3.501E-02	1.734E-06	2.603E-06	8.307E-04	3.609E-03	1.734E-06	1.799E-05
F17	3.515E-06	1.639E-05	3.065E-04	**9.263E-01**	1.734E-06	1.921E-06	1.734E-06	1.921E-06	1.734E-06	1.734E-06
F18	1.114E-03	**8.972E-02**	1.734E-06	**8.290E-01**	1.734E-06	**5.999E-01**	1.150E-04	1.734E-06	1.734E-06	1.734E-06
F19	1.360E-05	4.729E-06	3.112E-05	3.162E-03	1.734E-06	1.639E-05	8.919E-05	1.360E-05	1.734E-06	1.734E-06
F20	2.127E-06	1.734E-06	1.484E-03	2.052E-04	1.734E-06	1.734E-06	3.515E-06	1.734E-06	1.734E-06	1.734E-06
F21	8.466E-06	1.494E-05	2.255E-03	**9.426E-01**	1.734E-06	1.734E-06	1.734E-06	4.286E-06	1.734E-06	1.734E-06
F22	**1.109E-01**	1.734E-06	2.127E-06	**7.190E-02**	1.734E-06	1.734E-06	2.225E-04	2.183E-02	1.734E-06	2.127E-06
F23	1.734E-06	1.734E-06	1.734E-06	1.734E-06	1.734E-06	1.734E-06	3.112E-05	1.734E-06	1.734E-06	7.691E-06
F24	1.734E-06	2.127E-06	**3.286E-01**	3.405E-05	1.734E-06	9.316E-06	1.734E-06	1.734E-06	1.734E-06	1.734E-06
F25	7.691E-06	1.734E-06	1.734E-06	1.734E-06	3.182E-06	1.484E-03	1.734E-06	1.734E-06	1.734E-06	1.734E-06
F26	5.307E-05	1.734E-06	2.127E-06	4.286E-06	1.734E-06	5.320E-03	3.182E-06	1.734E-06	1.734E-06	1.734E-06
F27	**7.189E-01**	3.881E-04	**1.846E-01**	**5.170E-01**	**8.590E-02**	1.025E-05	2.415E-03	1.477E-04	2.957E-03	5.706E-04
F28	1.734E-06	1.734E-06	1.734E-06	1.734E-06	1.734E-06	1.734E-06	1.484E-03	1.734E-06	1.734E-06	**2.059E-01**
F29	1.734E-06	1.734E-06	4.196E-04	1.734E-06	1.734E-06	1.734E-06	1.734E-06	1.734E-06	1.734E-06	1.921E-06
F30	1.734E-06	1.734E-06	1.734E-06	1.734E-06	1.734E-06	1.734E-06	1.734E-06	1.734E-06	1.734E-06	1.360E-05

Table A5
The mean and variance values of the PSNR evaluation at various threshold levels

Image	Thresholds	Item	CLACO-MIS	ACOR-MIS	MVO-MIS	HHO-MIS	SCA-MIS	BLPSO-MIS	IGWO-MIS	IWOA-MIS	CLPSO-MIS
A	4	AVG	**1.959E + 01**	1.934 E+01	1.880 E+01	1.665 E+01	1.654 E+01	1.720 E+01	1.880 E+01	1.713 E+01	1.792 E+01
		STD	**1.066E + 00**	1.224 E+00	2.165 E+00	2.914 E+00	1.996 E+00	1.342 E+00	1.727 E+00	2.016 E+00	1.318 E+00
	5	AVG	**2.038E + 01**	2.022 E+01	2.012 E+01	1.844 E+01	1.705 E+01	1.871 E+01	1.985 E+01	1.887 E+01	1.915 E+01
		STD	1.358 E+00	1.149 E+00	1.239 E+00	1.731 E+00	2.671 E+00	**8.464E-01**	1.849 E+00	2.106 E+00	1.129 E+00
	6	AVG	**2.204E + 01**	2.127 E+01	2.140 E+01	1.829 E+01	1.785 E+01	2.003 E+01	2.078 E+01	1.983 E+01	1.990 E+01
		STD	**9.438E-01**	9.622E-01	1.259 E+00	2.739 E+00	2.252 E+00	1.626 E+00	1.652 E+00	1.872 E+00	1.106 E+00
	15	AVG	**2.782E + 01**	2.740 E+01	2.615 E+01	2.569 E+01	2.369 E+01	2.542 E+01	2.587 E+01	2.524 E+01	2.590 E+01
		STD	**8.048E-01**	8.418E-01	1.470 E+00	1.940 E+00	2.423 E+00	2.272 E+00	1.771 E+00	2.224 E+00	1.291 E+00
	20	AVG	**2.927E + 01**	2.838 E+01	2.756 E+01	2.779 E+01	2.510 E+01	2.665 E+01	2.747 E+01	2.747 E+01	2.690 E+01
		STD	1.229 E+00	**9.606E-01**	1.542 E+00	2.197 E+00	1.956 E+00	1.531 E+00	1.672 E+00	1.498 E+00	1.752 E+00
	25	AVG	**3.030E + 01**	3.008 E+01	2.941 E+01	2.858 E+01	2.760 E+01	2.941 E+01	2.905 E+01	2.955 E+01	2.924 E+01
		STD	1.584 E+00	**1.276E + 00**	1.838 E+00	2.334 E+00	2.214 E+00	1.382 E+00	1.649 E+00	2.028 E+00	1.422 E+00
B	4	AVG	1.722 E+01	**1.750E + 01**	1.685 E+01	1.692 E+01	1.399 E+01	1.648 E+01	1.651 E+01	1.655 E+01	1.697 E+01
		STD	1.063 E+00	**9.113E-01**	1.386 E+00	1.618 E+00	2.532 E+00	1.546 E+00	1.222 E+00	1.396 E+00	1.846 E+00
	5	AVG	1.921 E+01	**1.956E + 01**	1.866 E+01	1.775 E+01	1.504 E+01	1.817 E+01	1.752 E+01	1.844 E+01	1.760 E+01
		STD	**8.006E-01**	9.548E-01	1.232 E+00	1.856 E+00	2.622 E+00	1.531 E+00	2.022 E+00	1.609 E+00	2.134 E+00
	6	AVG	2.088 E+01	**2.122E + 01**	2.003 E+01	1.878 E+01	1.699 E+01	1.914 E+01	1.907 E+01	1.901 E+01	1.916 E+01
		STD	**8.633E-01**	9.209E-01	1.542 E+00	1.871 E+00	2.238 E+00	1.429 E+00	2.089 E+00	1.649 E+00	1.497 E+00
	15	AVG	**2.768E + 01**	2.672 E+01	2.604 E+01	2.453 E+01	2.424 E+01	2.535 E+01	2.492 E+01	2.507 E+01	2.498 E+01
		STD	**1.113E + 00**	1.640 E+00	1.830 E+00	2.704 E+00	2.177 E+00	1.515 E+00	1.637 E+00	2.217 E+00	1.816 E+00
	20	AVG	**2.938E + 01**	2.848 E+01	2.772 E+01	2.711 E+01	2.530 E+01	2.702 E+01	2.677 E+01	2.735 E+01	2.702 E+01
		STD	**1.177E + 00**	1.683 E+00	1.622 E+00	1.882 E+00	2.104 E+00	1.305 E+00	2.184 E+00	2.122 E+00	1.454 E+00
	25	AVG	**3.051E + 01**	2.997 E+01	2.952 E+01	2.934 E+01	2.738 E+01	2.895 E+01	2.877 E+01	2.857 E+01	2.822 E+01
		STD	1.321 E+00	1.446 E+00	1.956 E+00	1.480 E+00	1.480 E+00	1.745 E+00	**1.251E + 00**	2.478 E+00	1.757 E+00
C	4	AVG	1.946 E+01	1.929 E+01	**1.950E + 01**	1.785 E+01	1.763 E+01	1.801 E+01	1.924 E+01	1.895 E+01	1.812 E+01
		STD	**2.185E-01**	3.951E-01	5.338E-01	1.746 E+00	2.318 E+00	1.317 E+00	1.264 E+00	1.044 E+00	1.035 E+00
	5	AVG	**2.066E + 01**	2.034 E+01	2.011 E+01	1.865 E+01	1.860 E+01	1.913 E+01	2.031 E+01	1.892 E+01	1.901 E+01
		STD	**4.865E-01**	8.497E-01	1.348 E+00	2.090 E+00	2.254 E+00	9.773E-01	1.514 E+00	1.566 E+00	1.323 E+00
	6	AVG	2.171 E+01	**2.180E + 01**	2.143 E+01	2.053 E+01	1.910 E+01	2.067 E+01	2.101 E+01	1.927 E+01	2.029 E+01
		STD	**9.943E-01**	1.060 E+00	1.218 E+00	1.615 E+00	2.159 E+00	1.389 E+00	1.779 E+00	1.842 E+00	1.380 E+00
	15	AVG	**2.770E + 01**	2.687 E+01	2.659 E+01	2.574 E+01	2.460 E+01	2.518 E+01	2.565 E+01	2.532 E+01	2.584 E+01
		STD	**1.562E + 00**	1.671 E+00	1.913 E+00	2.378 E+00	1.657 E+00	1.613 E+00	1.917 E+00	1.845 E+00	1.964 E+00
	20	AVG	**2.960E + 01**	2.862 E+01	2.859 E+01	2.789 E+01	2.584 E+01	2.788 E+01	2.692 E+01	2.772 E+01	2.751 E+01
		STD	**1.491E + 00**	1.901 E+00	2.019 E+00	2.370 E+00	2.221 E+00	1.659 E+00	2.086 E+00	2.099 E+00	1.940 E+00
	25	AVG	**3.057E + 01**	3.046 E+01	2.934 E+01	2.917 E+01	2.798 E+01	2.991 E+01	2.901 E+01	2.891 E+01	2.931 E+01
		STD	1.879 E+00	1.527 E+00	2.385 E+00	2.418 E+00	2.705 E+00	**1.189E + 00**	2.132 E+00	2.402 E+00	1.741 E+00
D	4	AVG	**1.894E + 01**	1.876 E+01	1.803 E+01	1.645 E+01	1.511 E+01	1.684 E+01	1.773 E+01	1.649 E+01	1.722 E+01
		STD	**1.612E + 00**	1.618 E+00	2.316 E+00	2.330 E+00	2.630 E+00	1.983 E+00	2.352 E+00	2.261 E+00	1.940 E+00
	5	AVG	2.015 E+01	**2.021E + 01**	1.931 E+01	1.734 E+01	1.776 E+01	1.821 E+01	1.883 E+01	1.829 E+01	1.802 E+01
		STD	1.237 E+00	**1.087E + 00**	1.887 E+00	2.943 E+00	1.948 E+00	2.202 E+00	2.293 E+00	1.725 E+00	2.513 E+00
	6	AVG	**2.127E + 01**	2.104 E+01	2.069 E+01	1.809 E+01	1.696 E+01	1.947 E+01	1.942 E+01	1.890 E+01	1.941 E+01
		STD	**8.270E-01**	1.222 E+00	1.676 E+00	2.840 E+00	2.845 E+00	1.575 E+00	2.115 E+00	2.212 E+00	1.811 E+00
	15	AVG	**2.719E + 01**	2.707 E+01	2.647 E+01	2.480 E+01	2.282 E+01	2.552 E+01	2.548 E+01	2.592 E+01	2.560 E+01
		STD	1.446 E+00	**1.364E + 00**	1.610 E+00	3.439 E+00	2.459 E+00	1.790 E+00	1.858 E+00	2.340 E+00	1.487 E+00
	20	AVG	**2.937E + 01**	2.824 E+01	2.816 E+01	2.678 E+01	2.474 E+01	2.754 E+01	2.748 E+01	2.794 E+01	2.696 E+01
		STD	**1.376E + 00**	1.457 E+00	1.910 E+00	2.784 E+00	2.584 E+00	1.470 E+00	1.883 E+00	1.998 E+00	2.259 E+00
	25	AVG	**3.058E + 01**	2.985 E+01	2.925 E+01	2.963 E+01	2.749 E+01	2.889 E+01	2.878 E+01	2.864 E+01	2.906 E+01
		STD	1.726 E+00	1.730 E+00	1.650 E+00	1.952 E+00	2.209 E+00	**1.587E + 00**	1.630 E+00	2.624 E+00	1.612 E+00
E	4	AVG	**1.882E + 01**	1.864 E+01	1.833 E+01	1.641 E+01	1.533 E+01	1.720 E+01	1.760 E+01	1.677 E+01	1.721 E+01
		STD	1.177 E+00	**1.087E + 00**	1.306 E+00	2.316 E+00	2.221 E+00	1.546 E+00	1.547 E+00	1.810 E+00	1.504 E+00
	5	AVG	**2.047E + 01**	2.029 E+01	1.948 E+01	1.741 E+01	1.756 E+01	1.885 E+01	1.906 E+01	1.802 E+01	1.806 E+01
		STD	1.437 E+00	**1.170E + 00**	1.971 E+00	2.466 E+00	2.180 E+00	1.863 E+00	1.559 E+00	1.451 E+00	1.825 E+00
	6	AVG	2.164 E+01	**2.172E + 01**	2.140 E+01	1.860 E+01	1.825 E+01	1.844 E+01	1.959 E+01	1.893 E+01	1.906 E+01
		STD	1.081 E+00	**1.019E + 00**	1.091 E+00	2.727 E+00	1.867 E+00	1.947 E+00	1.636 E+00	1.752 E+00	1.669 E+00
	15	AVG	**2.745E + 01**	2.710 E+01	2.669 E+01	2.587 E+01	2.427 E+01	2.464 E+01	2.480 E+01	2.532 E+01	2.521 E+01
		STD	**1.182E + 00**	1.408 E+00	1.621 E+00	1.763 E+00	1.653 E+00	1.419 E+00	1.574 E+00	1.818 E+00	1.709 E+00
	20	AVG	**2.891E + 01**	2.857 E+01	2.833 E+01	2.651 E+01	2.552 E+01	2.737 E+01	2.672 E+01	2.633 E+01	2.704 E+01
		STD	1.696 E+00	1.460 E+00	1.717 E+00	2.345 E+00	2.489 E+00	**1.416E + 00**	1.676 E+00	2.367 E+00	1.945 E+00
	25	AVG	**3.048E + 01**	2.979 E+01	2.869 E+01	2.921 E+01	2.751 E+01	2.906 E+01	2.884 E+01	2.911 E+01	2.901 E+01
		STD	1.425 E+00	**1.091E + 00**	1.896 E+00	1.840 E+00	2.103 E+00	1.424 E+00	1.697 E+00	1.882 E+00	1.428 E+00
F	4	AVG	1.888 E+01	1.887 E+01	1.866 E+01	1.722 E+01	1.619 E+01	1.739 E+01	**1.937E + 01**	1.741 E+01	1.737 E+01
		STD	1.098 E+00	**9.216E-01**	1.299 E+00	2.048 E+00	2.426 E+00	1.172 E+00	1.293 E+00	2.108 E+00	1.432 E+00
	5	AVG	**1.986E + 01**	1.954 E+01	1.964 E+01	1.844 E+01	1.708 E+01	1.850 E+01	1.975 E+01	1.863 E+01	1.847 E+01
		STD	9.483E-01	**8.464E-01**	1.409 E+00	2.573 E+00	2.496 E+00	1.381 E+00	1.407 E+00	1.951 E+00	1.196 E+00
	6	AVG	**2.097E + 01**	2.069 E+01	2.066 E+01	1.982 E+01	1.880 E+01	1.978 E+01	2.029 E+01	1.945 E+01	1.966 E+01
		STD	7.260E-01	**6.737E-01**	1.936 E+00	2.457 E+00	2.486 E+00	8.686E-01	1.917 E+00	1.679 E+00	1.564 E+00
	15	AVG	**2.702E + 01**	2.653 E+01	2.565 E+01	2.500 E+01	2.379 E+01	2.485 E+01	2.536 E+01	2.493 E+01	2.507 E+01

(*continued on next page*)

Table A5 (*continued*)

Image	Thresholds	Item	CLACO-MIS	ACOR-MIS	MVO-MIS	HHO-MIS	SCA-MIS	BLPSO-MIS	IGWO-MIS	IWOA-MIS	CLPSO-MIS
		STD	**1.268E + 00**	1.279 E+00	2.150 E+00	2.621 E+00	2.571 E+00	1.945 E+00	1.519 E+00	2.216 E+00	2.044 E+00
	20	AVG	**2.879E + 01**	2.818 E+01	2.779 E+01	2.699 E+01	2.568 E+01	2.751 E+01	2.653 E+01	2.710 E+01	2.675 E+01
		STD	1.375 E+00	1.690 E+00	1.895 E+00	2.702 E+00	2.168 E+00	**1.373E + 00**	2.488 E+00	2.426 E+00	1.725 E+00
	25	AVG	2.963 E+01	**2.977E + 01**	2.878 E+01	2.884 E+01	2.735 E+01	2.904 E+01	2.805 E+01	2.871 E+01	2.915 E+01
		STD	2.037 E+00	1.839 E+00	1.672 E+00	2.262 E+00	1.954 E+00	2.342 E+00	1.766 E+00	1.912 E+00	**1.434E + 00**
G	4	AVG	2.021 E+01	**2.039E + 01**	1.996 E+01	1.888 E+01	1.736 E+01	1.736 E+01	1.993 E+01	1.896 E+01	1.823 E+01
		STD	9.290E-01	**2.820E-01**	1.545 E+00	2.107 E+00	1.770 E+00	1.870 E+00	8.923E-01	1.401 E+00	1.716 E+00
	5	AVG	2.150 E+01	**2.155E + 01**	2.065 E+01	1.859 E+01	1.822 E+01	1.937 E+01	2.093 E+01	1.926 E+01	1.870 E+01
		STD	**5.570E-01**	7.762E-01	2.008 E+00	2.386 E+00	2.033 E+00	2.017 E+00	1.345 E+00	2.189 E+00	1.907 E+00
	6	AVG	2.220 E+01	**2.278E + 01**	2.229 E+01	2.113 E+01	1.823 E+01	1.951 E+01	2.050 E+01	1.982 E+01	1.977 E+01
		STD	1.407 E+00	**6.127E-01**	1.454 E+00	1.893 E+00	2.739 E+00	1.529 E+00	1.845 E+00	2.303 E+00	2.437 E+00
	15	AVG	**2.731E + 01**	2.671 E+01	2.703 E+01	2.624 E+01	2.295 E+01	2.483 E+01	2.523 E+01	2.536 E+01	2.546 E+01
		STD	1.699 E+00	**1.484E + 00**	1.614 E+00	2.480 E+00	2.535 E+00	1.565 E+00	1.919 E+00	2.071 E+00	1.642 E+00
	20	AVG	**2.943E + 01**	2.915 E+01	2.826 E+01	2.803 E+01	2.596 E+01	2.754 E+01	2.750 E+01	2.796 E+01	2.824 E+01
		STD	1.267 E+00	1.348 E+00	2.094 E+00	3.132 E+00	2.137 E+00	1.894 E+00	1.883 E+00	2.051 E+00	**1.193E + 00**
	25	AVG	**3.017E + 01**	2.945 E+01	2.957 E+01	2.972 E+01	2.835 E+01	2.958 E+01	2.970 E+01	2.974 E+01	2.871 E+01
		STD	1.524 E+00	1.658 E+00	1.544 E+00	1.995 E+00	1.673 E+00	**1.506E + 00**	1.551 E+00	1.564 E+00	1.851 E+00
H	4	AVG	1.965 E+01	**2.004E + 01**	1.909 E+01	1.607 E+01	1.628 E+01	1.791 E+01	1.873 E+01	1.776 E+01	1.741 E+01
		STD	1.265 E+00	**7.748E-01**	1.296 E+00	2.344 E+00	2.147 E+00	1.720 E+00	1.298 E+00	1.660 E+00	2.063 E+00
	5	AVG	2.109 E+01	**2.138E + 01**	2.030 E+01	1.800 E+01	1.773 E+01	1.879 E+01	2.001 E+01	1.882 E+01	1.956 E+01
		STD	9.367E-01	**6.617E-01**	1.443 E+00	2.559 E+00	1.806 E+00	1.420 E+00	1.862 E+00	1.814 E+00	1.211 E+00
	6	AVG	**2.250E + 01**	2.219 E+01	2.125 E+01	1.934 E+01	1.816 E+01	1.982 E+01	2.102 E+01	1.939 E+01	1.981 E+01
		STD	**6.691E-01**	1.205 E+00	1.802 E+00	2.291 E+00	2.343 E+00	1.806 E+00	1.456 E+00	2.459 E+00	1.655 E+00
	15	AVG	**2.767E + 01**	2.680 E+01	2.648 E+01	2.609 E+01	2.473 E+01	2.527 E+01	2.455 E+01	2.567 E+01	2.543 E+01
		STD	**1.197E + 00**	1.652 E+00	2.067 E+00	1.661 E+00	2.376 E+00	1.760 E+00	2.201 E+00	1.430 E+00	1.820 E+00
	20	AVG	**2.966E + 01**	2.794 E+01	2.779 E+01	2.712 E+01	2.551 E+01	2.760 E+01	2.675 E+01	2.758 E+01	2.774 E+01
		STD	**1.164E + 00**	1.727 E+00	2.127 E+00	2.066 E+00	2.286 E+00	1.482 E+00	2.341 E+00	1.914 E+00	1.310 E+00
	25	AVG	**3.049E + 01**	3.022 E+01	3.006 E+01	2.946 E+01	2.798 E+01	2.890 E+01	2.918 E+01	2.981 E+01	2.941 E+01
		STD	1.596 E+00	1.134 E+00	1.557 E+00	2.082 E+00	1.489 E+00	1.660 E+00	1.880 E+00	1.625 E+00	**1.104E + 00**
I	4	AVG	**1.939E + 01**	1.896 E+01	1.848 E+01	1.642 E+01	1.650 E+01	1.684 E+01	1.778 E+01	1.686 E+01	1.635 E+01
		STD	**1.246E + 00**	1.626 E+00	1.631 E+00	2.342 E+00	2.119 E+00	2.412 E+00	1.735 E+00	1.923 E+00	2.238 E+00
	5	AVG	**2.032E + 01**	2.005 E+01	2.010 E+01	1.797 E+01	1.728 E+01	1.797 E+01	1.922 E+01	1.831 E+01	1.855 E+01
		STD	1.291 E+00	**1.252E + 00**	1.573 E+00	1.860 E+00	2.271 E+00	2.005 E+00	1.977 E+00	2.164 E+00	2.073 E+00
	6	AVG	**2.211E + 01**	2.166 E+01	2.145 E+01	1.854 E+01	1.866 E+01	1.966 E+01	2.019 E+01	1.933 E+01	1.945 E+01
		STD	1.156 E+00	**1.052E + 00**	1.438 E+00	2.518 E+00	1.873 E+00	1.888 E+00	1.810 E+00	2.027 E+00	2.008 E+00
	15	AVG	**2.795E + 01**	2.674 E+01	2.680 E+01	2.517 E+01	2.303 E+01	2.518 E+01	2.535 E+01	2.601 E+01	2.532 E+01
		STD	**1.385E + 00**	1.749 E+00	2.299 E+00	2.489 E+00	1.990 E+00	1.789 E+00	1.875 E+00	1.722 E+00	1.853 E+00
	20	AVG	**2.948E + 01**	2.886 E+01	2.774 E+01	2.742 E+01	2.597 E+01	2.724 E+01	2.748 E+01	2.778 E+01	2.730 E+01
		STD	1.548 E+00	1.779 E+00	2.356 E+00	2.923 E+00	2.847 E+00	**1.420E + 00**	2.098 E+00	1.497 E+00	1.763 E+00
	25	AVG	**3.096E + 01**	2.984 E+01	2.930 E+01	2.907 E+01	2.812 E+01	2.918 E+01	2.928 E+01	2.948 E+01	2.857 E+01
		STD	1.544 E+00	**1.078E + 00**	2.200 E+00	2.300 E+00	1.992 E+00	1.677 E+00	1.612 E+00	1.877 E+00	1.685 E+00

Table A6
The mean and variance values of the FSIM evaluation at various threshold levels

Image	Thresholds	Item	CLACO-MIS	ACOR-MIS	MVO-MIS	HHO-MIS	SCA-MIS	BLPSO-MIS	IGWO-MIS	IWOA-MIS	CLPSO-MIS
A	4	AVG	**8.484E-01**	8.399E-01	8.217E-01	7.569E-01	7.419E-01	7.662E-01	8.208E-01	7.658E-01	7.932E-01
		STD	4.071E-02	4.537E-02	6.682E-02	8.780E-02	6.248E-02	4.307E-02	5.978E-02	6.630E-02	**4.044E-02**
	5	AVG	**8.725E-01**	8.691E-01	8.625E-01	8.144E-01	7.604E-01	8.172E-01	8.522E-01	8.212E-01	8.279E-01
		STD	4.302E-02	3.778E-02	3.726E-02	5.096E-02	8.170E-02	**2.666E-02**	5.614E-02	6.654E-02	3.805E-02
	6	AVG	**9.173E-01**	8.989E-01	8.996E-01	8.058E-01	7.815E-01	8.521E-01	8.712E-01	8.433E-01	8.491E-01
		STD	**2.276E-02**	2.665E-02	3.439E-02	7.868E-02	6.517E-02	5.117E-02	4.571E-02	5.894E-02	3.268E-02
	15	AVG	**9.796E-01**	9.761E-01	9.566E-01	9.434E-01	9.121E-01	9.402E-01	9.471E-01	9.356E-01	9.499E-01
		STD	**6.867E-03**	7.505E-03	2.093E-02	2.943E-02	5.060E-02	4.040E-02	2.928E-02	3.977E-02	1.906E-02
	20	AVG	**9.821E-01**	9.767E-01	9.630E-01	9.603E-01	9.291E-01	9.509E-01	9.600E-01	9.616E-01	9.527E-01
		STD	**7.883E-03**	8.161E-03	2.033E-02	2.462E-02	3.250E-02	2.261E-02	2.065E-02	1.625E-02	2.370E-02
	25	AVG	9.815E-01	**9.817E-01**	9.733E-01	9.645E-01	9.560E-01	9.739E-01	9.719E-01	9.727E-01	9.720E-01
		STD	1.224E-02	**8.472E-03**	1.744E-02	2.730E-02	2.906E-02	1.147E-02	1.372E-02	2.372E-02	1.311E-02
B	4	AVG	7.304E-01	**7.341E-01**	7.269E-01	7.056E-01	6.816E-01	6.851E-01	7.168E-01	6.933E-01	7.090E-01
		STD	**1.717E-02**	2.114E-02	2.471E-02	3.072E-02	2.313E-02	3.681E-02	2.245E-02	3.181E-02	3.749E-02
	5	AVG	7.621E-01	**7.686E-01**	7.424E-01	7.288E-01	6.965E-01	7.084E-01	7.432E-01	7.297E-01	7.175E-01
		STD	1.959E-02	**1.715E-02**	3.614E-02	2.701E-02	3.098E-02	3.230E-02	2.398E-02	3.387E-02	3.998E-02
	6	AVG	**7.907E-01**	7.906E-01	7.770E-01	7.509E-01	7.127E-01	7.373E-01	7.539E-01	7.494E-01	7.400E-01
		STD	**1.966E-02**	2.033E-02	2.537E-02	3.058E-02	3.686E-02	3.413E-02	3.600E-02	3.169E-02	2.854E-02
	15	AVG	**9.147E-01**	8.994E-01	8.834E-01	8.608E-01	8.469E-01	8.603E-01	8.579E-01	8.621E-01	8.553E-01
		STD	**2.068E-02**	3.261E-02	2.985E-02	4.478E-02	3.488E-02	3.207E-02	3.055E-02	3.873E-02	3.973E-02
	20	AVG	**9.347E-01**	9.173E-01	9.086E-01	9.021E-01	8.617E-01	8.904E-01	8.896E-01	9.032E-01	8.924E-01
		STD	**1.718E-02**	2.878E-02	2.916E-02	3.526E-02	3.845E-02	2.413E-02	3.560E-02	3.439E-02	2.435E-02

(continued on next page)

Table A6 (*continued*)

Image	Thresholds	Item	CLACO-MIS	ACOR-MIS	MVO-MIS	HHO-MIS	SCA-MIS	BLPSO-MIS	IGWO-MIS	IWOA-MIS	CLPSO-MIS
	25	AVG	**9.442E-01**	9.345E-01	9.303E-01	9.274E-01	8.940E-01	9.143E-01	9.184E-01	9.163E-01	9.088E-01
		STD	**1.671E-02**	1.976E-02	2.368E-02	2.088E-02	2.531E-02	3.170E-02	1.862E-02	3.534E-02	2.674E-02
C	4	AVG	**7.927E-01**	7.915E-01	7.896E-01	7.527E-01	7.406E-01	7.560E-01	7.669E-01	7.685E-01	7.497E-01
		STD	**1.707E-02**	1.899E-02	2.273E-02	4.502E-02	4.853E-02	3.451E-02	2.745E-02	3.888E-02	3.850E-02
	5	AVG	**8.031E-01**	7.948E-01	7.874E-01	7.728E-01	7.701E-01	7.548E-01	7.761E-01	7.630E-01	7.688E-01
		STD	**1.751E-02**	2.609E-02	2.551E-02	4.132E-02	4.657E-02	3.328E-02	4.263E-02	3.881E-02	3.373E-02
	6	AVG	8.140E-01	8.104E-01	**8.164E-01**	7.973E-01	7.674E-01	7.871E-01	8.013E-01	7.812E-01	7.686E-01
		STD	1.952E-02	**1.635E-02**	3.041E-02	2.979E-02	4.847E-02	4.058E-02	3.874E-02	4.152E-02	4.052E-02
	15	AVG	**9.241E-01**	9.109E-01	9.052E-01	8.878E-01	8.597E-01	8.866E-01	8.806E-01	8.840E-01	8.874E-01
		STD	**1.766E-02**	2.679E-02	3.065E-02	3.790E-02	3.903E-02	3.565E-02	4.313E-02	3.505E-02	3.281E-02
	20	AVG	**9.414E-01**	9.286E-01	9.290E-01	9.129E-01	8.921E-01	9.176E-01	9.053E-01	9.182E-01	9.156E-01
		STD	**1.850E-02**	2.117E-02	2.887E-02	3.654E-02	3.351E-02	2.214E-02	3.816E-02	2.398E-02	2.632E-02
	25	AVG	**9.485E-01**	9.482E-01	9.329E-01	9.310E-01	9.162E-01	9.337E-01	9.288E-01	9.311E-01	9.298E-01
		STD	1.822E-02	**1.602E-02**	2.636E-02	2.196E-02	2.942E-02	1.721E-02	2.739E-02	2.809E-02	2.289E-02
D	4	AVG	**7.525E-01**	7.442E-01	7.339E-01	6.835E-01	6.764E-01	7.035E-01	7.187E-01	6.915E-01	7.047E-01
		STD	4.031E-02	4.374E-02	5.586E-02	5.068E-02	4.858E-02	4.097E-02	6.282E-02	5.934E-02	**4.023E-02**
	5	AVG	7.805E-01	**7.826E-01**	7.600E-01	7.175E-01	7.232E-01	7.373E-01	7.586E-01	7.366E-01	7.337E-01
		STD	4.024E-02	**3.551E-02**	5.260E-02	6.389E-02	4.454E-02	4.459E-02	5.487E-02	3.950E-02	5.784E-02
	6	AVG	**8.176E-01**	8.093E-01	8.033E-01	7.448E-01	7.093E-01	7.664E-01	7.703E-01	7.611E-01	7.687E-01
		STD	**2.553E-02**	3.514E-02	4.225E-02	5.582E-02	4.971E-02	3.838E-02	5.468E-02	4.787E-02	3.954E-02
	15	AVG	**9.419E-01**	9.360E-01	9.271E-01	8.915E-01	8.437E-01	9.004E-01	9.036E-01	9.087E-01	9.063E-01
		STD	**2.209E-02**	2.309E-02	2.720E-02	6.149E-02	6.141E-02	3.409E-02	3.398E-02	4.728E-02	2.954E-02
	20	AVG	**9.622E-01**	9.448E-01	9.404E-01	9.147E-01	8.811E-01	9.297E-01	9.307E-01	9.361E-01	9.209E-01
		STD	**1.570E-02**	2.204E-02	2.698E-02	4.710E-02	5.056E-02	2.392E-02	2.846E-02	3.000E-02	3.923E-02
	25	AVG	**9.674E-01**	9.599E-01	9.495E-01	9.534E-01	9.250E-01	9.458E-01	9.455E-01	9.406E-01	9.449E-01
		STD	**1.646E-02**	1.867E-02	2.195E-02	2.462E-02	3.501E-02	2.115E-02	2.340E-02	3.736E-02	2.319E-02
E	4	AVG	7.509E-01	**7.527E-01**	7.363E-01	7.236E-01	7.298E-01	7.140E-01	7.389E-01	7.196E-01	7.319E-01
		STD	1.638E-02	**8.176E-03**	3.199E-02	3.562E-02	3.568E-02	2.728E-02	2.658E-02	4.396E-02	3.186E-02
	5	AVG	**7.682E-01**	7.634E-01	7.541E-01	7.302E-01	7.454E-01	7.409E-01	7.541E-01	7.359E-01	7.325E-01
		STD	2.885E-02	2.996E-02	3.786E-02	4.391E-02	4.073E-02	3.299E-02	**2.831E-02**	3.392E-02	2.917E-02
	6	AVG	**7.960E-01**	7.849E-01	7.901E-01	7.459E-01	7.438E-01	7.435E-01	7.631E-01	7.482E-01	7.398E-01
		STD	2.664E-02	2.965E-02	**2.580E-02**	4.265E-02	3.332E-02	3.604E-02	3.406E-02	3.958E-02	3.033E-02
	15	AVG	**9.132E-01**	9.057E-01	9.025E-01	8.822E-01	8.528E-01	8.583E-01	8.619E-01	8.719E-01	8.681E-01
		STD	**1.994E-02**	2.618E-02	2.484E-02	3.668E-02	3.706E-02	2.589E-02	2.952E-02	3.516E-02	2.897E-02
	20	AVG	**9.323E-01**	9.249E-01	9.206E-01	8.908E-01	8.713E-01	8.986E-01	8.920E-01	8.878E-01	9.005E-01
		STD	2.678E-02	2.498E-02	2.877E-02	4.332E-02	4.224E-02	**2.437E-02**	3.108E-02	3.665E-02	3.518E-02
	25	AVG	**9.457E-01**	9.379E-01	9.192E-01	9.276E-01	9.014E-01	9.239E-01	9.187E-01	9.286E-01	9.240E-01
		STD	1.852E-02	**1.845E-02**	2.999E-02	2.909E-02	3.174E-02	2.001E-02	2.802E-02	2.556E-02	2.578E-02
F	4	AVG	8.658E-01	8.628E-01	8.564E-01	8.139E-01	7.546E-01	8.149E-01	**8.702E-01**	8.151E-01	8.133E-01
		STD	3.356E-02	**2.939E-02**	4.224E-02	5.517E-02	9.472E-02	3.748E-02	4.110E-02	6.037E-02	4.909E-02
	5	AVG	**8.891E-01**	8.802E-01	8.807E-01	8.414E-01	7.864E-01	8.422E-01	8.804E-01	8.413E-01	8.442E-01
		STD	2.643E-02	**2.336E-02**	3.907E-02	7.118E-02	9.087E-02	4.978E-02	3.969E-02	6.807E-02	3.541E-02
	6	AVG	**9.163E-01**	9.088E-01	9.035E-01	8.629E-01	8.349E-01	8.803E-01	8.878E-01	8.633E-01	8.729E-01
		STD	**1.521E-02**	1.773E-02	4.176E-02	7.072E-02	7.613E-02	2.809E-02	4.609E-02	6.057E-02	4.293E-02
	15	AVG	**9.756E-01**	9.697E-01	9.553E-01	9.430E-01	9.233E-01	9.402E-01	9.506E-01	9.432E-01	9.453E-01
		STD	**9.831E-03**	1.347E-02	2.670E-02	3.596E-02	5.248E-02	4.076E-02	2.144E-02	3.164E-02	3.037E-02
	20	AVG	**9.805E-01**	9.759E-01	9.707E-01	9.598E-01	9.488E-01	9.695E-01	9.565E-01	9.606E-01	9.612E-01
		STD	**8.329E-03**	1.193E-02	1.644E-02	2.401E-02	3.092E-02	1.310E-02	2.879E-02	2.868E-02	1.937E-02
	25	AVG	9.799E-01	**9.811E-01**	9.753E-01	9.729E-01	9.641E-01	9.717E-01	9.697E-01	9.732E-01	9.771E-01
		STD	1.464E-02	1.157E-02	1.310E-02	1.716E-02	1.855E-02	2.292E-02	1.572E-02	1.539E-02	**9.268E-03**
G	4	AVG	7.425E-01	7.473E-01	7.452E-01	7.412E-01	7.133E-01	6.998E-01	**7.496E-01**	7.334E-01	7.204E-01
		STD	2.017E-02	**8.573E-03**	2.868E-02	4.026E-02	4.258E-02	3.840E-02	1.947E-02	3.483E-02	3.584E-02
	5	AVG	7.752E-01	**7.798E-01**	7.658E-01	7.356E-01	7.281E-01	7.433E-01	7.746E-01	7.440E-01	7.225E-01
		STD	1.434E-02	**1.345E-02**	4.173E-02	4.934E-02	4.262E-02	4.318E-02	3.190E-02	4.987E-02	4.293E-02
	6	AVG	7.971E-01	8.076E-01	**8.078E-01**	7.978E-01	7.400E-01	7.469E-01	7.724E-01	7.578E-01	7.622E-01
		STD	3.026E-02	**1.881E-02**	3.372E-02	3.680E-02	5.366E-02	3.454E-02	4.621E-02	5.408E-02	5.453E-02
	15	AVG	**9.106E-01**	8.967E-01	9.049E-01	8.885E-01	8.166E-01	8.580E-01	8.661E-01	8.691E-01	8.679E-01
		STD	3.696E-02	3.037E-02	3.204E-02	5.442E-02	5.883E-02	**2.907E-02**	4.153E-02	4.591E-02	3.835E-02
	20	AVG	**9.413E-01**	9.347E-01	9.185E-01	9.123E-01	8.757E-01	9.003E-01	9.055E-01	9.117E-01	9.158E-01
		STD	**2.141E-02**	2.378E-02	4.171E-02	5.903E-02	4.763E-02	4.165E-02	3.069E-02	4.290E-02	2.369E-02
	25	AVG	**9.424E-01**	9.322E-01	9.334E-01	9.361E-01	9.200E-01	9.298E-01	9.351E-01	9.380E-01	9.183E-01
		STD	**2.319E-02**	2.643E-02	2.403E-02	2.991E-02	2.823E-02	2.623E-02	2.663E-02	2.327E-02	3.018E-02
H	4	AVG	7.315E-01	**7.356E-01**	7.245E-01	6.779E-01	6.897E-01	6.962E-01	7.276E-01	7.002E-01	6.949E-01
		STD	2.676E-02	**1.101E-02**	2.159E-02	4.609E-02	3.437E-02	3.651E-02	2.443E-02	3.268E-02	2.455E-02
	5	AVG	7.637E-01	**7.684E-01**	7.437E-01	7.093E-01	7.140E-01	7.167E-01	7.475E-01	7.287E-01	7.369E-01
		STD	2.170E-02	**1.729E-02**	3.891E-02	5.248E-02	3.871E-02	3.275E-02	4.263E-02	3.701E-02	3.239E-02
	6	AVG	**7.972E-01**	7.840E-01	7.666E-01	7.539E-01	7.078E-01	7.513E-01	7.696E-01	7.506E-01	7.503E-01
		STD	**1.662E-02**	3.440E-02	4.952E-02	3.856E-02	5.289E-02	2.513E-02	4.233E-02	4.327E-02	3.598E-02
	15	AVG	**9.149E-01**	8.973E-01	8.996E-01	8.843E-01	8.531E-01	8.609E-01	8.532E-01	8.756E-01	8.676E-01
		STD	**2.300E-02**	3.201E-02	2.693E-02	3.266E-02	5.105E-02	3.644E-02	3.234E-02	2.591E-02	3.294E-02

(*continued on next page*)

Table A6 (*continued*)

Image	Thresholds	Item	CLACO-MIS	ACOR-MIS	MVO-MIS	HHO-MIS	SCA-MIS	BLPSO-MIS	IGWO-MIS	IWOA-MIS	CLPSO-MIS
	20	AVG	**9.392E-01**	9.097E-01	9.136E-01	8.990E-01	8.709E-01	8.995E-01	8.859E-01	9.060E-01	9.068E-01
		STD	**2.048E-02**	2.905E-02	3.073E-02	3.189E-02	4.083E-02	2.815E-02	4.348E-02	3.205E-02	2.326E-02
	25	AVG	**9.471E-01**	9.417E-01	9.387E-01	9.279E-01	9.043E-01	9.178E-01	9.252E-01	9.341E-01	9.263E-01
		STD	1.832E-02	**1.555E-02**	2.301E-02	2.814E-02	2.545E-02	2.839E-02	2.551E-02	2.524E-02	1.789E-02
I	4	AVG	**7.804E-01**	7.745E-01	7.527E-01	7.212E-01	7.278E-01	7.322E-01	7.413E-01	7.226E-01	7.117E-01
		STD	**3.384E-02**	3.757E-02	5.209E-02	4.575E-02	4.768E-02	4.700E-02	4.474E-02	4.094E-02	4.171E-02
	5	AVG	**7.993E-01**	7.954E-01	7.989E-01	7.618E-01	7.492E-01	7.533E-01	7.732E-01	7.603E-01	7.593E-01
		STD	**3.520E-02**	3.654E-02	3.957E-02	4.441E-02	4.804E-02	5.200E-02	4.933E-02	4.346E-02	4.531E-02
	6	AVG	**8.361E-01**	8.243E-01	8.283E-01	7.671E-01	7.722E-01	7.844E-01	7.954E-01	7.828E-01	7.794E-01
		STD	2.900E-02	**2.807E-02**	3.832E-02	5.075E-02	4.925E-02	4.401E-02	4.499E-02	4.824E-02	4.694E-02
	15	AVG	**9.459E-01**	9.269E-01	9.242E-01	8.997E-01	8.607E-01	8.874E-01	8.969E-01	9.086E-01	8.986E-01
		STD	**2.070E-02**	3.257E-02	4.346E-02	4.479E-02	3.288E-02	3.954E-02	3.761E-02	3.389E-02	3.439E-02
	20	AVG	**9.581E-01**	9.481E-01	9.302E-01	9.285E-01	9.017E-01	9.248E-01	9.285E-01	9.344E-01	9.232E-01
		STD	**1.959E-02**	2.559E-02	3.974E-02	4.531E-02	4.816E-02	2.282E-02	3.593E-02	2.351E-02	3.511E-02
	25	AVG	**9.682E-01**	9.576E-01	9.468E-01	9.453E-01	9.300E-01	9.447E-01	9.471E-01	9.505E-01	9.355E-01
		STD	1.382E-02	**1.346E-02**	3.021E-02	2.823E-02	3.441E-02	2.193E-02	2.377E-02	2.272E-02	2.518E-02

Table A7
The mean and variance values of the SSIM evaluation at various threshold levels

Image	Thresholds	Item	CLACO-MIS	ACOR-MIS	MVO-MIS	HHO-MIS	SCA-MIS	BLPSO-MIS	IGWO-MIS	IWOA-MIS	CLPSO-MIS
A	4	AVG	**5.796E-01**	5.663E-01	5.608E-01	4.961E-01	5.172E-01	5.072E-01	5.659E-01	5.088E-01	5.335E-01
		STD	4.528E-02	5.057E-02	7.063E-02	9.947E-02	6.419E-02	**4.163E-02**	6.636E-02	6.404E-02	4.814E-02
	5	AVG	**6.155E-01**	6.090E-01	6.115E-01	5.696E-01	5.352E-01	5.647E-01	6.137E-01	5.735E-01	5.807E-01
		STD	5.617E-02	4.662E-02	4.746E-02	5.972E-02	7.978E-02	**2.197E-02**	6.225E-02	7.262E-02	4.314E-02
	6	AVG	**6.863E-01**	6.570E-01	6.647E-01	5.782E-01	5.603E-01	6.162E-01	6.562E-01	6.141E-01	6.138E-01
		STD	3.966E-02	4.054E-02	5.153E-02	8.314E-02	6.436E-02	4.538E-02	5.849E-02	6.649E-02	**3.670E-02**
	15	AVG	**8.762E-01**	8.664E-01	8.343E-01	8.187E-01	7.555E-01	8.049E-01	8.195E-01	8.062E-01	8.226E-01
		STD	**1.893E-02**	2.207E-02	3.788E-02	4.815E-02	7.299E-02	6.319E-02	4.832E-02	5.557E-02	3.605E-02
	20	AVG	**9.011E-01**	8.816E-01	8.624E-01	8.656E-01	7.991E-01	8.410E-01	8.559E-01	8.585E-01	8.434E-01
		STD	2.566E-02	**2.266E-02**	3.535E-02	4.847E-02	4.918E-02	3.708E-02	4.225E-02	3.830E-02	3.968E-02
	25	AVG	**9.142E-01**	9.107E-01	8.957E-01	8.782E-01	8.585E-01	8.927E-01	8.889E-01	8.987E-01	8.930E-01
		STD	2.689E-02	**2.259E-02**	3.674E-02	5.062E-02	5.034E-02	2.928E-02	3.142E-02	4.204E-02	2.726E-02
B	4	AVG	**7.230E-01**	7.174E-01	7.071E-01	6.582E-01	6.728E-01	6.466E-01	7.044E-01	6.491E-01	6.692E-01
		STD	**1.372E-02**	3.120E-02	4.095E-02	6.336E-02	2.787E-02	5.317E-02	4.830E-02	6.668E-02	4.629E-02
	5	AVG	**7.336E-01**	7.312E-01	7.067E-01	6.635E-01	6.804E-01	6.767E-01	7.211E-01	6.853E-01	6.748E-01
		STD	2.722E-02	**2.669E-02**	5.249E-02	6.539E-02	4.270E-02	3.930E-02	4.536E-02	4.210E-02	5.938E-02
	6	AVG	**7.519E-01**	7.437E-01	7.271E-01	7.059E-01	6.957E-01	6.999E-01	7.216E-01	7.077E-01	7.017E-01
		STD	2.523E-02	**2.501E-02**	4.632E-02	5.296E-02	4.281E-02	4.334E-02	3.649E-02	4.581E-02	3.764E-02
	15	AVG	**8.458E-01**	8.338E-01	8.276E-01	8.137E-01	7.985E-01	8.144E-01	8.105E-01	8.119E-01	8.092E-01
		STD	**1.770E-02**	2.726E-02	2.372E-02	3.345E-02	2.693E-02	2.125E-02	2.246E-02	2.931E-02	2.647E-02
	20	AVG	**8.780E-01**	8.647E-01	8.581E-01	8.529E-01	8.189E-01	8.443E-01	8.415E-01	8.524E-01	8.483E-01
		STD	**1.455E-02**	2.291E-02	2.254E-02	3.217E-02	2.956E-02	1.799E-02	2.733E-02	2.806E-02	1.583E-02
	25	AVG	**8.943E-01**	8.879E-01	8.848E-01	8.834E-01	8.548E-01	8.692E-01	8.693E-01	8.759E-01	8.661E-01
		STD	**1.554E-02**	1.705E-02	2.028E-02	1.831E-02	1.875E-02	2.508E-02	1.787E-02	2.473E-02	2.065E-02
C	4	AVG	5.590E-01	5.601E-01	5.653E-01	5.610E-01	**6.098E-01**	5.402E-01	5.926E-01	5.751E-01	5.400E-01
		STD	**2.209E-02**	2.734E-02	3.682E-02	7.324E-02	7.882E-02	4.050E-02	6.724E-02	7.196E-02	5.305E-02
	5	AVG	5.981E-01	5.844E-01	5.824E-01	5.958E-01	**6.774E-01**	5.924E-01	6.395E-01	6.043E-01	5.915E-01
		STD	6.864E-02	6.518E-02	6.394E-02	8.674E-02	8.309E-02	**5.615E-02**	8.772E-02	9.490E-02	7.428E-02
	6	AVG	6.490E-01	6.487E-01	6.415E-01	**6.948E-01**	6.621E-01	6.362E-01	6.882E-01	6.370E-01	6.206E-01
		STD	**6.716E-02**	7.715E-02	7.716E-02	8.273E-02	9.748E-02	7.084E-02	9.830E-02	8.089E-02	7.834E-02
	15	AVG	**8.594E-01**	8.413E-01	8.294E-01	8.095E-01	8.077E-01	8.293E-01	8.064E-01	8.145E-01	8.452E-01
		STD	4.242E-02	4.601E-02	6.406E-02	7.351E-02	5.452E-02	4.961E-02	6.945E-02	6.723E-02	**2.580E-02**
	20	AVG	**8.887E-01**	8.824E-01	8.792E-01	8.683E-01	8.273E-01	8.658E-01	8.498E-01	8.562E-01	8.640E-01
		STD	3.642E-02	**2.496E-02**	4.172E-02	4.535E-02	7.426E-02	2.953E-02	5.400E-02	5.458E-02	4.444E-02
	25	AVG	9.094E-01	**9.096E-01**	8.855E-01	8.762E-01	8.788E-01	8.940E-01	8.840E-01	8.852E-01	8.886E-01
		STD	1.650E-02	1.669E-02	4.991E-02	6.192E-02	2.243E-02	**1.496E-02**	4.476E-02	3.913E-02	2.743E-02
D	4	AVG	**6.478E-01**	6.306E-01	6.110E-01	5.671E-01	5.984E-01	5.970E-01	6.029E-01	5.723E-01	5.890E-01
		STD	**3.083E-02**	3.865E-02	5.790E-02	5.883E-02	5.091E-02	3.438E-02	6.445E-02	6.001E-02	5.731E-02
	5	AVG	6.476E-01	**6.547E-01**	6.348E-01	5.996E-01	6.271E-01	6.135E-01	6.268E-01	6.228E-01	6.098E-01
		STD	3.659E-02	**3.160E-02**	4.402E-02	7.121E-02	4.150E-02	5.291E-02	5.216E-02	3.875E-02	6.036E-02
	6	AVG	**6.683E-01**	6.643E-01	6.644E-01	6.220E-01	5.996E-01	6.467E-01	6.521E-01	6.322E-01	6.533E-01
		STD	**2.154E-02**	2.751E-02	4.061E-02	6.193E-02	7.406E-02	3.811E-02	4.891E-02	4.803E-02	3.850E-02
	15	AVG	**8.227E-01**	8.224E-01	8.124E-01	7.861E-01	7.351E-01	7.910E-01	7.929E-01	8.071E-01	7.987E-01
		STD	3.256E-02	3.188E-02	3.576E-02	6.074E-02	5.063E-02	3.701E-02	3.787E-02	4.489E-02	**2.896E-02**
	20	AVG	**8.729E-01**	8.491E-01	8.507E-01	8.302E-01	7.879E-01	8.361E-01	8.342E-01	8.446E-01	8.256E-01
		STD	**2.412E-02**	2.881E-02	3.494E-02	4.884E-02	5.270E-02	2.662E-02	3.715E-02	3.846E-02	3.715E-02
	25	AVG	**8.917E-01**	8.776E-01	8.704E-01	8.757E-01	8.336E-01	8.627E-01	8.610E-01	8.606E-01	8.669E-01

(*continued on next page*)

Table A7 (*continued*)

Image	Thresholds	Item	CLACO-MIS	ACOR-MIS	MVO-MIS	HHO-MIS	SCA-MIS	BLPSO-MIS	IGWO-MIS	IWOA-MIS	CLPSO-MIS
		STD	2.508E-02	3.076E-02	2.656E-02	3.358E-02	4.206E-02	2.495E-02	2.733E-02	4.740E-02	**2.476E-02**
E	4	AVG	7.141E-01	**7.183E-01**	6.861E-01	6.350E-01	6.822E-01	6.508E-01	6.966E-01	6.329E-01	6.759E-01
		STD	2.629E-02	**1.030E-02**	4.882E-02	9.758E-02	4.561E-02	4.708E-02	4.835E-02	6.287E-02	4.541E-02
	5	AVG	**7.153E-01**	7.132E-01	6.852E-01	6.633E-01	6.870E-01	6.736E-01	7.064E-01	6.650E-01	6.726E-01
		STD	**2.488E-02**	3.285E-02	5.622E-02	6.566E-02	5.835E-02	4.834E-02	3.577E-02	5.293E-02	4.611E-02
	6	AVG	**7.332E-01**	7.161E-01	7.169E-01	6.653E-01	6.977E-01	6.789E-01	6.943E-01	6.820E-01	6.746E-01
		STD	**2.265E-02**	2.472E-02	3.812E-02	6.230E-02	3.810E-02	4.952E-02	4.741E-02	5.362E-02	3.776E-02
	15	AVG	**8.316E-01**	8.223E-01	8.291E-01	8.120E-01	7.877E-01	7.936E-01	7.918E-01	8.065E-01	7.962E-01
		STD	**1.915E-02**	2.265E-02	2.577E-02	3.064E-02	3.554E-02	2.763E-02	2.281E-02	2.737E-02	2.520E-02
	20	AVG	**8.631E-01**	8.523E-01	8.558E-01	8.276E-01	8.109E-01	8.354E-01	8.215E-01	8.226E-01	8.366E-01
		STD	2.300E-02	2.515E-02	2.468E-02	4.128E-02	3.617E-02	**2.150E-02**	2.688E-02	3.141E-02	3.073E-02
	25	AVG	**8.827E-01**	8.749E-01	8.618E-01	8.682E-01	8.462E-01	8.641E-01	8.581E-01	8.703E-01	8.645E-01
		STD	2.001E-02	**1.633E-02**	2.504E-02	2.516E-02	2.441E-02	1.734E-02	2.513E-02	2.579E-02	2.029E-02
F	4	AVG	5.989E-01	5.947E-01	5.852E-01	5.238E-01	4.737E-01	5.320E-01	**6.174E-01**	5.320E-01	5.311E-01
		STD	5.321E-02	**4.582E-02**	6.759E-02	1.019E-01	1.185E-01	5.514E-02	6.424E-02	1.014E-01	6.284E-02
	5	AVG	6.436E-01	6.276E-01	6.353E-01	5.812E-01	5.189E-01	5.834E-01	**6.445E-01**	5.915E-01	5.868E-01
		STD	4.536E-02	**4.126E-02**	6.403E-02	1.156E-01	1.226E-01	6.580E-02	6.089E-02	9.012E-02	5.493E-02
	6	AVG	**6.956E-01**	6.826E-01	6.830E-01	6.513E-01	6.029E-01	6.469E-01	6.696E-01	6.294E-01	6.410E-01
		STD	3.267E-02	**3.167E-02**	7.975E-02	1.012E-01	1.170E-01	3.659E-02	8.091E-02	8.011E-02	6.637E-02
	15	AVG	**8.890E-01**	8.742E-01	8.475E-01	8.285E-01	7.817E-01	8.208E-01	8.386E-01	8.244E-01	8.248E-01
		STD	**2.902E-02**	3.402E-02	5.781E-02	6.982E-02	8.999E-02	6.227E-02	4.123E-02	6.469E-02	6.215E-02
	20	AVG	**9.159E-01**	9.036E-01	8.936E-01	8.706E-01	8.401E-01	8.884E-01	8.583E-01	8.734E-01	8.713E-01
		STD	**2.550E-02**	3.074E-02	3.859E-02	5.363E-02	5.898E-02	2.661E-02	6.141E-02	5.356E-02	3.886E-02
	25	AVG	9.225E-01	**9.251E-01**	9.090E-01	9.051E-01	8.762E-01	9.054E-01	8.925E-01	9.046E-01	9.132E-01
		STD	3.523E-02	2.948E-02	3.284E-02	4.464E-02	4.314E-02	4.783E-02	3.621E-02	3.720E-02	**2.603E-02**
G	4	AVG	6.838E-01	6.855E-01	6.889E-01	6.830E-01	6.612E-01	6.330E-01	**6.980E-01**	6.667E-01	6.638E-01
		STD	2.726E-02	**1.331E-02**	4.409E-02	4.790E-02	5.015E-02	6.228E-02	1.629E-02	4.499E-02	5.970E-02
	5	AVG	7.068E-01	7.069E-01	6.895E-01	6.738E-01	6.741E-01	6.790E-01	**7.102E-01**	6.847E-01	6.652E-01
		STD	**1.417E-02**	1.968E-02	6.051E-02	7.466E-02	6.784E-02	4.350E-02	2.465E-02	5.105E-02	5.463E-02
	6	AVG	7.160E-01	7.277E-01	**7.341E-01**	7.258E-01	6.851E-01	6.866E-01	7.114E-01	6.896E-01	6.982E-01
		STD	3.055E-02	**1.509E-02**	2.552E-02	4.079E-02	5.850E-02	4.186E-02	4.294E-02	5.919E-02	6.789E-02
	15	AVG	8.259E-01	8.169E-01	**8.302E-01**	8.240E-01	7.596E-01	7.921E-01	7.977E-01	8.050E-01	7.989E-01
		STD	3.323E-02	2.500E-02	3.065E-02	4.799E-02	5.194E-02	**2.177E-02**	3.778E-02	3.919E-02	3.318E-02
	20	AVG	**8.695E-01**	8.610E-01	8.530E-01	8.521E-01	8.166E-01	8.314E-01	8.385E-01	8.450E-01	8.472E-01
		STD	**2.181E-02**	2.371E-02	3.693E-02	5.474E-02	3.889E-02	3.448E-02	3.308E-02	4.053E-02	2.190E-02
	25	AVG	**8.788E-01**	8.693E-01	8.729E-01	8.767E-01	8.605E-01	8.682E-01	8.720E-01	8.733E-01	8.586E-01
		STD	2.469E-02	2.439E-02	2.467E-02	3.082E-02	2.696E-02	2.377E-02	2.545E-02	2.672E-02	**2.242E-02**
H	4	AVG	6.793E-01	**6.814E-01**	6.513E-01	5.590E-01	6.306E-01	6.351E-01	6.756E-01	6.246E-01	6.161E-01
		STD	6.370E-02	**4.418E-02**	7.277E-02	1.300E-01	8.977E-02	6.506E-02	6.472E-02	9.002E-02	9.942E-02
	5	AVG	7.001E-01	**7.050E-01**	6.800E-01	6.331E-01	6.637E-01	6.626E-01	6.970E-01	6.595E-01	6.923E-01
		STD	3.398E-02	**2.647E-02**	5.287E-02	9.680E-02	6.926E-02	5.341E-02	7.544E-02	5.700E-02	4.166E-02
	6	AVG	**7.286E-01**	7.176E-01	7.096E-01	6.719E-01	6.684E-01	6.797E-01	7.240E-01	6.636E-01	6.952E-01
		STD	**1.966E-02**	3.061E-02	5.393E-02	8.638E-02	5.783E-02	6.634E-02	3.065E-02	8.346E-02	4.821E-02
	15	AVG	**8.387E-01**	8.284E-01	8.268E-01	8.227E-01	7.983E-01	8.018E-01	7.904E-01	8.105E-01	8.050E-01
		STD	**2.238E-02**	3.021E-02	3.721E-02	2.954E-02	4.531E-02	2.816E-02	3.902E-02	2.576E-02	3.795E-02
	20	AVG	**8.747E-01**	8.472E-01	8.508E-01	8.518E-01	8.217E-01	8.400E-01	8.367E-01	8.537E-01	8.494E-01
		STD	**1.969E-02**	2.833E-02	3.522E-02	2.461E-02	3.396E-02	2.328E-02	3.455E-02	2.563E-02	2.184E-02
	25	AVG	**8.905E-01**	8.852E-01	8.812E-01	8.776E-01	8.532E-01	8.654E-01	8.726E-01	8.788E-01	8.709E-01
		STD	1.907E-02	1.901E-02	2.445E-02	2.730E-02	2.386E-02	2.431E-02	2.936E-02	2.262E-02	**1.739E-02**
I	4	AVG	**6.609E-01**	6.595E-01	6.401E-01	5.885E-01	6.204E-01	6.076E-01	6.202E-01	5.918E-01	5.929E-01
		STD	**2.431E-02**	3.656E-02	4.673E-02	5.856E-02	5.380E-02	6.375E-02	4.865E-02	4.164E-02	5.040E-02
	5	AVG	6.600E-01	**6.661E-01**	6.647E-01	6.273E-01	6.319E-01	6.403E-01	6.421E-01	6.224E-01	6.345E-01
		STD	**3.058E-02**	4.017E-02	4.217E-02	4.204E-02	5.574E-02	4.966E-02	4.030E-02	4.037E-02	3.924E-02
	6	AVG	**6.891E-01**	6.813E-01	6.860E-01	6.380E-01	6.521E-01	6.639E-01	6.610E-01	6.500E-01	6.587E-01
		STD	2.129E-02	**2.072E-02**	3.610E-02	4.788E-02	5.264E-02	4.005E-02	4.099E-02	4.800E-02	3.943E-02
	15	AVG	**8.333E-01**	8.081E-01	8.174E-01	7.933E-01	7.552E-01	7.800E-01	7.849E-01	7.978E-01	7.930E-01
		STD	2.914E-02	3.989E-02	4.142E-02	5.041E-02	**2.735E-02**	3.376E-02	3.982E-02	3.473E-02	3.440E-02
	20	AVG	**8.670E-01**	8.539E-01	8.406E-01	8.367E-01	8.043E-01	8.269E-01	8.325E-01	8.377E-01	8.255E-01
		STD	2.699E-02	3.323E-02	4.237E-02	5.000E-02	5.009E-02	**2.436E-02**	3.818E-02	2.682E-02	3.236E-02
	25	AVG	**8.895E-01**	8.732E-01	8.720E-01	8.602E-01	8.427E-01	8.603E-01	8.626E-01	8.705E-01	8.498E-01
		STD	2.489E-02	**1.857E-02**	3.109E-02	3.922E-02	3.538E-02	2.816E-02	2.949E-02	2.976E-02	3.029E-02

Table A8
The analytical results of PSNR evaluation gained by using the WSRT

Thresholds	Item	CLACO-MIS	ACOR-MIS	MVO-MIS	HHO-MIS	SCA-MIS	BLPSO-MIS	IGWO-MIS	IWOA-MIS	CLPSO-MIS
4	+/−/ =	~	1/0/8	3/0/6	8/0/1	9/0/0	9/0/0	6/0/3	9/0/0	8/0/1
	Mean	**1.556**	1.889	3.111	7.444	8.667	6.444	4.000	5.889	6.000
	Rank	**1**	2	3	8	9	7	4	5	6
5	+/−/ =	~	0/0/9	3/0/6	9/0/0	9/0/0	9/0/0	6/0/3	9/0/0	9/0/0
	Mean	**1.444**	1.889	3.111	8.000	8.778	5.889	4.000	5.778	6.111
	Rank	**1**	2	3	8	9	6	4	5	7
6	+/−/ =	~	1/1/7	4/0/5	9/0/0	9/0/0	9/0/0	7/0/2	9/0/0	9/0/0
	Mean	**1.556**	1.667	2.778	7.000	8.889	5.667	4.444	7.000	6.000
	Rank	**1**	2	3	7	9	5	4	7	6
15	+/−/ =	~	3/0/6	6/0/3	9/0/0	9/0/0	9/0/0	9/0/0	9/0/0	9/0/0
	Mean	**1.000**	2.222	2.778	5.889	8.889	7.000	6.333	5.667	5.222
	Rank	**1**	2	3	6	9	8	7	5	4
20	+/−/ =	~	5/0/4	7/0/2	8/0/1	9/0/0	9/0/0	9/0/0	9/0/0	9/0/0
	Mean	**1.000**	2.000	3.222	5.667	9.000	5.778	7.000	5.222	6.111
	Rank	**1**	2	3	5	9	6	8	4	7
25	+/−/ =	~	1/0/8	6/0/3	7/0/2	9/0/0	6/0/3	8/0/1	5/0/4	8/0/1
	Mean	**1.111**	2.444	4.778	4.889	9.000	5.111	6.444	5.111	6.111
	Rank	1	2	3	4	9	5	8	5	7

Table A9
The analytical results of FSIM evaluation gained by using the WSRT

Thresholds	Item	CLACO-MIS	ACOR-MIS	MVO-MIS	HHO-MIS	SCA-MIS	BLPSO-MIS	IGWO-MIS	IWOA-MIS	CLPSO-MIS
4	+/−/ =	~	0/0/9	3/0/6	8/0/1	9/0/0	9/0/0	4/0/5	8/0/1	9/0/0
	Mean	**1.778**	1.778	3.333	7.222	8.111	6.778	3.222	6.222	6.556
	Rank	**1**	1	4	8	9	7	3	5	6
5	+/−/ =	~	0/0/9	3/0/6	9/0/0	9/0/0	9/0/0	4/0/5	9/0/0	9/0/0
	Mean	**1.444**	1.889	3.111	7.222	7.889	6.889	3.556	6.333	6.667
	Rank	**1**	2	3	8	9	7	4	5	6
6	+/−/ =	~	1/0/8	3/0/6	8/0/1	9/0/0	9/0/0	8/0/1	9/0/0	9/0/0
	Mean	**1.444**	2.444	2.333	6.333	8.667	6.333	4.000	6.556	6.889
	Rank	**1**	3	2	5	9	5	4	7	8
15	+/−/ =	~	4/0/5	8/0/1	9/0/0	9/0/0	9/0/0	9/0/0	9/0/0	9/0/0
	Mean	**1.000**	2.222	2.778	5.222	9.000	7.222	6.556	5.333	5.667
	Rank	**1**	2	3	4	9	8	7	5	6
20	+/−/ =	~	5/0/4	7/0/2	8/0/1	9/0/0	9/0/0	9/0/0	9/0/0	9/0/0
	Mean	**1.000**	2.222	2.889	6.333	9.000	6.222	6.778	4.889	5.667
	Rank	**1**	2	3	7	9	6	8	4	5
25	+/−/ =	~	1/0/8	6/0/3	8/0/1	9/0/0	8/0/1	8/0/1	7/0/2	8/0/1
	Mean	**1.222**	2.222	4.333	5.000	8.889	5.889	6.333	4.556	6.556
	Rank	**1**	2	3	5	9	6	7	4	8

Table A10
The analytical results of SSIM evaluation gained by using the WSRT

Thresholds	Item	CLACO-MIS	ACOR-MIS	MVO-MIS	HHO-MIS	SCA-MIS	BLPSO-MIS	IGWO-MIS	IWOA-MIS	CLPSO-MIS
4	+/−/ =	~	1/0/8	4/1/4	7/0/2	7/1/1	9/0/0	3/2/4	7/0/2	8/0/1
	Mean	**2.333**	2.444	3.444	7.667	5.444	7.111	2.889	6.778	6.889
	Rank	**1**	2	4	9	5	8	3	6	7
5	+/−/ =	~	0/0/9	2/0/7	8/0/1	7/1/1	7/0/2	1/1/7	7/0/2	7/0/2
	Mean	**2.111**	2.778	4.222	8.000	5.889	6.556	2.667	6.111	6.667
	Rank	**1**	3	4	9	5	7	2	6	8
6	+/−/ =	~	2/0/7	2/1/6	6/1/2	8/0/1	8/0/1	4/0/5	8/0/1	6/0/3
	Mean	**1.667**	3.000	2.667	6.222	7.444	6.444	4.000	7.000	6.556
	Rank	**1**	3	2	5	9	6	4	8	7
15	+/−/ =	~	1/0/8	4/0/5	8/0/1	9/0/0	9/0/0	9/0/0	8/0/1	9/0/0
	Mean	1.111	2.556	2.667	5.222	8.778	6.889	6.889	5.444	5.444
	Rank	**1**	2	3	4	9	7	7	5	5
20	+/−/ =	~	5/0/4	6/0/3	8/0/1	9/0/0	9/0/0	9/0/0	9/0/0	9/0/0
	Mean	**1.000**	2.667	3.000	4.778	9.000	6.222	7.222	5.000	6.111
	Rank	**1**	2	3	4	9	7	8	5	6
25	+/−/ =	~	1/0/8	5/0/4	6/0/3	9/0/0	7/0/2	8/0/1	5/0/4	8/0/1
	Mean	**1.222**	2.222	4.111	5.333	8.778	6.000	6.556	4.778	6.000
	Rank	**1**	2	3	5	9	6	8	4	6

Table A11
The maximum 2D Kapur's entropy obtained by each method

Image	Thresholds	CLACO-MIS	ACOR-MIS	MVO-MIS	HHO-MIS	SCA-MIS	BLPSO-MIS	IGWO-MIS	IWOA-MIS	CLPSO-MIS
A	4	**3.872E + 01**	3.871 E+01	3.867 E+01	3.813 E+01	3.802 E+01	3.749 E+01	3.851 E+01	3.842 E+01	3.796 E+01
	5	**4.417E + 01**	4.417 E+01	4.413 E+01	4.316 E+01	4.216 E+01	4.274 E+01	4.391 E+01	4.361 E+01	4.251 E+01
	6	**4.933E + 01**	4.930 E+01	4.926 E+01	4.871 E+01	4.647 E+01	4.792 E+01	4.887 E+01	4.841 E+01	4.805 E+01
	15	**8.775E + 01**	8.751 E+01	8.634 E+01	8.559 E+01	7.675 E+01	8.081 E+01	8.254 E+01	8.268 E+01	8.233 E+01
	20	**1.028E + 02**	1.020 E+02	1.005 E+02	9.757 E+01	8.820 E+01	9.494 E+01	9.569 E+01	9.714 E+01	9.503 E+01
	25	1.135 E+02	**1.137E + 02**	1.098 E+02	1.128 E+02	1.039 E+02	1.042 E+02	1.070 E+02	1.075 E+02	1.084 E+02
B	4	**3.865E + 01**	3.864 E+01	3.862 E+01	3.846 E+01	3.762 E+01	3.567 E+01	3.855 E+01	3.810 E+01	3.759 E+01
	5	**4.431E + 01**	4.430 E+01	4.426 E+01	4.399 E+01	4.221 E+01	4.189 E+01	4.423 E+01	4.321 E+01	4.271 E+01
	6	4.958 E+01	**4.964E + 01**	4.942 E+01	4.839 E+01	4.632 E+01	4.638 E+01	4.911 E+01	4.825 E+01	4.743 E+01
	15	**8.630E + 01**	8.601 E+01	8.525 E+01	8.372 E+01	7.764 E+01	7.842 E+01	8.241 E+01	8.274 E+01	8.108 E+01
	20	**1.006E + 02**	9.966 E+01	9.838 E+01	9.810 E+01	8.751 E+01	9.208 E+01	9.616 E+01	9.597 E+01	9.633 E+01
	25	**1.129E + 02**	1.127 E+02	1.104 E+02	1.098 E+02	9.739 E+01	1.010 E+02	1.055 E+02	1.077 E+02	1.023 E+02
C	4	**3.852E + 01**	3.852 E+01	3.852 E+01	3.834 E+01	3.765 E+01	3.707 E+01	3.843 E+01	3.844 E+01	3.778 E+01
	5	**4.441E + 01**	4.440 E+01	4.426 E+01	4.333 E+01	4.274 E+01	4.272 E+01	4.427 E+01	4.400 E+01	4.322 E+01
	6	**4.989E + 01**	4.978 E+01	4.969 E+01	4.874 E+01	4.610 E+01	4.768 E+01	4.899 E+01	4.855 E+01	4.819 E+01
	15	**8.657E + 01**	8.582 E+01	8.538 E+01	8.534 E+01	7.757 E+01	8.216 E+01	8.379 E+01	8.280 E+01	8.370 E+01
	20	**1.008E + 02**	1.007 E+02	9.858 E+01	9.994 E+01	8.893 E+01	9.576 E+01	9.614 E+01	9.788 E+01	9.522 E+01
	25	**1.131E + 02**	1.126 E+02	1.104 E+02	1.118 E+02	9.940 E+01	1.050 E+02	1.052 E+02	1.072 E+02	1.069 E+02
D	4	3.885 E+01	**3.902E + 01**	3.876 E+01	3.882 E+01	3.738 E+01	3.726 E+01	3.865 E+01	3.855 E+01	3.784 E+01
	5	**4.492E + 01**	4.488 E+01	4.474 E+01	4.427 E+01	4.300 E+01	4.402 E+01	4.422 E+01	4.398 E+01	4.415 E+01
	6	**5.036E + 01**	5.033 E+01	4.994 E+01	4.913 E+01	4.704 E+01	4.750 E+01	4.932 E+01	4.982 E+01	4.877 E+01
	15	**8.722E + 01**	8.689 E+01	8.485 E+01	8.464 E+01	7.853 E+01	8.119 E+01	8.202 E+01	8.303 E+01	8.249 E+01
	20	**1.017E + 02**	1.003 E+02	9.961 E+01	9.715 E+01	8.864 E+01	9.314 E+01	9.553 E+01	9.707 E+01	9.525 E+01
	25	1.124 E+02	**1.129E + 02**	1.092 E+02	1.101 E+02	9.887 E+01	1.036 E+02	1.040 E+02	1.093 E+02	1.049 E+02
E	4	**3.865E + 01**	3.865 E+01	3.863 E+01	3.830 E+01	3.768 E+01	3.667 E+01	3.862 E+01	3.793 E+01	3.802 E+01
	5	**4.441E + 01**	4.440 E+01	4.431 E+01	4.362 E+01	4.130 E+01	4.339 E+01	4.427 E+01	4.325 E+01	4.255 E+01
	6	**4.983E + 01**	4.978 E+01	4.950 E+01	4.785 E+01	4.550 E+01	4.685 E+01	4.884 E+01	4.853 E+01	4.744 E+01
	15	8.665 E+01	**8.685E + 01**	8.558 E+01	8.411 E+01	7.637 E+01	8.089 E+01	8.119 E+01	8.292 E+01	8.142 E+01
	20	**1.015E + 02**	1.008 E+02	9.929 E+01	1.000 E+02	8.995 E+01	9.157 E+01	9.487 E+01	9.547 E+01	9.727 E+01
	25	**1.123E + 02**	1.104 E+02	1.107 E+02	1.085 E+02	1.018 E+02	1.010 E+02	1.048 E+02	1.065 E+02	1.057 E+02
F	4	3.840 E+01	3.840 E+01	**3.841E + 01**	3.784 E+01	3.776 E+01	3.713 E+01	3.833 E+01	3.793 E+01	3.729 E+01
	5	**4.401E + 01**	4.401 E+01	4.397 E+01	4.266 E+01	4.200 E+01	4.259 E+01	4.368 E+01	4.343 E+01	4.258 E+01
	6	**4.935E + 01**	4.931 E+01	4.920 E+01	4.825 E+01	4.788 E+01	4.773 E+01	4.873 E+01	4.798 E+01	4.780 E+01
	15	**8.629E + 01**	8.578 E+01	8.366 E+01	8.381 E+01	7.716 E+01	8.164 E+01	8.158 E+01	8.177 E+01	8.120 E+01
	20	**1.010E + 02**	9.946 E+01	9.867 E+01	9.667 E+01	8.795 E+01	9.335 E+01	9.390 E+01	9.553 E+01	9.386 E+01
	25	**1.104E + 02**	1.100 E+02	1.092 E+02	1.090 E+02	9.695 E+01	1.018 E+02	1.037 E+02	1.058 E+02	1.036 E+02
G	4	**3.853E + 01**	3.852 E+01	3.852 E+01	3.840 E+01	3.799 E+01	3.684 E+01	3.849 E+01	3.838 E+01	3.807 E+01
	5	**4.419E + 01**	4.419 E+01	4.404 E+01	4.388 E+01	4.216 E+01	4.209 E+01	4.382 E+01	4.337 E+01	4.305 E+01
	6	**4.965E + 01**	4.960 E+01	4.952 E+01	4.857 E+01	4.699 E+01	4.733 E+01	4.876 E+01	4.851 E+01	4.781 E+01
	15	**8.654E + 01**	8.628 E+01	8.516 E+01	8.422 E+01	7.655 E+01	8.056 E+01	8.173 E+01	8.288 E+01	8.189 E+01
	20	**1.012E + 02**	9.994 E+01	9.914 E+01	9.842 E+01	8.960 E+01	9.466 E+01	9.586 E+01	9.686 E+01	9.504 E+01
	25	1.113 E+02	**1.126E + 02**	1.088 E+02	1.101 E+02	9.681 E+01	1.039 E+02	1.055 E+02	1.078 E+02	1.070 E+02
H	4	**3.872E + 01**	3.872 E+01	3.869 E+01	3.853 E+01	3.739 E+01	3.690 E+01	3.868 E+01	3.854 E+01	3.751 E+01
	5	**4.456E + 01**	4.456 E+01	4.445 E+01	4.374 E+01	4.210 E+01	4.213 E+01	4.427 E+01	4.407 E+01	4.401 E+01
	6	**4.984E + 01**	4.981 E+01	4.978 E+01	4.898 E+01	4.706 E+01	4.739 E+01	4.958 E+01	4.908 E+01	4.835 E+01
	15	**8.639E + 01**	8.604 E+01	8.468 E+01	8.366 E+01	7.692 E+01	7.984 E+01	8.077 E+01	8.267 E+01	8.172 E+01
	20	**1.005E + 02**	9.956 E+01	1.003 E+02	9.869 E+01	8.698 E+01	9.315 E+01	9.450 E+01	9.597 E+01	9.416 E+01
	25	1.109 E+02	1.100 E+02	**1.112E + 02**	1.105 E+02	9.802 E+01	1.038 E+02	1.061 E+02	1.075 E+02	1.054 E+02
I	4	**3.883E + 01**	3.881 E+01	3.824 E+01	3.765 E+01	3.713 E+01	3.736 E+01	3.849 E+01	3.765 E+01	3.774 E+01
	5	4.418 E+01	4.411 E+01	**4.421E + 01**	4.316 E+01	4.246 E+01	4.276 E+01	4.344 E+01	4.293 E+01	4.313 E+01
	6	**4.958E + 01**	4.949 E+01	4.935 E+01	4.830 E+01	4.677 E+01	4.760 E+01	4.893 E+01	4.865 E+01	4.801 E+01
	15	8.695 E+01	**8.736E + 01**	8.550 E+01	8.484 E+01	7.611 E+01	8.014 E+01	8.233 E+01	8.229 E+01	8.123 E+01
	20	**1.010E + 02**	9.974 E+01	1.003 E+02	9.938 E+01	8.744 E+01	9.282 E+01	9.474 E+01	9.648 E+01	9.595 E+01
	25	**1.127E + 02**	1.111 E+02	1.109 E+02	1.095 E+02	9.719 E+01	1.033 E+02	1.084 E+02	1.090 E+02	1.041 E+02

Appendix B

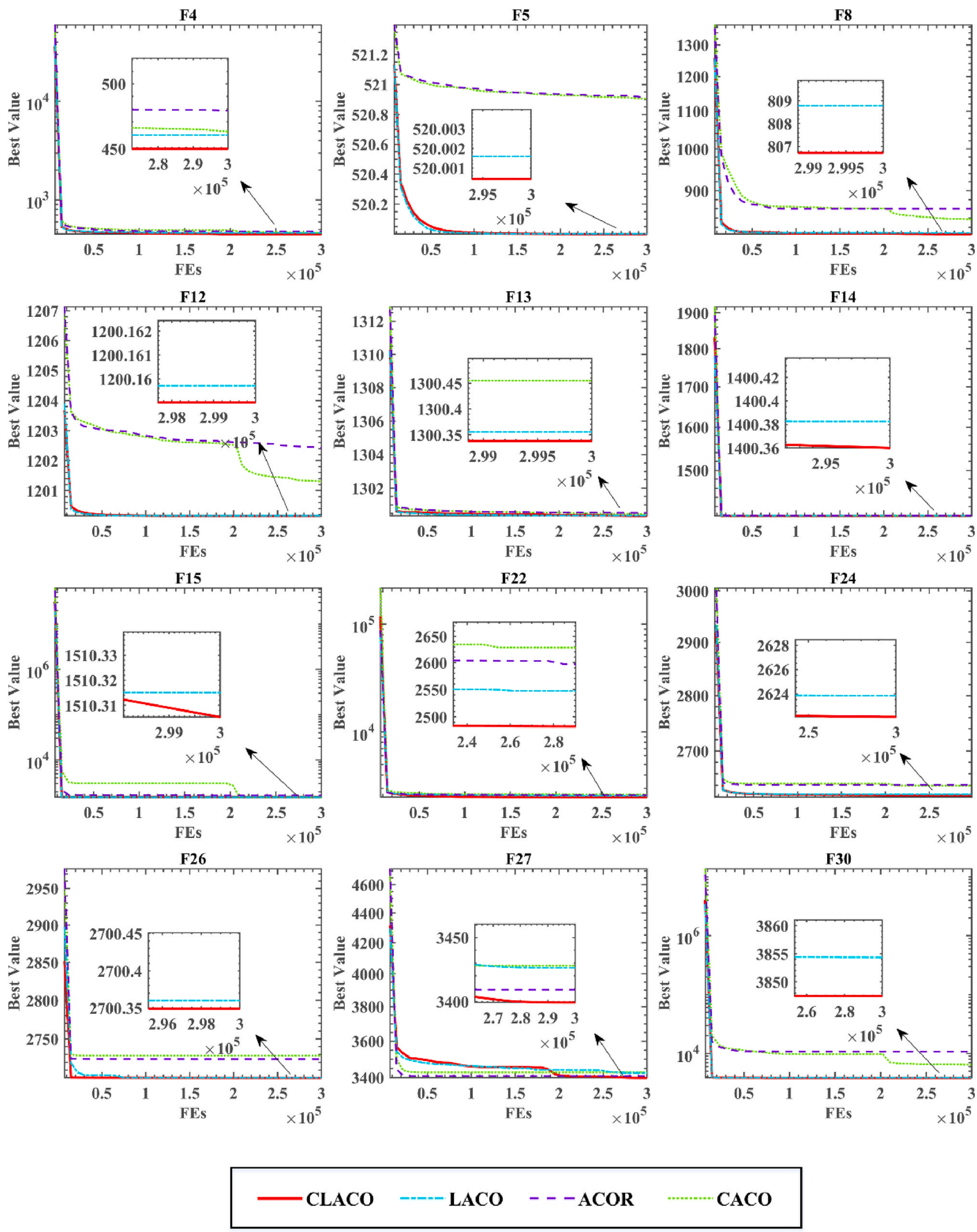

Fig. B1. Some convergence curves obtained by four variants

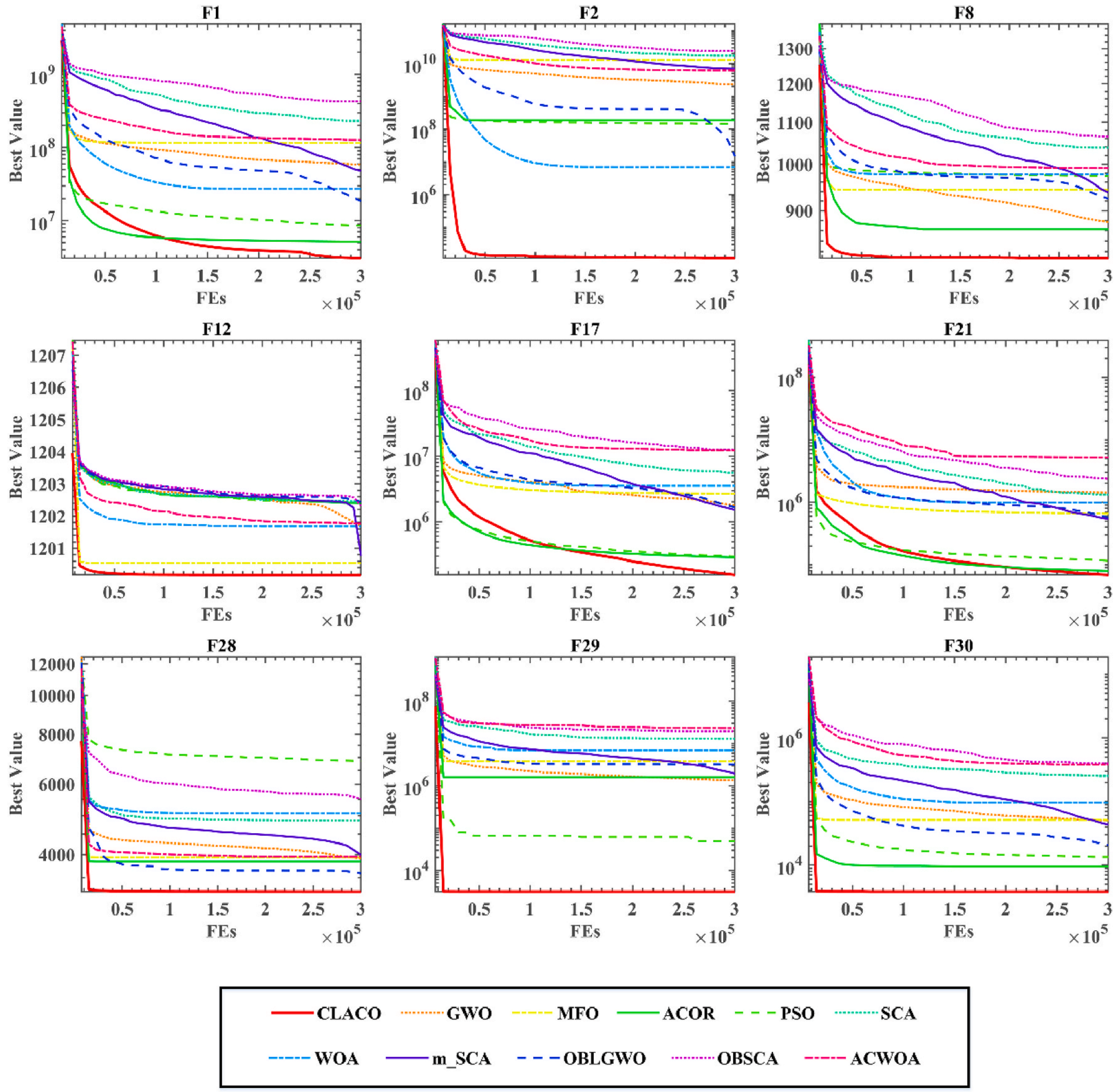

Fig. B2. Some convergence curves obtained by CLACO and some excellent peer

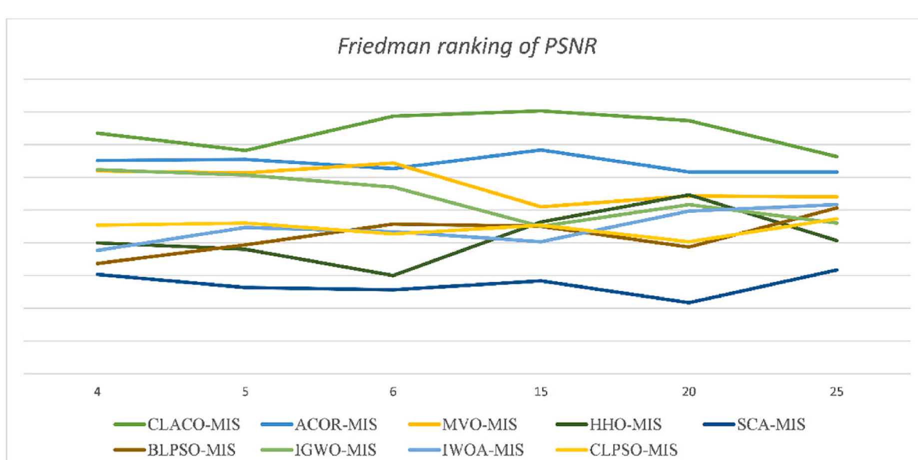

Fig. B3. The Friedman ranking of PSNR at different threshold levels

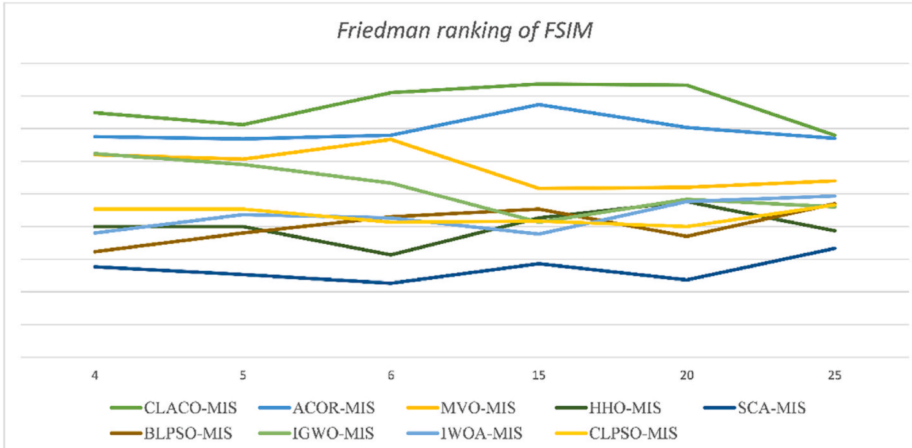

Fig. B4. The Friedman ranking of FSIM at different threshold levels

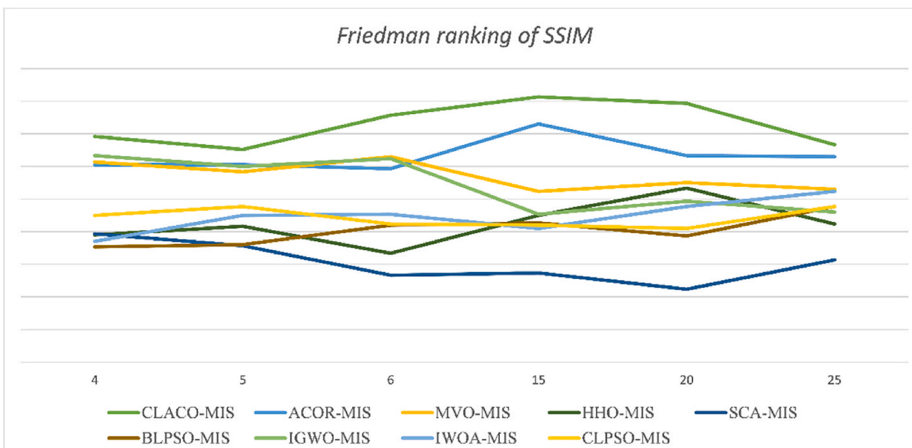

Fig. B5. The Friedman ranking of SSIM at different threshold levels

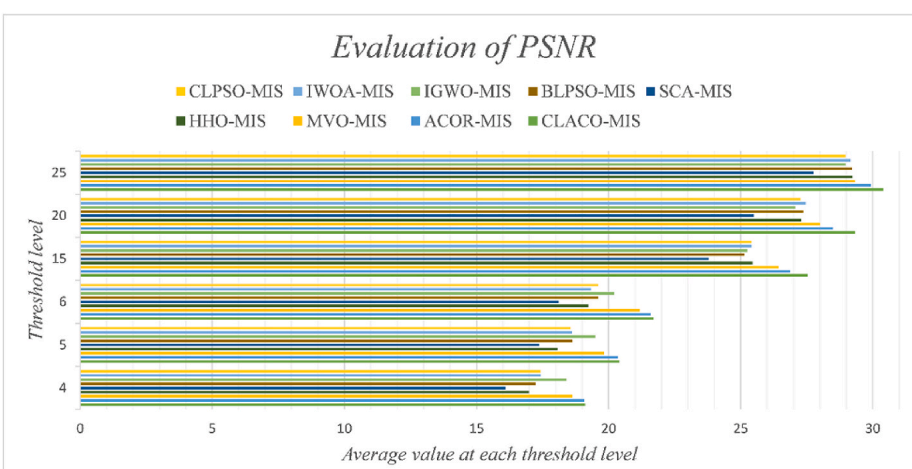

Fig. B6. Overall average results of PSNR evaluation at each threshold level

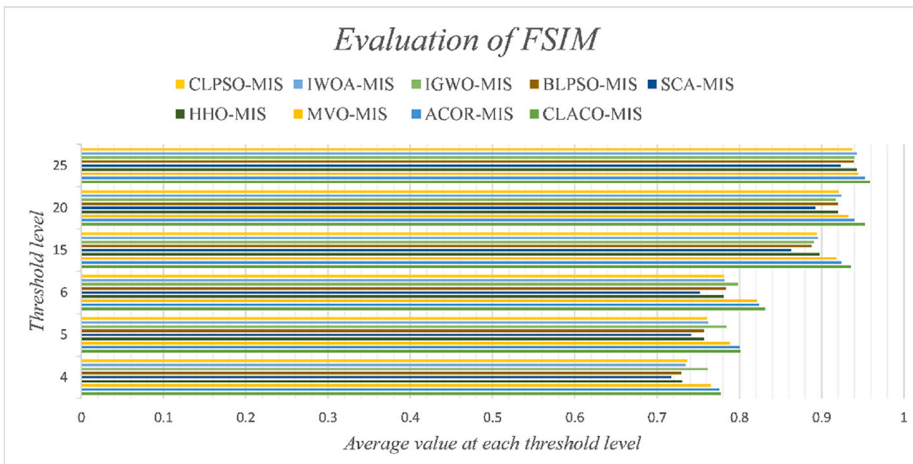

Fig. B7. Overall average results of FSIM evaluation at each threshold level

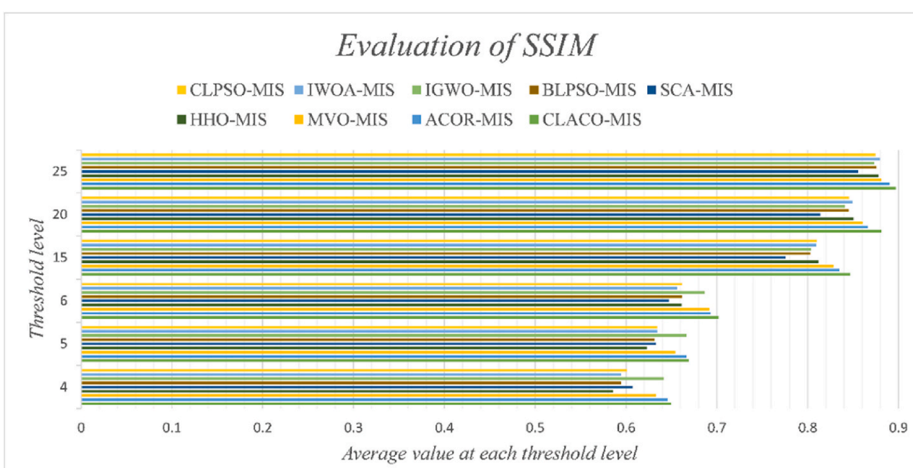

Fig. B8. Overall average results of SSIM evaluation at each threshold level

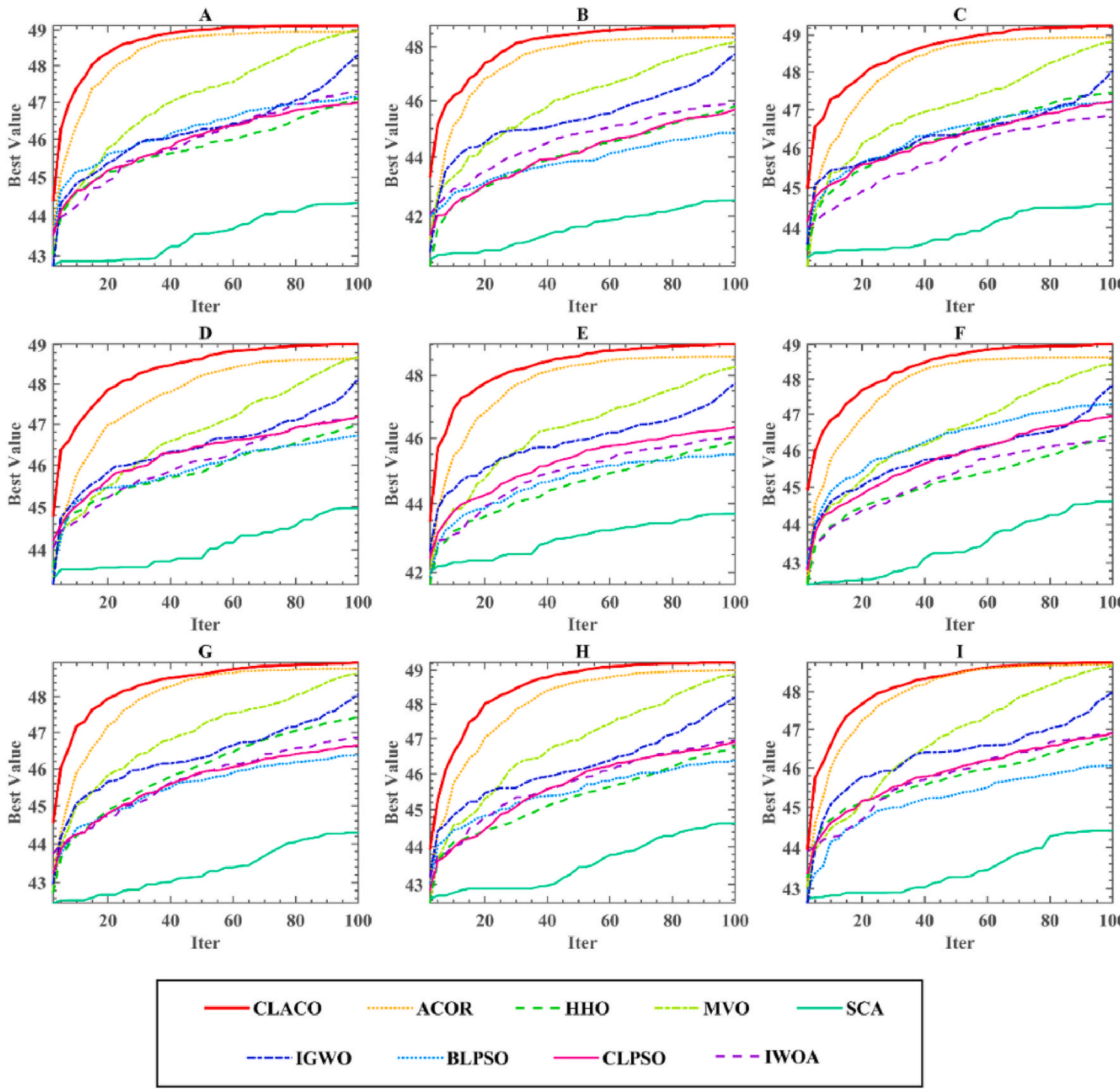

Fig. B9. All convergence curves obtained by CLACO-MIS and its peers at threshold level 6

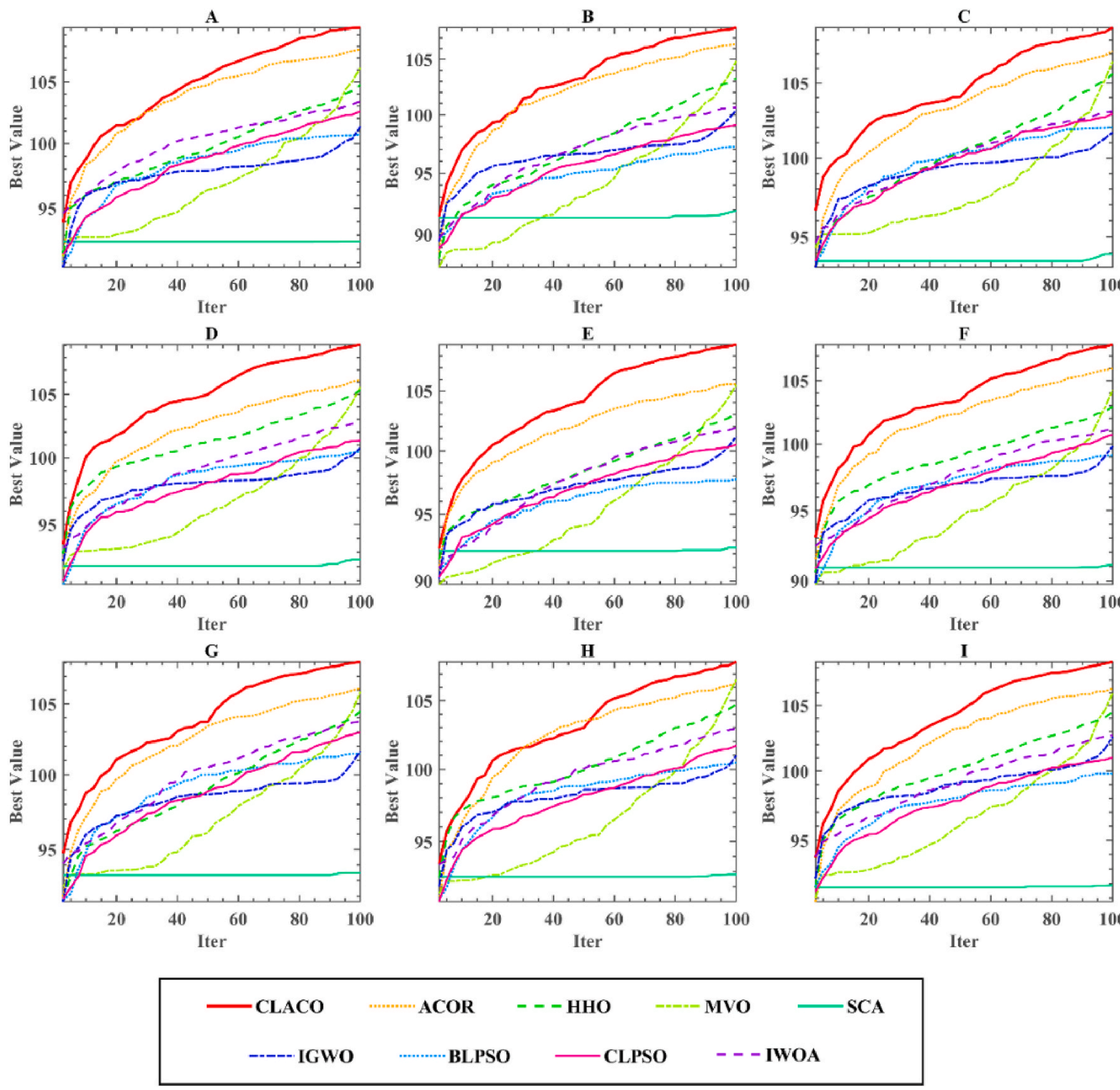

Fig. B10. All convergence curves obtained by CLACO-MIS and its peers at threshold level 25

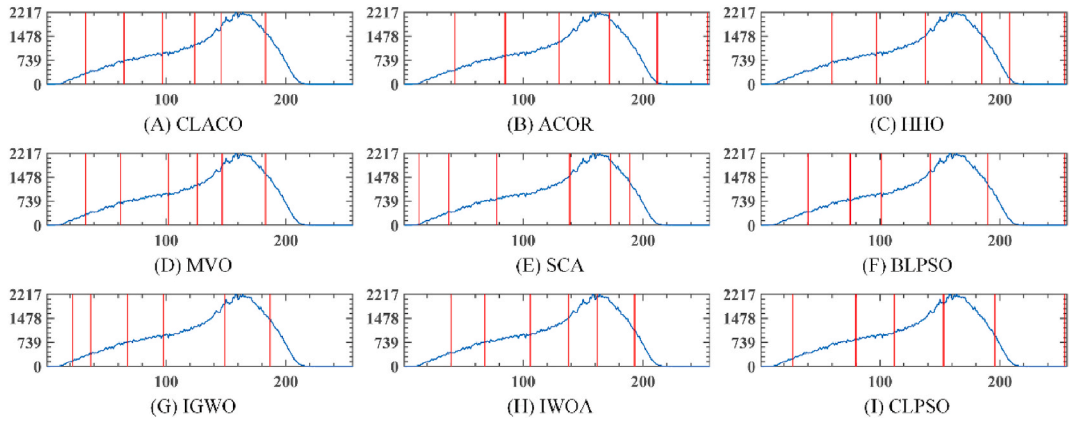

Fig. B11. The optimal threshold segmentation image of A at threshold level 6

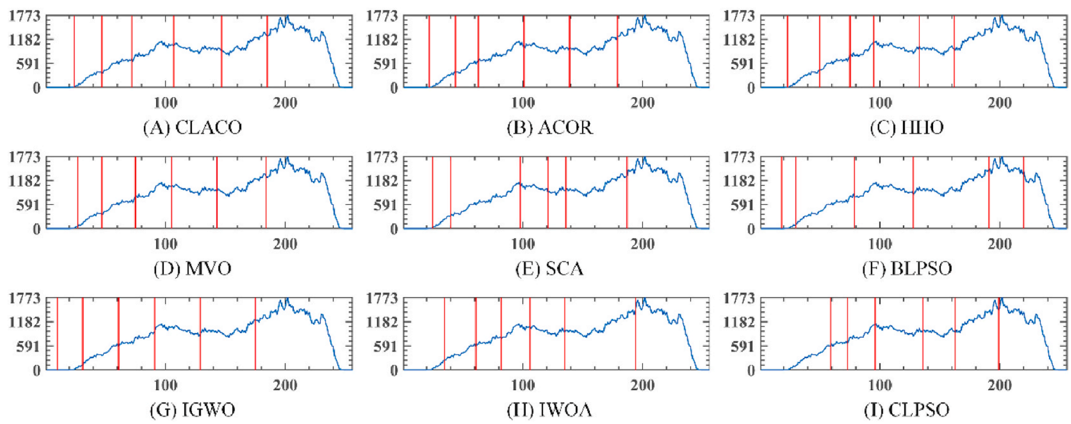

Fig. B12. The optimal threshold segmentation image of B at threshold level 6

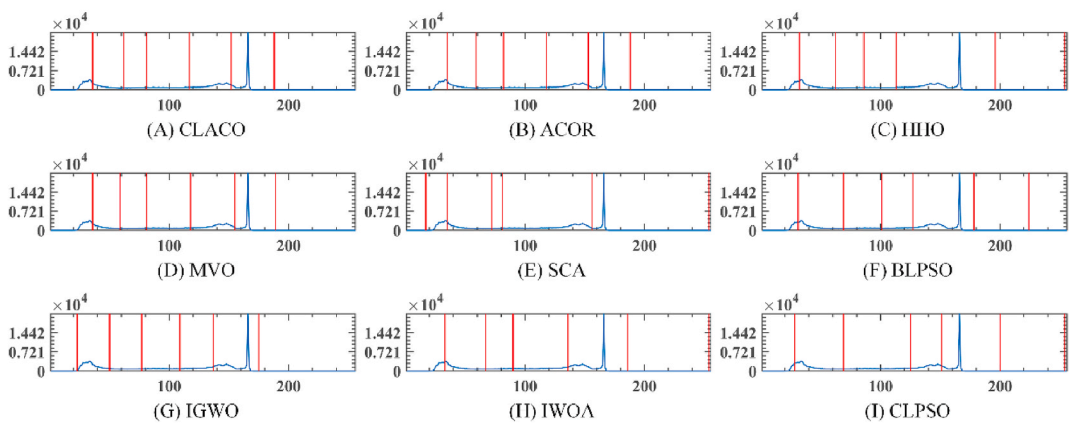

Fig. B13. The optimal threshold segmentation image of C at threshold level 6

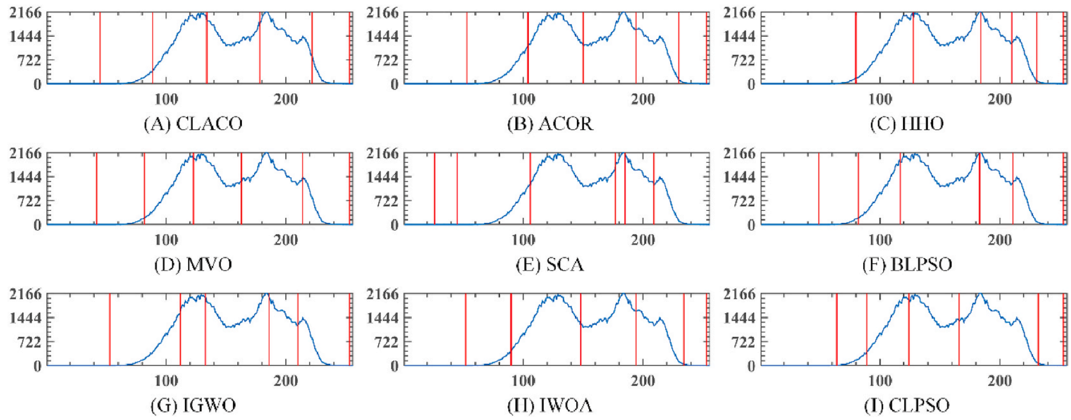

Fig. B14. The optimal threshold segmentation image of D at threshold level 6

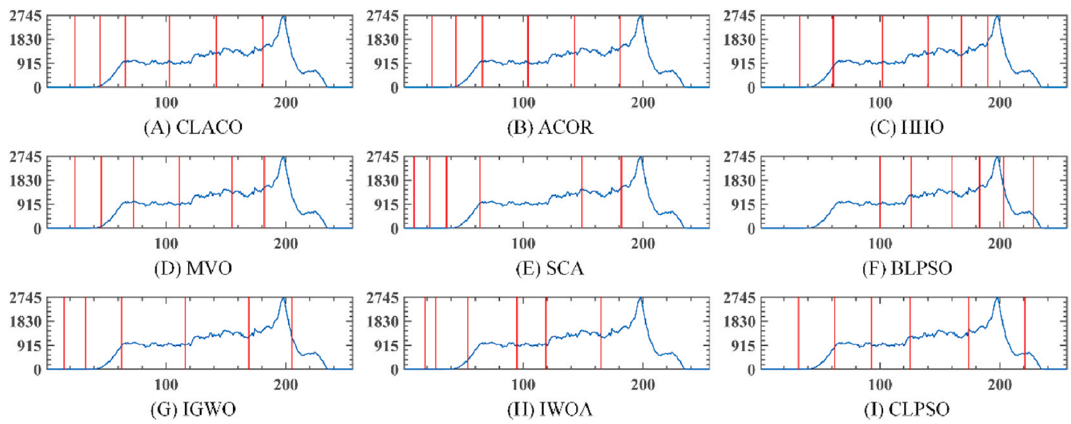

Fig. B15. The optimal threshold segmentation image of E at threshold level 6

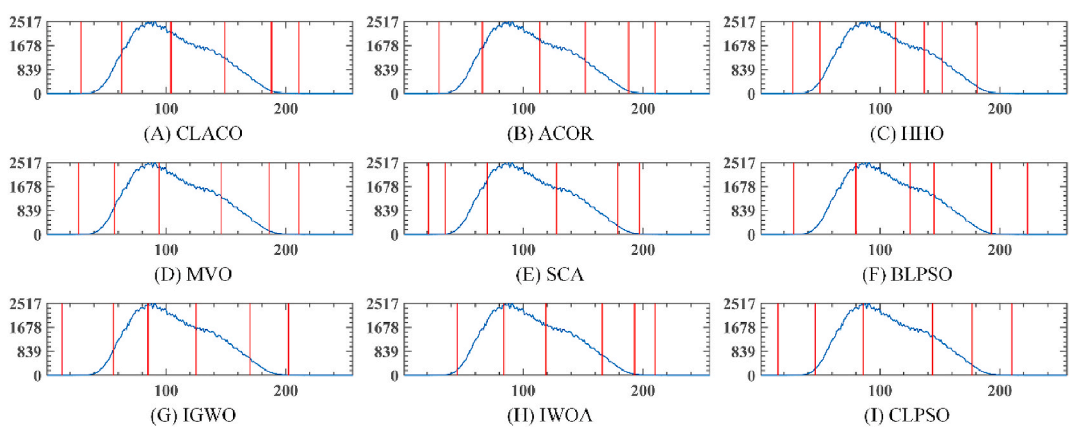

Fig. B16. The optimal threshold segmentation image of F at threshold level 6

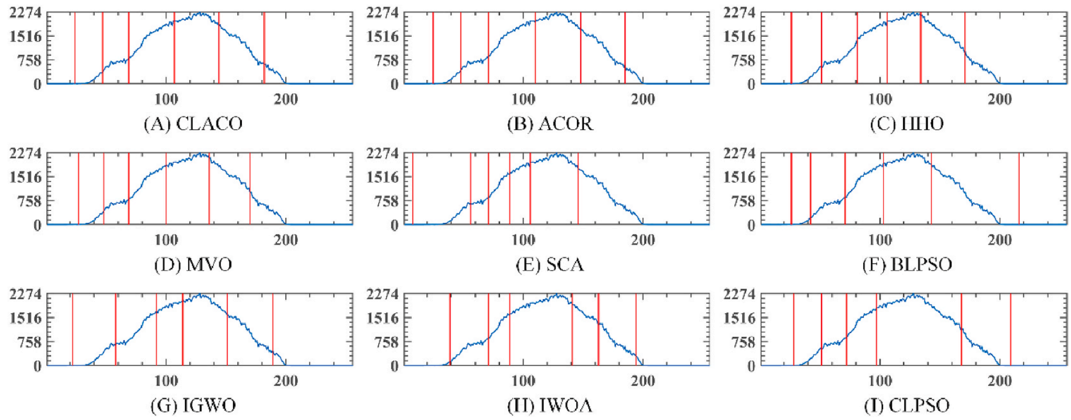

Fig. B17. The optimal threshold segmentation image of G at threshold level 6

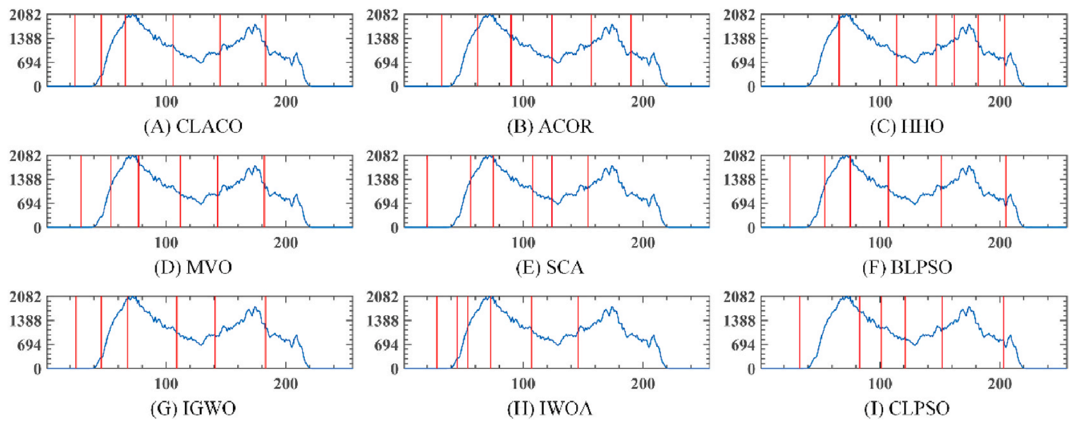

Fig. B18. The optimal threshold segmentation image of H at threshold level 6

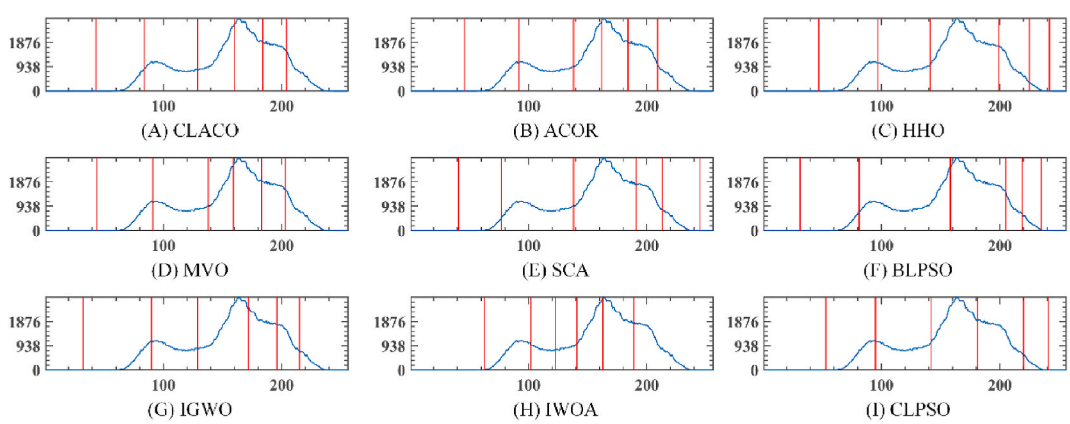

Fig. B19. The optimal threshold segmentation image of I at threshold level 6

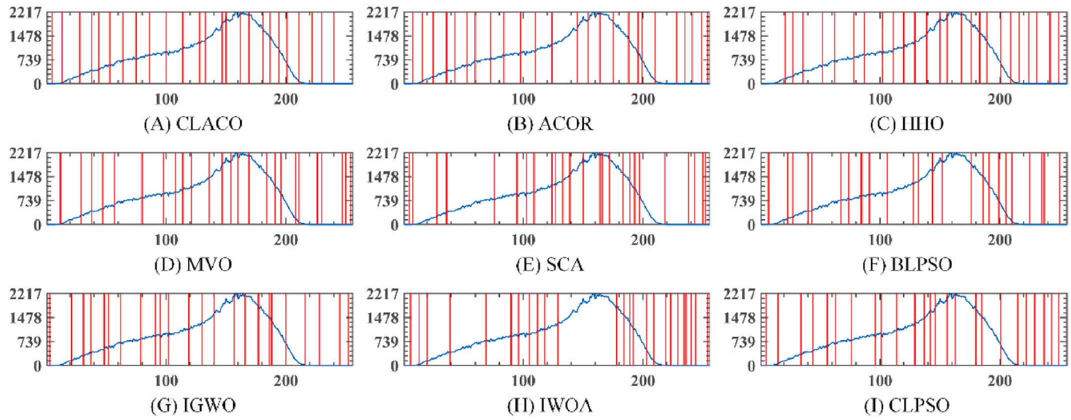

Fig. B20. The optimal threshold segmentation image of A at threshold level 25

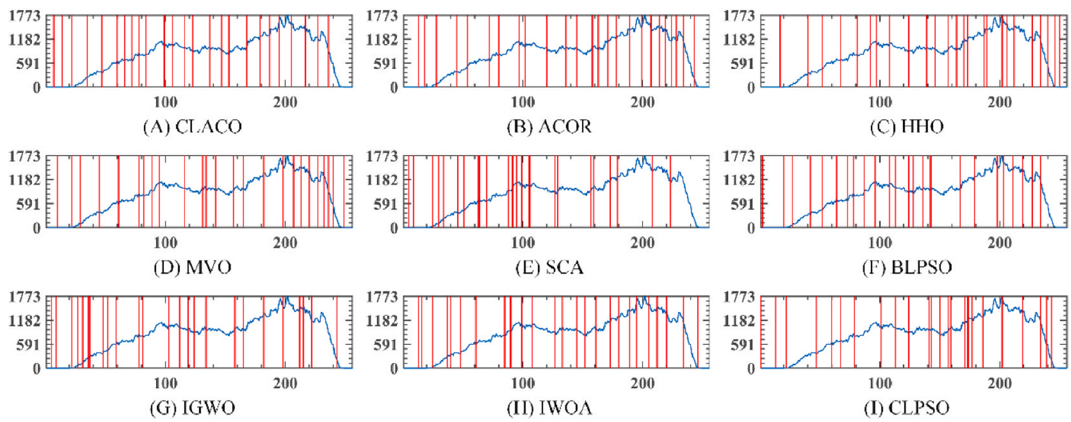

Fig. B21. The optimal threshold segmentation image of B at threshold level 25

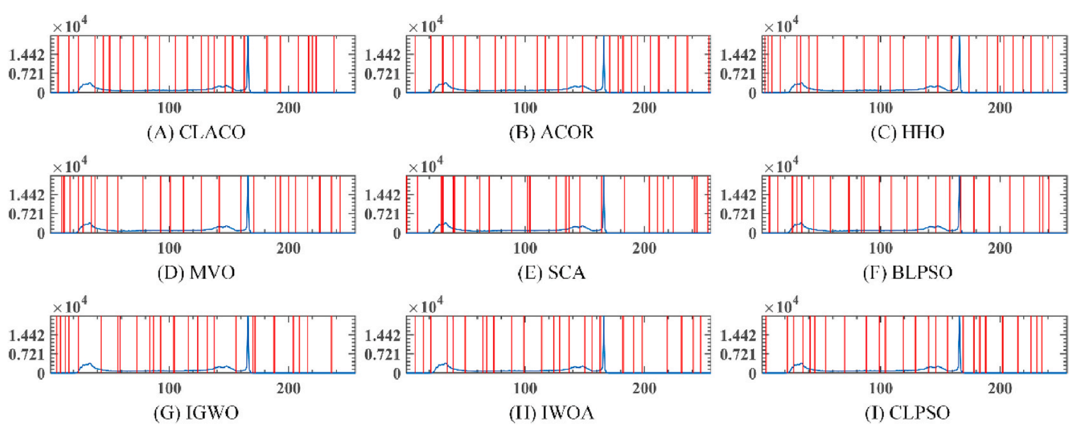

Fig. B22. The optimal threshold segmentation image of C at threshold level 25

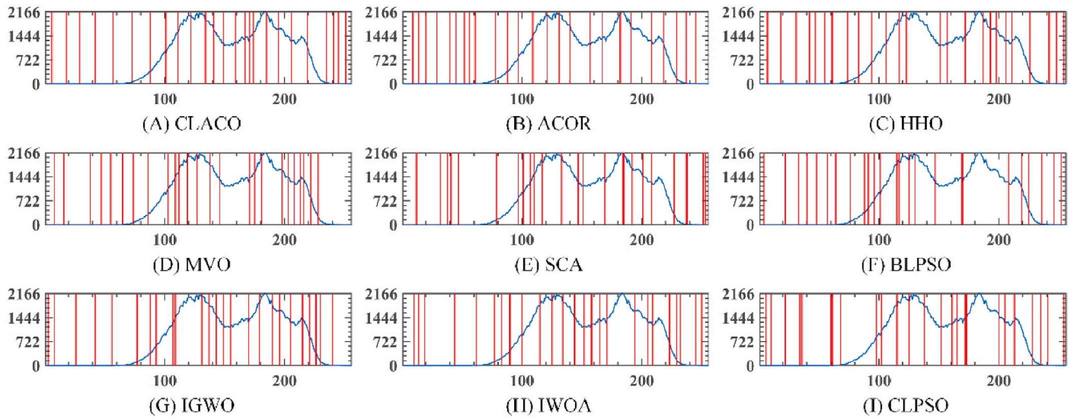

Fig. B23. The optimal threshold segmentation image of D at threshold level 25

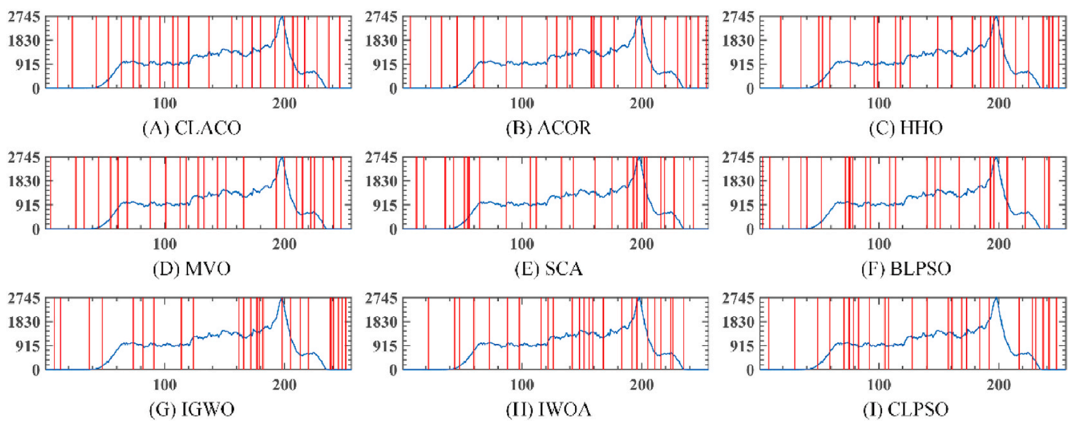

Fig. B24. The optimal threshold segmentation image of E at threshold level 25

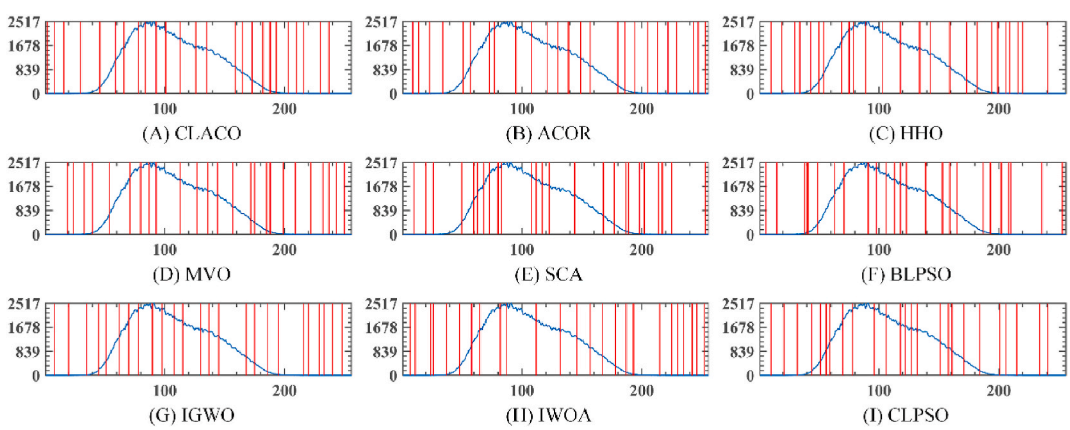

Fig. B25. The optimal threshold segmentation image of F at threshold level 25

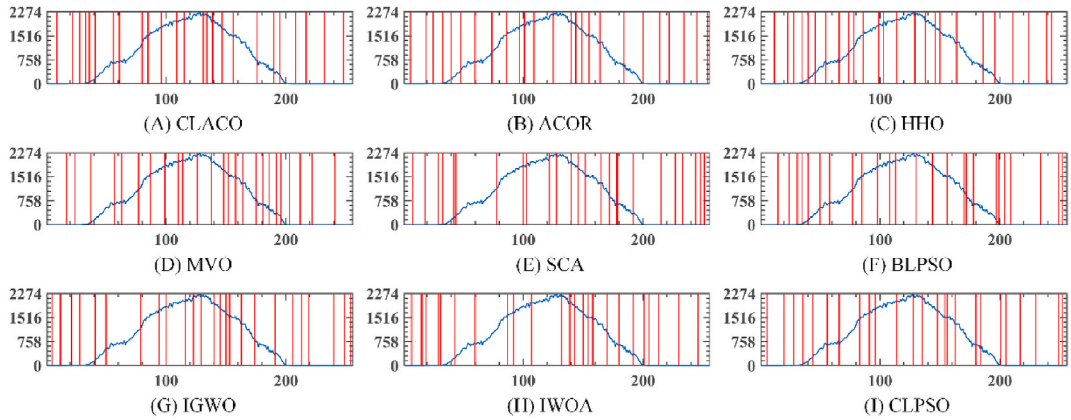

Fig. B26. The optimal threshold segmentation image of G at threshold level 25

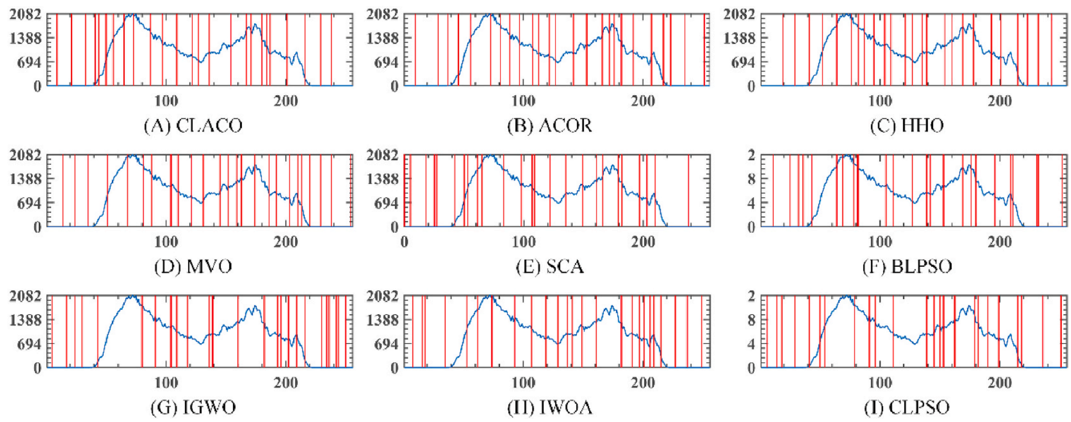

Fig. B27. The optimal threshold segmentation image of H at threshold level 25

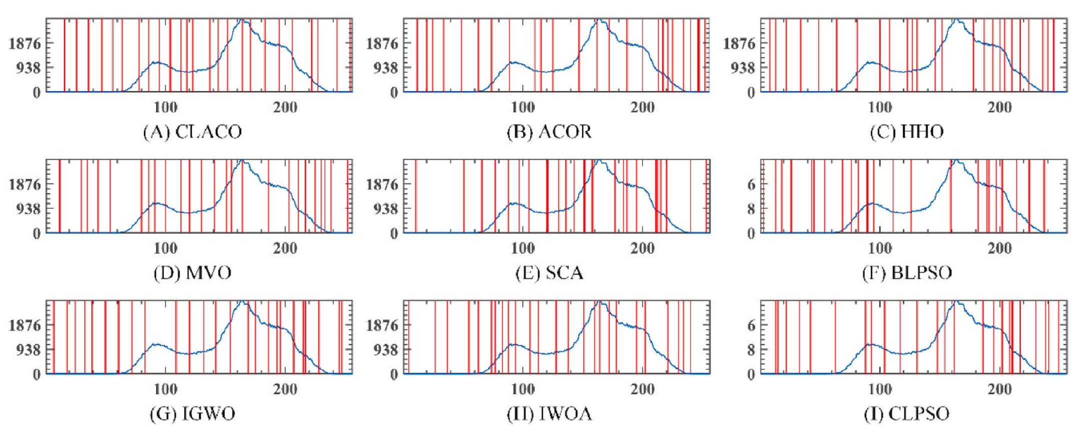

Fig. B28. The optimal threshold segmentation image of I at threshold level 25

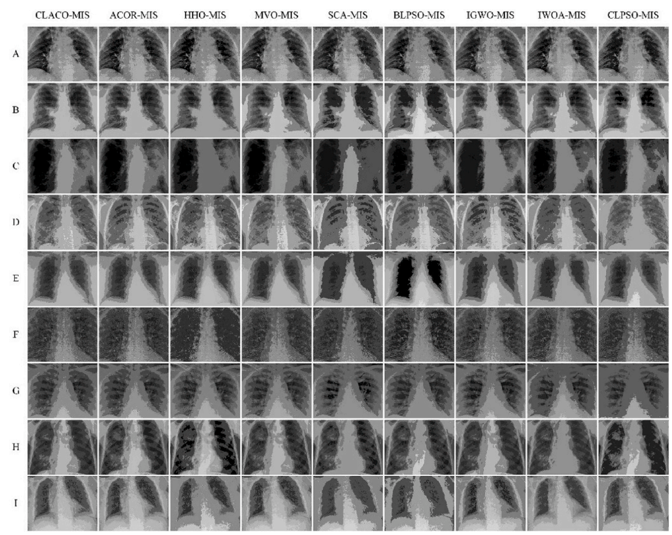

Fig. B29. All segmentation results of CLACO-MIS and its peers at threshold level 6

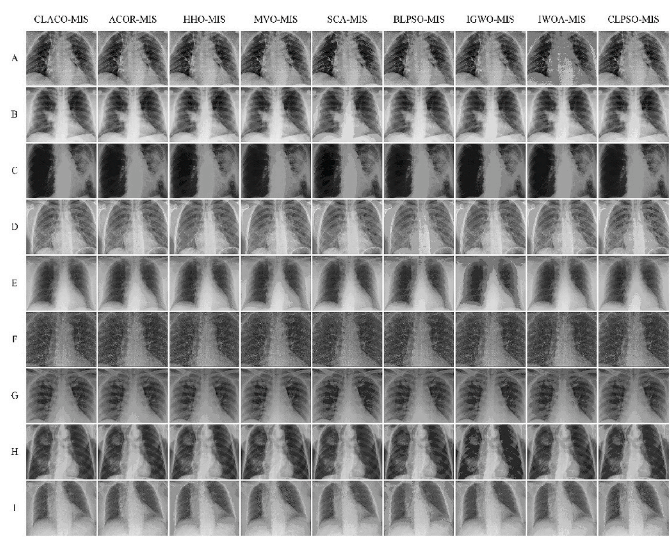

Fig. B30. All segmentation results of CLACO-MIS and its peers at threshold level 25

Appendix C. An overview of ACOR

It is a version of the continuous ACO presented by Socha et al. [75], which enables the original ACO algorithm to break through the limitation that it can only be used to solve discrete problems. In ACOR, its core is mainly achieved by transforming discrete probability distribution to the continuous probability distribution, as well as by using some solutions to form a solution archive, which is applied to realize the update of pheromones.

In the case of continuous probability density functions, the Gaussian kernel function is adopted by ACOR as the probability density distribution function, in which the Gaussian kernel function $G^i(x)$, shown in Eq. (16) [75], is obtained by weighting together with certain 1D Gaussian functions.

$$G^i(x) = \sum_{l=1}^{k} w_l g_l^i(x) = \sum_{l=1}^{k} w_l \frac{1}{\sigma_l^i \sqrt{2\pi}} e^{-\frac{\left(x-\mu_l^i\right)^2}{2\sigma_l^{i\,2}}} \tag{16}$$

where k refers to the number of Gaussian functions in a single dimension, $w = \{w_1, \ldots, w_k\}$refers to the weight vector, $\mu^i = \{\mu_1^i, \ldots, \mu_k^i\}$ refers to the mean vector, and $\sigma^i = \{\sigma_1^i, \ldots, \sigma_k^i\}$ refers to the standard deviation vector.

Besides, in the constructed solution profile, each solution is stored along with the objective function value as well as the corresponding weight value of each solution. Just as seen in Fig. C1, the solution ranking is decided by an order of the quality corresponding to the value of the appropriate objective function, and the better the quality is, the lower the order is.

In this way, assuming that the magnitude of the function value of the individual solution meets the condition $f(x_1) \le \ldots f(x_l) \le \ldots f(x_k)$, it can be introduced that the individual weights w_l then satisfy $w_1 \ge \ldots w_l \ge \ldots w_k$, where the value of w_l can be obtained by using Eq. (17) [75].

$$w_l = \frac{1}{qk\sqrt{2\pi}} e^{-\frac{(l-1)^2}{2q^2k^2}} \tag{17}$$

where q is a parameter of ACOR. If q is smaller, then the weight of the optimal solution is higher, which means that the probability of the optimal solution being selected is higher, thus this parameter can be used to optimize the local and global optima.

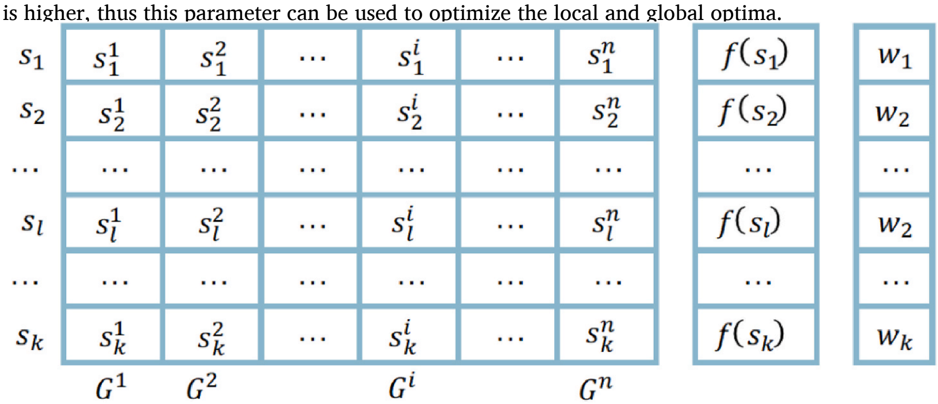

Fig. C1. The archive with k ants kept in ACOR

What the sampling process is implemented in practice is first to calculate the weight size w_l , to choose a Gaussian function $g_l^i(x)$ based on the probability p_l, and to determine the guiding solution s_l, which is subsequently sampled around each position vector of the guiding solution s_l employing a Gaussian function, where p_l is computed according to Eq. (18) [75], μ_l^i is obtained according to Eq. (19) [75], andσ_l^i is computed according to Eq. (20) [75].

$$p_l = \frac{w_l}{\sum_{r=1}^{k} w_r} \tag{18}$$

$$\mu^i = \{\mu_1^i, \dots, \mu_k^i\} = \{s_1^i, \dots, s_k^i\} \tag{19}$$

$$\sigma_l^i = \xi \sum_{e=1}^{k} \frac{|s_e^i - s_l^i|}{k-1} \tag{20}$$

where ξ is a parameter and $\xi > 0$ that plays the same role as the pheromone volatilization rate in the original ACO, where the larger the value of ξ is, the slower the convergence rate is.

The pheromone update process in ACOR is replaced by the update process of the solution in the solution archive. The process of updating the solutions is to merge the m new solutions constructed by the ant and the k old solutions in the solution archive in each iteration, and select the k better solutions from these $m + k$ solutions to put it into the solution archive after sorting, while the rest of the m worse solutions are discarded. A flowchart of the ACOR algorithm is presented in Fig. C2.

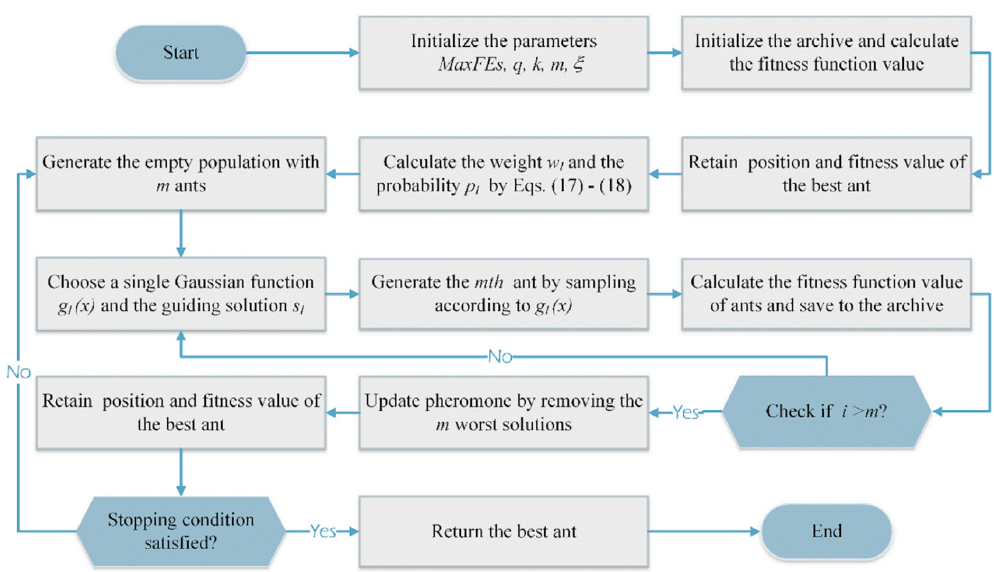

Fig. C2. Flowchart of ACOR

References

[1] T.E. Simos, C. Tsitouras, V.N. Kovalnogov, R.V. Fedorov, D.A. Generalov, Real-time estimation of R0 for COVID-19 spread, Mathematics 9 (2021) 664.
[2] A.M. Ismael, A. Şengür, Deep learning approaches for COVID-19 detection based on chest X-ray images, Expert Syst. Appl. 164 (2021) 114054.
[3] G. Maguolo, L. Nanni, A critic evaluation of methods for covid-19 automatic detection from x-ray images, Inf. Fusion 76 (2021) 1–7.
[4] E.E.-D. Hemdan, M.A. Shouman, M.E. Karar, Covidx-net: A Framework of Deep Learning Classifiers to Diagnose Covid-19 in X-Ray Images, 2020 arXiv preprint arXiv:2003.11055.
[5] B.-H. Li, Y. Liu, A.-M. Zhang, W.-H. Wang, S. Wan, A survey on blocking technology of entity resolution, J. Comput. Sci. Technol. 35 (2020) 769–793.
[6] L. Chen, X. Xu, Effect evaluation of the long-term care insurance (LTCI) system on the health Care of the Elderly: a review, J. Multidiscip. Healthc. 13 (2020) 863.
[7] D. Jiang, F.-X. Chen, H. Zhou, Y.-Y. Lu, H. Tan, S.-J. Yu, J. Yuan, H. Liu, W. Meng, Z.-B. Jin, Bioenergetic crosstalk between mesenchymal stem cells and various ocular cells through the intercellular trafficking of mitochondria, Theranostics 10 (2020) 7260.
[8] D. Pan, X.-X. Xia, H. Zhou, S.-Q. Jin, Y.-Y. Lu, H. Liu, M.-L. Gao, Z.-B. Jin, COCO enhances the efficiency of photoreceptor precursor differentiation in early human embryonic stem cell-derived retinal organoids, Stem Cell Res. Ther. 11 (2020) 1–12.
[9] Y. Liu, X. Lv, Z. Tang, The Impact of Mortality Salience on Quantified Self Behavior during the COVID-19 Pandemic, Personality and Individual Differences, 2021, p. 110972.
[10] Y. Zhao, X. Yu, H. Wu, Y. Zhou, X. Sun, S. Yu, S. Yu, H. Liu, A Fast 2-D Otsu lung tissue image segmentation algorithm based on improved PSO, Microprocess. Microsyst. 80 (2021) 103527.
[12] E. Rodríguez-Esparza, L.A. Zanella-Calzada, D. Oliva, A.A. Heidari, D. Zaldivar, M. Pérez-Cisneros, L.K. Foong, An efficient Harris hawks-inspired image segmentation method, Expert Syst. Appl. 155 (2020) 113428.
[13] A.M. Anter, S. Bhattacharyya, Z. Zhang, Multi-stage fuzzy swarm intelligence for automatic hepatic lesion segmentation from CT scans, Appl. Soft Comput. 96 (2020) 106677.
[14] M. Abdel-Basset, V. Chang, R. Mohamed, HSMA_WOA: a hybrid novel Slime mould algorithm with whale optimization algorithm for tackling the image segmentation problem of chest X-ray images, Appl. Soft Comput. 95 (2020) 106642.
[15] R.K. Sambandam, S. Jayaraman, Self-adaptive dragonfly based optimal thresholding for multilevel segmentation of digital images, Journal of King Saud University - Computer and Information Sciences 30 (2018) 449–461.
[16] H. Verma, D. Verma, P.K. Tiwari, A population based hybrid FCM-PSO algorithm for clustering analysis and segmentation of brain image, Expert Syst. Appl. (2020) 114121.
[17] R. Radha, R. Gopalakrishnan, A medical analytical system using intelligent fuzzy level set brain image segmentation based on improved quantum particle swarm optimization, Microprocess. Microsyst. 79 (2020) 103283.
[18] D. Yu, Y. Mao, B. Gu, S. Nojavan, K. Jermsittiparsert, M. Nasseri, A new LQG optimal control strategy applied on a hybrid wind turbine/solid oxide fuel cell/in the presence of the interval uncertainties, Sustainable Energy, Grids and Networks 21 (2020) 100296.
[19] B. Wang, F. Zou, J. Cheng, S. Zhong, Fault detection filter design for continuous-time nonlinear Markovian jump systems with mode-dependent delay and time-varying transition probabilities, Adv. Differ. Equ. 2017 (2017) 1–23.
[20] X. Pang, K. Gong, X. Zhang, S. Wu, Y. Cui, B.-Z. Qian, Osteopontin as a multifaceted driver of bone metastasis and drug resistance, Pharmacol. Res. 144 (2019) 235–244.
[21] H. Tang, Y. Xu, A. Lin, A.A. Heidari, M. Wang, H. Chen, Y. Luo, C. Li, Predicting green consumption behaviors of students using efficient firefly grey wolf-assisted K-nearest neighbor classifiers, IEEE Access 8 (2020) 35546–35562.
[22] G. Liu, W. Jia, M. Wang, A.A. Heidari, H. Chen, Y. Luo, C. Li, Predicting cervical hyperextension injury: a covariance guided sine cosine support vector machine, IEEE access 8 (2020) 46895–46908.
[23] Y. Zhang, R. Liu, X. Wang, H. Chen, C. Li, Boosted binary Harris hawks optimizer and feature selection, Eng. Comput. (2020) 1–30.
[24] Q. Li, H. Chen, H. Huang, X. Zhao, Z. Cai, C. Tong, W. Liu, X. Tian, An enhanced grey wolf optimization based feature selection wrapped kernel extreme learning machine for medical diagnosis, Computational and mathematical methods in medicine (2017) 2017.
[25] T. Liu, L. Hu, C. Ma, Z.-Y. Wang, H.-L. Chen, A fast approach for detection of erythemato-squamous diseases based on extreme learning machine with maximum relevance minimum redundancy feature selection, Int. J. Syst. Sci. 46 (2015) 919–931.
[26] A.A. Heidari, R.A. Abbaspour, H. Chen, Efficient boosted grey wolf optimizers for global search and kernel extreme learning machine training, Appl. Soft Comput. 81 (2019) 105521.
[27] M. Wang, H. Chen, B. Yang, X. Zhao, L. Hu, Z. Cai, H. Huang, C. Tong, Toward an optimal kernel extreme learning machine using a chaotic moth-flame optimization strategy with applications in medical diagnoses, Neurocomputing 267 (2017) 69–84.
[28] M. Wang, H. Chen, Chaotic multi-swarm whale optimizer boosted support vector machine for medical diagnosis, Appl. Soft Comput. 88 (2020) 105946, https://doi.org/10.1016/j.asoc.2019.105946.
[29] X. Liang, Z. Cai, M. Wang, X. Zhao, H. Chen, C. Li, Chaotic oppositional sine–cosine method for solving global optimization problems, Eng. Comput. (2020) 1–17.
[30] H. Yu, W. Li, C. Chen, J. Liang, W. Gui, M. Wang, H. Chen, Dynamic Gaussian bare-bones fruit fly optimizers with abandonment mechanism: method and analysis, Eng. Comput. (2020) 1–29.
[31] B. Nautiyal, R. Prakash, V. Vimal, G. Liang, H. Chen, Improved Salp Swarm Algorithm with mutation schemes for solving global optimization and engineering problems, Eng. Comput. (2021) 1–23.
[32] G.-Q. Zeng, K.-D. Lu, Y.-X. Dai, Z.-J. Zhang, M.-R. Chen, C.-W. Zheng, D. Wu, W.-W.J.N. Peng, Binary-coded extremal optimization for the design of PID controllers, Neurocomputing 138 (2014) 180–188.
[33] G.-Q. Zeng, J. Chen, Y.-X. Dai, L.-M. Li, C.-W. Zheng, M.-R.J.N. Chen, Design of fractional order PID controller for automatic regulator voltage system based on multi-objective extremal optimization, Neurocomputing 160 (2015) 173–184.
[34] G.-Q. Zeng, X.-Q. Xie, M.-R. Chen, J. Weng, Adaptive population extremal optimization-based PID neural network for multivariable nonlinear control systems, Swarm and Evolutionary Computation 44 (2019) 320–334.
[35] A. Lin, Q. Wu, A.A. Heidari, Y. Xu, H. Chen, W. Geng, C. Li, Predicting intentions of students for master programs using a chaos-induced sine cosine-based fuzzy K-nearest neighbor classifier, Ieee Access 7 (2019) 67235–67248.
[36] J. Tu, A. Lin, H. Chen, Y. Li, C. Li, Predict the entrepreneurial intention of fresh graduate students based on an adaptive support vector machine framework, Math. Probl Eng. 2019 (2019) 1–16.
[37] Y. Wei, N. Ni, D. Liu, H. Chen, M. Wang, Q. Li, X. Cui, H. Ye, An improved grey wolf optimization strategy enhanced SVM and its application in predicting the second major, Math. Probl Eng. 2017 (2017) 1–12.
[38] Guo-qiang Zeng, Yong-zai Lu, Wei-Jie Mao, Modified extremal optimization for the hard maximum satisfiability problem, J. Zhejiang Univ. Sci. C 12 (2011) 589–596.
[39] G. Zeng, Y. Lu, Y. Dai, Z. Wu, W. Mao, Z. Zhang, C. Zheng, Backbone guided extremal optimization for the hard maximum satisfiability problem, Int. J. Innovat. Comput. Inf. Contr. 8 (2012) 8355–8366.
[40] X. Zhao, D. Li, B. Yang, C. Ma, Y. Zhu, H. Chen, Feature selection based on improved ant colony optimization for online detection of foreign fiber in cotton, Appl. Soft Comput. 24 (2014) 585–596.
[41] X. Zhao, D. Li, B. Yang, H. Chen, X. Yang, C. Yu, S. Liu, A two-stage feature selection method with its application, Comput. Electr. Eng. 47 (2015) 114–125.
[42] C. Li, L. Hou, B.Y. Sharma, H. Li, C. Chen, Y. Li, X. Zhao, H. Huang, Z. Cai, H. Chen, Developing a new intelligent system for the diagnosis of tuberculous pleural effusion, Comput. Methods Progr. Biomed. 153 (2018) 211–225.
[43] X. Zhao, X. Zhang, Z. Cai, X. Tian, X. Wang, Y. Huang, H. Chen, L. Hu, Chaos enhanced grey wolf optimization wrapped ELM for diagnosis of paraquat-poisoned patients, Comput. Biol. Chem. 78 (2019) 481–490.
[44] H. Huang, S. Zhou, J. Jiang, H. Chen, Y. Li, C. Li, A new fruit fly optimization algorithm enhanced support vector machine for diagnosis of breast cancer based on high-level features, BMC Bioinf. 20 (2019) 1–14.
[45] J. Pang, H. Zhou, Y.-C. Tsai, F.-D. Chou, A scatter simulated annealing algorithm for the bi-objective scheduling problem for the wet station of semiconductor manufacturing, Comput. Ind. Eng. 123 (2018) 54–66.
[46] H. Zhou, J. Pang, P.-K. Chen, F.-D. Chou, A modified particle swarm optimization algorithm for a batch-processing machine scheduling problem with arbitrary release times and non-identical job sizes, Comput. Ind. Eng. 123 (2018) 67–81.
[47] M. Chen, G. Zeng, K. Lu, J. Weng, A two-layer nonlinear combination method for short-term wind speed prediction based on ELM, ENN, and LSTM, IEEE Internet of Things Journal 6 (2019) 6997–7010.
[48] Y. Zhang, R. Liu, A.A. Heidari, X. Wang, Y. Chen, M. Wang, H. Chen, Towards Augmented Kernel Extreme Learning Models for Bankruptcy Prediction: Algorithmic Behavior and Comprehensive Analysis, Neurocomputing, 2020, https://doi.org/10.1016/j.neucom.2020.1010.1038.
[49] J. Luo, H. Chen, Y. Xu, H. Huang, X. Zhao, An improved grasshopper optimization algorithm with application to financial stress prediction, Appl. Math. Model. 64 (2018) 654–668.
[50] M. Wang, H. Chen, H. Li, Z. Cai, X. Zhao, C. Tong, J. Li, X. Xu, Grey wolf optimization evolving kernel extreme learning machine: application to bankruptcy prediction, Eng. Appl. Artif. Intell. 63 (2017) 54–68.
[51] W. Deng, H. Liu, J. Xu, H. Zhao, Y. Song, An improved quantum-inspired differential evolution algorithm for deep belief network, IEEE Trans. Instrum. Meas. (2020), https://doi.org/10.1109/TIM.2020.2983233.
[52] H. Zhao, H. Liu, J. Xu, W. Deng, Performance prediction using high-order differential mathematical morphology gradient spectrum entropy and extreme learning machine, IEEE Trans. Instrum. Meas. (2019), https://doi.org/10.1109/TIM.2019.2948414.
[53] W. Deng, J. Xu, H. Zhao, Y. Song, A novel gate resource allocation method using improved PSO-based QEA, IEEE Trans. Intell. Transport. Syst. (2020), https://doi.org/10.1109/TITS.2020.3025796.
[54] D. W, X. Jj, S. Yj, Z. Hm, An effective improved Co-evolution ant colony optimization algorithm with multi-strategies and its application, Int. J. Bio-Inspired Comput. 16 (13) (2020) 158–170.
[57] J. Kennedy, R. Eberhart, Particle swarm optimization, in: Proceedings of ICNN'95 - International Conference on Neural Networks, 1944, 1995, pp. 1942–1948.
[61] A.A. Heidari, S. Mirjalili, H. Faris, I. Aljarah, M. Mafarja, H. Chen, Harris hawks optimization: algorithm and applications, Future Generation Computer Systems-the International Journal of Escience 97 (2019) 849–872.

[62] S. Li, H. Chen, M. Wang, A.A. Heidari, S. Mirjalili, Slime mould algorithm: a new method for stochastic optimization, Future Generat. Comput. Syst. 111 (2020) 300–323.
[63] Y. Yang, H. Chen, A. Asghar Heidari, A.H. Gandomi, Hunger games search: visions, conception, implementation, deep analysis, perspectives, and towards performance shifts, Expert Syst. Appl. (2021) 114864, https://doi.org/10.1016/j.eswa.2021.114864.
[64] I. Ahmadianfar, A. Asghar Heidari, A.H. Gandomi, X. Chu, H. Chen, RUN beyond the metaphor: an efficient optimization algorithm based on Runge Kutta method, Expert Syst. Appl. (2021) 115079.
[65] C. Qu, Z. Zeng, J. Dai, Z. Yi, W. He, A modified sine-cosine algorithm based on neighborhood search and greedy levy mutation, 2018, Comput. Intell. Neurosci. (2018), 4231647-4231647.
[66] A.A. Heidari, R. Ali Abbaspour, H. Chen, Efficient boosted grey wolf optimizers for global search and kernel extreme learning machine training, Appl. Soft Comput. 81 (2019) 105521.
[67] M. Abd Elaziz, D. Oliva, S. Xiong, An improved opposition-based sine cosine algorithm for global optimization, Expert Syst. Appl. 90 (2017) 484–500.
[68] M.A. Elhosseini, A.Y. Haikal, M. Badawy, N. Khashan, Biped robot stability based on an A–C parametric Whale Optimization Algorithm, Journal of Computational Science 31 (2019) 17–32.
[69] X. Chen, H. Tianfield, C. Mei, W. Du, G. Liu, Biogeography-based learning particle swarm optimization, Soft Computing 21 (2017) 7519–7541.
[70] J.J. Liang, A.K. Qin, P.N. Suganthan, S. Baskar, Comprehensive learning particle swarm optimizer for global optimization of multimodal functions, IEEE Trans. Evol. Comput. 10 (2006) 281–295.
[71] C. Chen, X. Wang, H. Yu, M. Wang, H. Chen, Dealing with multi-modality using synthesis of Moth-flame optimizer with sine cosine mechanisms, Math. Comput. Simulat. (2021).
[72] C. Chen, X. Wang, H. Yu, N. Zhao, M. Wang, H. Chen, An enhanced comprehensive learning particle swarm optimizer with the elite-based dominance scheme, Complexity (2020) 2020.
[73] Z. Cai, J. Gu, J. Luo, Q. Zhang, H. Chen, Z. Pan, Y. Li, C. Li, Evolving an optimal kernel extreme learning machine by using an enhanced grey wolf optimization strategy, Expert Syst. Appl. 138 (2019) 112814.
[74] M. Tubishat, M.A.M. Abushariah, N. Idris, I. Aljarah, Improved whale optimization algorithm for feature selection in Arabic sentiment analysis, Appl. Intell. 49 (2019) 1688–1707.
[75] K. Socha, M. Dorigo, Ant colony optimization for continuous domains, Eur. J. Oper. Res. 185 (2008) 1155–1173.
[76] M. Dorigo, Optimization, Learning and Natural Algorithms, 1992.
[77] M. Dorigo, G.D. Caro, The Ant Colony Optimization Meta-Heuristic, New Ideas in Optimization, McGraw-Hill Ltd., UK, 1999, pp. 11–32.
[78] D. Zhao, L. Liu, F. Yu, A.A. Heidari, M. Wang, D. Oliva, K. Muhammad, H. Chen, Ant colony optimization with horizontal and vertical crossover search: fundamental visions for multi-threshold image segmentation, Expert Syst. Appl. (2020) 114122.
[79] C.-C. Chen, L.P. Shen, Improve the accuracy of recurrent fuzzy system design using an efficient continuous ant colony optimization, Int. J. Fuzzy Syst. 20 (2018) 817–834.
[80] D. Zhao, L. Liu, F. Yu, A.A. Heidari, M. Wang, G. Liang, K. Muhammad, H. Chen, Chaotic random spare ant colony optimization for multi-threshold image segmentation of 2D Kapur entropy, Knowl. Base Syst. (2020) 106510, https://doi.org/10.1016/j.knosys.2020.106510.
[81] Y. Wu, W. Ma, Q. Miao, S. Wang, Multimodal continuous ant colony optimization for multisensor remote sensing image registration with local search, Swarm and Evolutionary Computation 47 (2019) 89–95.
[82] A. Kumar, M. Thakur, G. Mittal, A new ants interaction scheme for continuous optimization problems, International Journal of System Assurance Engineering and Management 9 (2018) 784–801.
[83] Z. Chen, R.-L. Wang, Ant colony optimization with different crossover schemes for global optimization, Cluster Computing-the Journal of Networks Software Tools and Applications 20 (2017) 1247–1257.
[84] I. Karakonstantis, A. Vlachos, Hybrid ant colony optimization for continuous domains for solving emission and economic dispatch problems, J. Inf. Optim. Sci. 39 (2018) 651–671.
[85] S. García, A. Fernández, J. Luengo, F. Herrera, Advanced nonparametric tests for multiple comparisons in the design of experiments in computational intelligence and data mining: experimental analysis of power, Inf. Sci. 180 (2010) 2044–2064.
[86] J. Derrac, S. García, D. Molina, F. Herrera, A practical tutorial on the use of nonparametric statistical tests as a methodology for comparing evolutionary and swarm intelligence algorithms, Swarm and Evolutionary Computation 1 (2011) 3–18.
[87] Q. Huynh-Thu, M. Ghanbari, Scope of Validity of PSNR in Image/video Quality Assessment, Electronics Letters, Institution of Engineering and Technology, 2008, pp. 800–801.
[88] W. Zhou, A.C. Bovik, H.R. Sheikh, E.P. Simoncelli, Image quality assessment: from error visibility to structural similarity, IEEE Trans. Image Process. 13 (2004) 600–612.
[89] L. Zhang, L. Zhang, X. Mou, D. Zhang, FSIM: a feature similarity Index for image quality assessment, IEEE Trans. Image Process. 20 (2011) 2378–2386.
[90] R. Salgotra, U. Singh, Application of mutation operators to flower pollination algorithm, Expert Syst. Appl. 79 (2017) 112–129.
[91] Y. Xu, H. Chen, J. Luo, Q. Zhang, S. Jiao, X. Zhang, Enhanced Moth-flame optimizer with mutation strategy for global optimization, Inf. Sci. 492 (2019) 181–203.
[92] H. Wang, H. Li, Y. Liu, C. Li, S. Zeng, Opposition-based Particle Swarm Algorithm with Cauchy Mutation, 2007 IEEE Congress on Evolutionary Computation, IEEE, 2007, pp. 4750–4756.
[93] C. Qu, Z. Zeng, J. Dai, Z. Yi, W. He, A modified sine-cosine algorithm based on neighborhood search and greedy levy mutation, Comput. Intell. Neurosci. (2018) 2018.
[94] X.-S. Yang, Nature-inspired Metaheuristic Algorithms, Luniver press, 2010.
[95] A. Buades, B. Coll, J. Morel, A Non-local Algorithm for Image Denoising, 62, 2005 IEEE Computer Society Conference on Computer Vision and Pattern Recognition (CVPR'05), 2005, pp. 60–65.
[96] H. Mittal, M. Saraswat, An optimum multi-level image thresholding segmentation using non-local means 2D histogram and exponential Kbest gravitational search algorithm, Eng. Appl. Artif. Intell. 71 (2018) 226–235.
[97] T.J.C.g. Pun, i. processing, Entropic thresholding, a new approach 16 (1981) 210–239.
[98] J.N. Kapur, P.K. Sahoo, A.K.J.C.v. Wong, graphics, i. processing, A new method for gray-level picture thresholding using the entropy of the histogram 29 (1985) 273–285.
[99] J.P. Cohen, P. Morrison, L. Dao, K. Roth, T.Q. Duong, M.J.a.p.a. Ghassemi, Covid-19 image data collection: prospective predictions are the future [Online]. Available, https://github.com/ieee8023/covid-chestxray-dataset, 2020.
[100] C.C. Hou, T.E. Simos, I.T. Famelis, Neural network solution of pantograph type differential equations, Math. Methods Appl. Sci. 43 (2020) 3369–3374.
[101] I. Aljarah, M. Mafarja, A.A. Heidari, H. Faris, S. Mirjalili, Multi-verse optimizer: theory, literature review, and application in data clustering, in: S. Mirjalili, J. Song Dong, A. Lewis (Eds.), Nature-Inspired Optimizers: Theories, Literature Reviews and Applications, Springer International Publishing, Cham, 2020, pp. 123–141.
[102] M. Mafarja, A.A. Heidari, H. Faris, S. Mirjalili, I. Aljarah, Dragonfly algorithm: theory, literature review, and application in feature selection, in: S. Mirjalili, J. Song Dong, A. Lewis (Eds.), Nature-Inspired Optimizers: Theories, Literature Reviews and Applications, Springer International Publishing, Cham, 2020, pp. 47–67.
[103] R. Yang, M. Xu, T. Liu, Z. Wang, Z. Guan, Enhancing quality for HEVC compressed videos, IEEE Trans. Circ. Syst. Video Technol. 29 (2018) 2039–2054.
[104] M. Xu, C. Li, Z. Chen, Z. Wang, Z. Guan, Assessing visual quality of omnidirectional videos, IEEE transactions on circuits and systems for video technology 29 (2018) 3516–3530.
[105] C. Zuo, Q. Chen, L. Tian, L. Waller, A. Asundi, Transport of intensity phase retrieval and computational imaging for partially coherent fields: the phase space perspective, Opt Laser. Eng. 71 (2015) 20–32.
[106] C. Zuo, J. Sun, J. Li, J. Zhang, A. Asundi, Q. Chen, High-resolution transport-of-intensity quantitative phase microscopy with annular illumination, Sci. Rep. 7 (2017) 1–22.
[107] B. Zhang, Z. Niu, J. Wang, D. Ji, T. Zhou, Y. Liu, Y. Feng, Y. Hu, J. Zhang, Y. Fan, Four-hundred gigahertz broadband multi-branch waveguide coupler, IET Microwaves, Antennas & Propagation 14 (2020) 1175–1179.
[108] Y. Wang, W. Lu, J. Liu, M. Zhang, Y. Miao, Random seismic noise attenuation based on data augmentation and CNN, Acta Geophysica Sinica 62 (2019) 421–433.
[109] Z.-q. Niu, B. Zhang, D.-t. Li, D.-f. Ji, Y. Liu, Y.-n. Feng, T.-c. Zhou, Y.-h. Zhang, Y. Fan, A mechanical reliability study of 3dB waveguide hybrid couplers in the submillimeter and terahertz band, J. Zhejiang Univ. - Sci. 1 (1998).
[110] S.J. Wang, H.L. Chen, W.J. Yan, Y.H. Chen, X. Fu, Face recognition and micro-expression recognition based on discriminant tensor subspace analysis plus extreme learning machine, Neural Process. Lett. 39 (2014) 25–43.
[111] S.-J. Wang, Y. He, J. Li, X. Fu, MESNet: a convolutional neural network for spotting multi-scale micro-expression intervals in long videos, IEEE Trans. Image Process. (2021).
[112] X. Wang, F. Sohel, M. Bennamoun, Y. Guo, H. Lei, Scale space clustering evolution for salient region detection on 3D deformable shapes, Pattern Recogn. 71 (2017) 414–427.
[113] X. Wang, M. Bennamoun, F. Sohel, H. Lei, Diffusion geometry derived keypoints and local descriptors for 3d deformable shape analysis, J. Circ. Syst. Comput. 30 (2021) 2150016.
[114] J. Li, C. Soladie, R. Seguier, Local temporal pattern and data augmentation for micro-expression spotting, IEEE Transactions on Affective Computing (2020), https://doi.org/10.1109/TAFFC.2020.3023821.
[115] X. Xue, S.F. Wang, L.J. Zhan, Z.Y. Feng, Y.D. Guo, Social learning evolution (SLE): computational experiment-based modeling framework of social manufacturing, Ieee Transactions on Industrial Informatics 15 (2019) 3343–3355.
[116] X. Xue, Z. Chen, S. Wang, Z. Feng, Y. Duan, Z. Zhou, Value Entropy: A Systematic Evaluation Model of Service Ecosystem Evolution, IEEE Transactions on Services Computing, 2020, https://doi.org/10.1109/TSC.2020.3016660.
[117] C. Yang, H. Zhao, L. Bruzzone, J.A. Benediktsson, Y. Liang, B. Liu, X. Zeng, R. Guan, C. Li, Z. Ouyang, Lunar impact crater identification and age estimation with Chang'E data by deep and transfer learning, Nat. Commun. 11 (2020) 6358.
[118] X. Liu, B. Yang, H. Chen, K. Musial, H. Chen, Y. Li, W. Zuo, A scalable redefined stochastic blockmodel, ACM Trans. Knowl. Discov. Data 15 (2021) 1–28.
[119] X. Cao, T. Cao, F. Gao, X. Guan, Risk-averse storage planning for improving RES hosting capacity under uncertain siting choice, IEEE Transactions on Sustainable Energy (2021), https://doi.org/10.1109/TSTE.2021.3075615.
[120] J. Xia, H. Chen, Q. Li, M. Zhou, L. Chen, Z. Cai, Y. Fang, H. Zhou, Ultrasound-based differentiation of malignant and benign thyroid Nodules: an extreme learning machine approach, Comput. Methods Progr. Biomed. 147 (2017) 37–49.

[121] C. Chen, Q. Wu, Z. Li, L. Xiao, Z.Y. Hu, Diagnosis of Alzheimer's Disease Based on Deeply-Fused Nets, Combinatorial Chemistry & High Throughput Screening, 2020.
[122] Y. Li, L. Liu, Y. Guo, X. Liao, B. Hu, T. Yu, Spatio-temporal-spectral hierarchical graph convolutional network with semi-supervised active learning for patient-specific seizure prediction, IEEE Transactions on Cybernetics (2021), https://doi.org/10.1109/TCYB.2021.3071860.
[123] C. Feng, Z. Zhu, Z. Cui, V. Ushakov, J.C. Dreher, W. Luo, R. Gu, X. Wu, F.J.H.b. m. Krueger, Prediction of trust propensity from intrinsic brain morphology and functional connectome, Hum. Brain Mapp. 42 (2021) 175–191.
[124] Z. Li, X. Wu, X. Xu, H. Wang, Z. Guo, Z. Zhan, L. Yao, The recognition of multiple anxiety levels based on electroencephalograph, IEEE Trans. Affect. Comput. (2019), https://doi.org/10.1109/TAFFC.2019.2936198.
[128] Y. Liu, B. Zhang, Y. Feng, X. Lv, D. Ji, Z. Niu, Y. Fan, Development of 340-GHz transceiver front end based on GaAs monolithic integration technology for THz active imaging array, Appl. Sci. 10 (21) (2020) 7924.
[129] Z. Niu, B. Zhang, J. Wang, K. Liu, Z. Chen, K. Yang, Y. Liu, The research on 220GHz multicarrier high-speed communication system, China Commun. 17 (3) (2020) 131–139.
[130] Z.Q. Niu, B. Zhang, D.T. Li, D.F. Ji, Y. Liu, Y.N. Feng, Y. Fan, A mechanical reliability study of 3dB waveguide hybrid couplers in the submillimeter and terahertz band, J. Zhejiang Univ. Sci. 1 (1) (1998) 1, https://doi.org/10.1631/FITEE.2000229.
[131] B. Zhang, D. Ji, D. Fang, S. Liang, Y. Fan, X. Chen, A novel 220-GHz GaN diode on-chip tripler with high driven power, IEEE Electron. Device Lett. 40 (5) (2019) 780–783.
[132] Q. Jiang, F. Shao, W. Lin, K. Gu, G. Jiang, H. Sun, Optimizing multistage discriminative dictionaries for blind image quality assessment, IEEE Trans. Multimed. 20 (8) (2017) 2035–2048.
[133] Y. Yang, Y. Liu, X. Lv, J. Ai, Y. Li, Anthropomorphism and customers' willingness to use artificial intelligence service agents, J. Hospit. Market. Manag. (2021) 1–23.
[134] S. Mirjalili, I. Aljarah, M. Mafarja, A.A. Heidari, H. Faris, Grey Wolf optimizer: theory, literature review, and application in computational fluid dynamics problems, Nature-Inspired Optimizers (2020) 87–105.
[135] S. Mirjalili, J.S. Dong, A. Lewis, Nature-inspired optimizers: theories, literature reviews and applications, Springer 811 (2019).
[136] A.R. Jordehi, An improved particle swarm optimisation for unit commitment in microgrids with battery energy storage systems considering battery degradation and uncertainties, Int. J. Energy Res. 45 (1) (2021) 727–744.
[137] A.R. Jordehi, Particle swarm optimisation with opposition learning-based strategy: an efficient optimisation algorithm for day-ahead scheduling and reconfiguration in active distribution systems, Soft comput. 24 (24) (2020) 18573–18590.
[138] A.R. Jordehi, A mixed binary-continuous particle swarm optimisation algorithm for unit commitment in microgrids considering uncertainties and emissions, Int. Trans. Electr. Energy Syst. 30 (11) (2020), e12581.
[139] A.R. Jordehi, Enhanced leader particle swarm optimisation (ELPSO): a new algorithm for optimal scheduling of home appliances in demand response programs, Artif. Intell. Rev. (2019) 1–31.
[140] A.R. Jordehi, Binary particle swarm optimisation with quadratic transfer function: A new binary optimisation algorithm for optimal scheduling of appliances in smart homes, Appl. Soft Comput. 78 (2019) 465–480.
[141] A.R. Jordehi, Enhanced leader PSO (ELPSO): a new PSO variant for solving global optimisation problems, Appl. Soft Comput. 26 (2015) 401–417.
[142] A.R. Jordehi, Time varying acceleration coefficients particle swarm optimisation (TVACPSO): A new optimisation algorithm for estimating parameters of PV cells and modules, Energy Convers. Manag. 129 (2016) 262–274.
[144] P. Wu, H. Ye, X. Cai, C. Li, S. Li, M. Chen, M. Wang, A.A. Heidari, M. Chen, J. Li, H. Chen, An effective machine learning approach for identifying non-severe and severe coronavirus disease 2019 patients in a rural Chinese population: the wenzhou retrospective study, IEEE Access 9 (2021) 45486–45503.
[145] H. Ye, P. Wu, T. Zhu, Z. Xiao, X. Zhang, L. Zheng, J. Li, Diagnosing coronavirus disease 2019 (COVID-19): Efficient Harris Hawks-inspired fuzzy K-nearest neighbor prediction methods, IEEE Access 9 (2021) 17787–17802.